NUCLEAR INSTRUMENTS

A JOURNAL ON ACCELERATORS, INSTRUMENTATION
AND TECHNIQUES IN NUCLEAR PHYSICS

EDITOR K. SIEGBAHN - UPPSALA

VOLUME 3

JULY 1958 — DECEMBER 1958

NORTH-HOLLAND PUBLISHING COMPANY — AMSTERDAM

PRINTED IN THE NETHERLANDS
DRUKKERIJ MEIJER N.V. — WORMERVEER AND AMSTERDAM

NUCLEAR INSTRUMENTS

EDITORIAL BOARD:

J. B. ADAMS (CERN)
E. AMALDI (Rome)
H. L. ANDERSON (Chicago)
K. T. BAINBRIDGE (Cambridge, Mass.)
C. J. BAKKER (CERN)
P. R. BELL (Oak Ridge)
R. E. BELL (Montreal)
A. BERTHELOT (Saclay)
H. BRINKMAN (Groningen)
S. DE BENEDETTI (Pittsburgh)
M. DE HEMPTINNE (Louvain)
A. DE-SHALIT (Rehovoth)
M. DEUTSCH (Cambridge, Mass.)
S. DU TOIT (Pretoria)
B. S. DŽELEPOV (Leningrad)
W. GENTNER (CERN)
P. C. GUGELOT (Amsterdam)
H. HALBAN (Paris)
O. HAXEL (Heidelberg)
P. HUBER (Basel)
D. J. HUGHES (Brookhaven)
S. KIKUCHI (Tokyo)
J. KOCH (Copenhagen)
M. S. KOZODAEV (Moscow)
S. LIVINGSTON (Cambridge, Mass.)
E. M. MCMILLAN (Berkeley)
M. G. MEŠČERJAKOV (Moscow)
P. B. MOON (Birmingham)
M. L. OLIPHANT (Canberra)
W. PAUL (Bonn)
A. S. RAO (Bombay)
G. SALVINI (Rome)
P. SAVIĆ (Belgrade)
P. SCHERRER (Zürich)
CH. SCHMELZER (CERN)
M. W. B. SKINNER (Liverpool)
R. TANGEN (Blindern)
V. I. VEKSLER (Moscow)
O. WERNHOLM (Stockholm)
D. TAYLOR (Harwell)
G. VON DARDEL (CERN)
R. R. WILSON (Cornell)
S. D. WINTER (Saclay)

JULY 1958 VOLUME 3 (1958) No. 1

GREGG M. SINCLAIR LIBRARY
UNIVERSITY OF HAWAII
8-7-63

NUCLEAR INSTRUMENTS

A JOURNAL ON ACCELERATORS, INSTRUMENTATION AND TECHNIQUES IN NUCLEAR PHYSICS

EDITOR: K. SIEGBAHN – UPPSALA

CONTENTS

I. LINDGREN, Atomic beam resonance apparatus with six-pole magnets for radioactive isotopes 1
A. BISI and L. ZAPPA, Statistical spread in pulse size of the scintillation spectrometer 17
G. HETTINGER and N. STARFELT, Improved NaI scintillation spectrometer for the study of continuous X-ray spectra 25
O. BECKMAN, Photographic bent crystal gamma spectrometer 27
J. O. BURGMAN and G. ANDERSSON, Ion source for radioisotope separation 33
G. C. PHILLIPS, E. B. PAUL, A. T. G. FERGUSON, A. B. WHITEHEAD, T. GRJEBINE, R. MOREAU and B. OLKOWSKY, Natural modulation of high frequency ion source beams 43
T. R. OPHEL, Response curves of alkali halide scintillators with special reference to the $Li^6(n,\alpha)$ reaction in lithium iodide 45
B. JOHANSSON and T. ALVÄGER, Proposition for a new method for measuring short half-lives 49
J. VAN BLADEL, General formulas for gap-excited linear ducts 52

NORTH-HOLLAND PUBLISHING COMPANY – AMSTERDAM

NUCLEAR INSTRUMENTS

A journal on accelerators, instrumentation and techniques in nuclear physics

EDITOR: K. SIEGBAHN, UPPSALA

EDITORIAL BOARD:

J. B. ADAMS (CERN)
E. AMALDI (Rome)
H. L. ANDERSON (Chicago)
K. T. BAINBRIDGE (Cambridge, Mass.)
C. J. BAKKER (CERN)
P. R. BELL (Oak Ridge)
R. E. BELL (Montreal)
A. BERTHELOT (Saclay)
H. BRINKMAN (Groningen)
S. DE BENEDETTI (Pittsburgh)
M. DE HEMPTINNE (Louvain)
A. DE-SHALIT (Rehovoth)
M. DEUTSCH (Cambridge, Mass.)
S. DU TOIT (Pretoria)
B. S. DŽELEPOV (Leningrad)
W. GENTNER (CERN)
P. C. GUGELOT (Amsterdam)
H. HALBAN (Paris)
O. HAXEL (Heidelberg)
P. HUBER (Basel)
D. J. HUGHES (Brookhaven)
S. KIKUCHI (Tokyo)
J. KOCH (Copenhagen)
M. S. KOZODAEV (Moscow)
S. LIVINGSTON (Cambridge, Mass.)
E. M. MCMILLAN (Berkeley)
M. G. MEŠČERJAKOV (Moscow)
P. B. MOON (Birmingham)
M. L. OLIPHANT (Canberra)
W. PAUL (Bonn)
A. S. RAO (Bombay)
G. SALVINI (Rome)
P. SAVIĆ (Belgrade)
P. SCHERRER (Zürich)
CH. SCHMELZER (CERN)
H. W. B. SKINNER (Liverpool)
R. TANGEN (Blindern)
D. TAYLOR (Harwell)
V. I. VEKSLER (Moscow)
O. WERNHOLM (Stockholm)
G. VON DARDEL (CERN)
R. R. WILSON (Cornell)
S. D. WINTER (Saclay)

Contributions may be sent to the Editor, Professor K. Siegbahn, Institute of Physics, the University of Uppsala, either directly or through the intermediary of one of the members of the Editorial Board of the country or region in which the author is working. Contributions may be written in English, French or German, with an abstract in English.

Books for review should be sent to Professor Siegbahn.

Nuclear Instruments is published monthly. The subscription price of a volume of 360 pages is $ 17.00 (130 s), postage free.

Subscriptions should be sent to the publishers, North-Holland Publishing Company, P.O.Box 103, Amsterdam or to any subscription-agent.

No part of this issue may be reproduced in any form, by print, photoprint, microfilm or any other means without written permission from the publisher. Reprints, photoprints or microfilms are obtainable at cost from the publisher.

nuclear instruments

outstanding in

PRECISION & STABILITY

Hamner

Non-Overload Amplifier and Single Channel Pulse Height Analyzer Model N-302

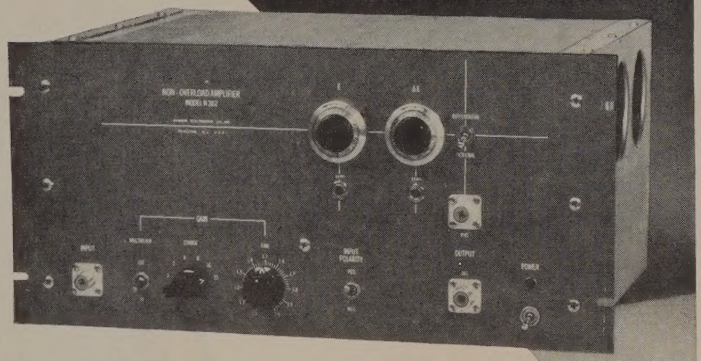

For: Scintillation Spectroscopy • Single Component Monitoring • Proportional Counter Pulse Analysis

• Amplifier: Risetime, 0.2 microseconds; feedback stabilized gain, 20,000 max. (10,000 max. with 1 microsecond delay line clipping); 0-100 volts output with better than 0.2% linearity; handles large overloads with minimum base line shift.

• Pulse Height Selector: Resolving time, 1.2 microseconds; 0-100 volt base line with 50 millivolt per day stability; 0-10 volt window with 1% stability at 1 volt; rate dependence, less than 10 millivolts window shift at 200,000 C.P.S.

• Combination provides the ultimate in reliability and stability. Designed to handle most pulse amplification and height analysis problems encountered in the nuclear field today.

Regulated High Voltage Power Supply Model N-401

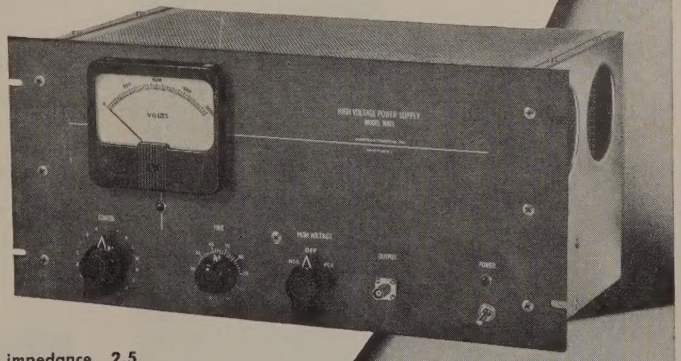

Continuously Variable • The Ultimate in Stability

• The Model N-401 is a new concept in regulated power supply design—it provides up to 5 MA of current and negative or positive DC voltage—continuously variable from 500 to 1800 volts.

• Unmatched stability against line change; less than 0.003% per volt—Regulation, 0.0025% per MA @ 1000 volts—Output impedance, 2.5 ohms.

• Low noise and ripple; less than 1 MV RMS.

• Designed for use with scintillation and proportional counters or for general laboratory use—anywhere the ultimate in stability is required at a reasonable price.

WRITE FOR DESCRIPTIVE BROCHURES AND PRICES:

Hamner Electronics Co., Inc.

P.O. BOX [redacted], PRINCETON, NEW JERSEY, U.S.A. • Phone: Pennington 7-1320

531

Export Department: H.E.C.I., 202 East 44th Street, New York, New York, U.S.A.

Hamner's complete line of nuclear instruments includes: Mercury Switch Pulsers, Scalers, Photomultiplier Preamplifiers, Scintillation Counters, High Voltage Power Supplies, Recording and Manual Spectrometers, Log Count Rate Meters, High Gain Non-Overloading Amplifiers, etc. Complete Catalog Available.

PHILIPS

equipment for Nuclear Physics and Atomic Energy

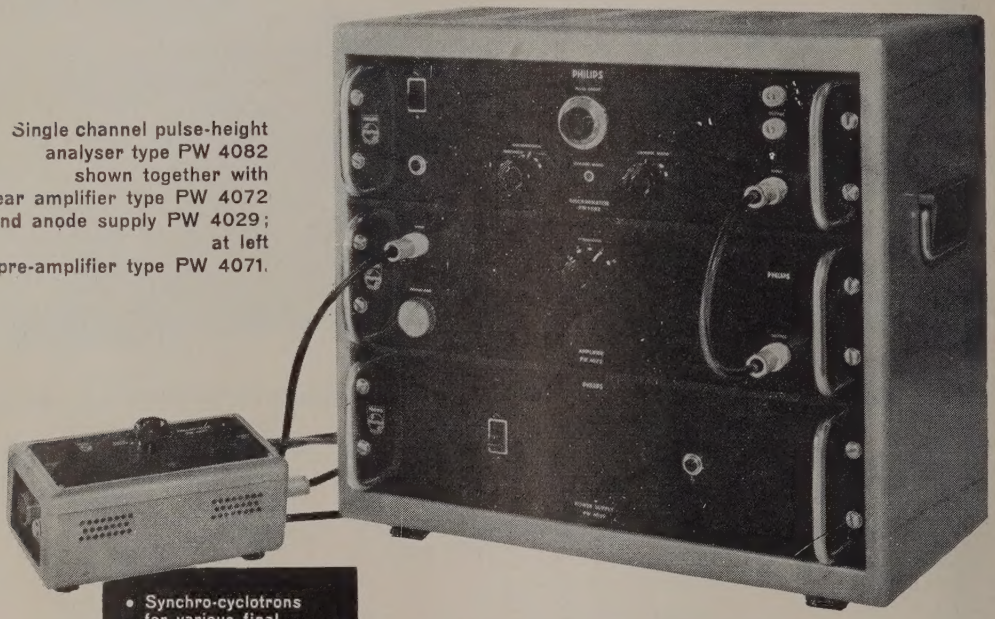

Single channel pulse-height analyser type PW 4082 shown together with linear amplifier type PW 4072 and anode supply PW 4029; at left pre-amplifier type PW 4071.

- Synchro-cyclotrons for various final energies.
- Cockcroft-Walton accelerators.
- Generators for very high d.c. voltages.
- Linear electron accelerators.
- Reactor control instrumentation.
- Radiation measuring and detection equipment.
- Civil defence instruments.
- Area monitoring instrumentation.
- Geiger counter tubes.
- Photomultipliers.
- Radio-active isotopes.
- Air liquefiers.

In conjunction with a proportional or scintillation detector, a linear amplifier and a scaler or ratemeter, this single channel pulse-height discriminator, with features such as:

- High resolving power,
- 10 different channel widths,
- Provision for threshold discrimination,
- Provision for connecting an automatic scanning unit,

permits accurate analysis of energy spectrums of radioisotopes.

PHILIPS

Nuclear Equipment

for further information please apply to:

N.V. PHILIPS' GLOEILAMPENFABRIEKEN, Scientific Equipment Department, Eindhoven-Holland
RESEARCH & CONTROL INSTRUMENTS LTD., Instrument House, 207/215, King's Cross Road, London WC 1

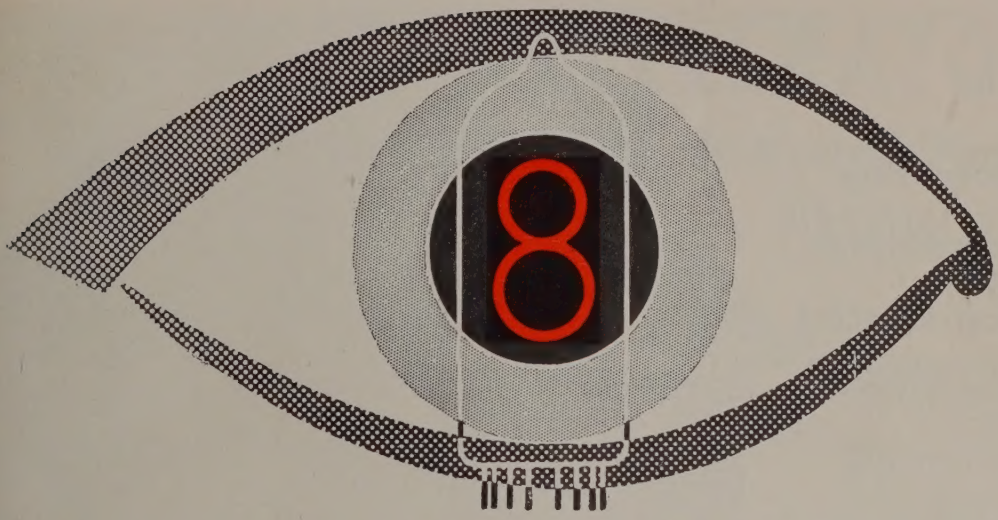

INSTANTANEOUS READOUT

with the wide-angle side-viewing

DIGITRON*

The new Ericsson register tube which gives direct numerical display for all digital applications.

The Digitron consists of 10 cathode assemblies arranged to display the numbers 0 to 9 according to the cathode energised.

Number delineation takes full advantage of the essentially rectangular vertical cross-section of the glass envelope and is based on a display area of 30 mm x 17 mm. This represents a considerable increase in both character size and visibility range over end viewing presentation. Further, by adopting such a method of display, an unrestricted view of the numbers is obtained over viewing angles of 60° either side of tube normal without any distortion.

Displayed data can therefore be quickly assimilated without ambiguity by either individuals or groups at distances up to 50 feet over a viewing arc of 120°.

Developments in hand indicate that other symbols and characters can be supplied in "DIGITRON" form for special applications.

If you would like more information about the DIGITRON TYPE GRIOG or have any problems concerning digital display please write to:

THE TECHNICAL SERVICES DEPT.,

ERICSSON

TUBE DIVISION, BEESTON, NOTTINGHAM.

ERICSSON TELEPHONES LIMITED, HEAD OFFICE: 22 LINCOLN'S INN FIELDS, LONDON W.C.2. Tel HOLborn 6936.

T E L ENGLAND

* DIGITRON IS AN ERICSSON TRADE MARK

E89A-71A

A Beta-Ray Spectrometer in commercial production, engineered to highest standards of performance

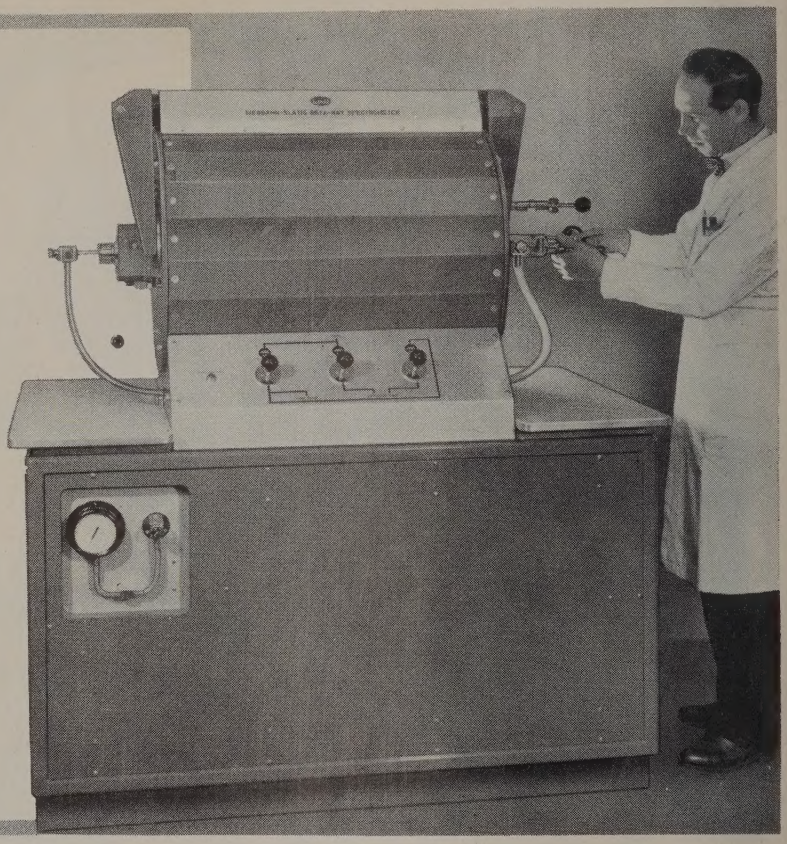

▲ Operator inserting source holder into spectrometer chamber through lock valve. Control console and 50 kW motor-generator set not shown.

The LKB 3024B Siegbahn-Slätis Intermediate Image Beta-Ray Spectrometer

Features distinguishing the LKB Beta-Ray Spectrometer include:

Energy Range: 1 keV to 8.3 MeV electrons, or, when used as pair spectrometer, up to 17.6 MeV gammas.

Transmission: up to 8% of 4π.

Resolution: 0.7% at 1% transmission or 1.2% at 6% transmission.

Linearity: $B\rho$ proportional to magnet current within ±0.11% between 36 keV and 8.3 MeV.

Shielding: Spectrometer is iron-jacketed, insuring extremely low stray-field level.

Operation: Safe and fast. There are protective devices against all possible kinds of failure. Precision electronic regulator with follow-up servo facilitates current setting.

To be shown at the Geneva "Atoms for Peace" Exhibition, Sept. 1–14, 1958

Other LKB Products for the Nuclear Physicist:
Custom-built Precision-Stabilized and Transient-Free High Current D. C. Power Supplies.
Autovac Vacuum Gauge.

LKB

Write for details and references to:

LKB-PRODUKTER

Fabriksaktiebolag

P.O. Box 12220, Stockholm 12, Sweden

Distributors throughout the world

PARTICLE ACCELERATORS

in Nuclear Physics, Chemistry, and Biology

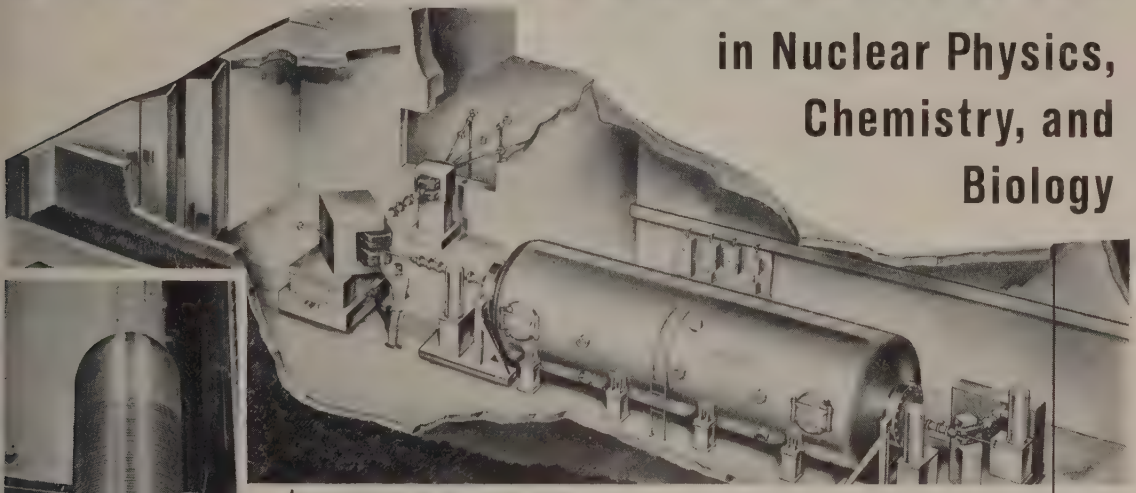

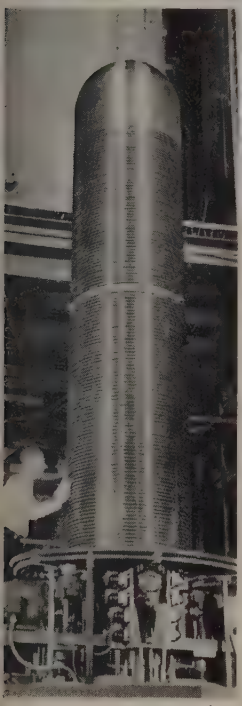

5.5 Mev Van de Graaff Model CN

This machine, widely used for neutron cross-section studies and nuclear-energy-level determinations, will be displayed at the Second International Exhibition of the Peaceful Uses of Atomic Energy, in Geneva, Switzerland.

10-Mev Tandem Van de Graaff® Positive-ion Accelerator, Model EN. Designed for nuclear research at the Chalk River establishment of Atomic Energy of Canada Limited, this is the first of three high-energy machines being built by HIGH VOLTAGE for installation in various parts of North America. With this new design, physicists will, for the first time, be able to explore with precision the binding-energy physics of higher atomic numbers.

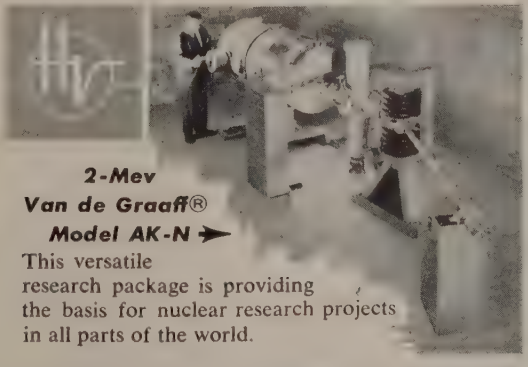

2-Mev Van de Graaff® Model AK-N

This versatile research package is providing the basis for nuclear research projects in all parts of the world.

0.25-Mev Van de Graaff®, Model PN-250

The most recent development in particle accelerators, this new, low-energy machine is designed as a pulsed-neutron source for use with subcritical assemblies in reactor research and teaching.

Van de Graaffs®

1 Mev – Model EN
Economical neutron source for reactor research

1 Mev – Model JN
Simplified electron source for transistor and crystal research

2 Mev Model AK-N
Precise, multiple-purpose instrument for general physics research and teaching

2 Mev Model AK-S
Moderate-power electron source for quantitive radiation research

2 Mev Model KN
Powerful neutron source and effective instrument for binding-energy physics

5.5 Mev Model CN
Ideal positive-ion accelerator for broad-range nuclear research programs

10 Mev Model EN
New, precise, high-energy, tandem accelerator for binding-energy investigation of heavy nuclei

Microwave Linear Electron Accelerators — 5 to 50 Mev Linacs
A series of high-energy, high-powered electron accelerators for research and production

Write us for the name of your nearest distributor and for informative reprints in your field of interest

HIGH VOLTAGE ENGINEERING CORPORATION
BURLINGTON MASSACHUSETTS

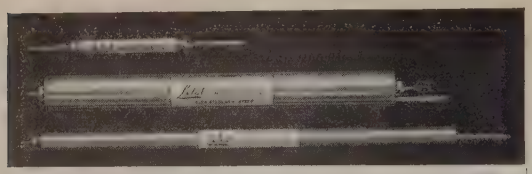

LELAB METAL-WALLED G-M TUBES

for anti-coincidence applications where uniformity counts !

Lelab Counter Tubes are individually constructed, filled, and tested. Each is fabricated almost entirely of metal. All components are confined within the diameter of the tube shell to permit close stacking.

Compare our low prices on these superior tubes!

(Makers of Lelab [Robinson-Selverstone Type] Probe Counters for neurosurgery and where a fine needle-like probe for highly localized measurements is useful.)

Write for complete information

H. W. Leighton Laboratories

York & Sunset Lane-Hatboro, Pa. U.S.A.

FOR SCINTILLATION & PROPORTIONAL COUNTING

Non-overloading linear Amplifiers

MODELS 108 and 108 p

* GAIN–40,000, continuously variable
* RISE TIME–0.2 microsecond
* ACCEPTS + AND — PULSES

Tremendous Dynamic Range

EXCEEDS 1,000,000 (0.1 mv to 100 V)

Excellent linearity for small pulses in the presence of tremendous overloads that paralyze other amplifiers.

PULSE HEIGHT SELECTOR (Supplied only on Model 108 P—Precision trigger-type).

MODEL 108 . . . $ 545.00 — MODEL 108 p . . . $ 595.00

Precision High Voltage Supply

MODEL 515 . . . $ 385.00

* 500–1500 volts, 1 m.a. (2 m.a. to 1KV)
* Continuously variable
* Polarity switch makes this highly regulated supply equivalent to two separate precision instruments
* Drift less than .01% over several hours; less than .02% per day Regulation .0002% per % change in line voltage for line voltages between 70 and 140
* Precision voltage divider for precise reading of output voltage
* 4½" panel meter. Dual teflon connectors

RADIATION INSTRUMENT CO.

P.O. BOX 733 SILVER SPRING, MARYLAND, U.S.A.

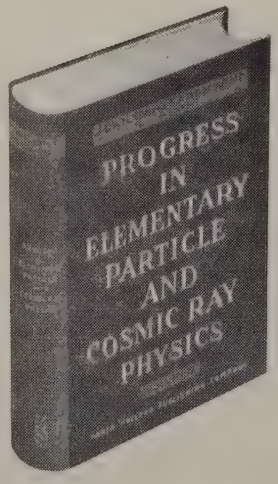

PROGRESS IN ELEMENTARY PARTICLE AND COSMIC RAY PHYSICS VOL. IV

Editors

J. G. WILSON, *Professor of Physics, University of Leeds*

and

S. A. WOUTHUYSEN, *Professor of Physics, University of Amsterdam*

6 × 9″ XII + 482 p. 110 illus. Guilders 45.00 (90 s)

CONTENTS

1. *Some Theoretical Aspects of the Strong Interactions of the New Particles* (B. D'Espagnat and J. Prentki). 2. *The Properties and Production of K-mesons* (W. D. Walker). 3. *The Interaction of μ-Mesons with Matter* (G. N. Fowler and A. W. Wolfendale). 4. *The Primary Cosmic Radiation and its Time Variations* (S. F. Singer). 5. *The Origin of Cosmic Radiation* (V. L. Ginzburg).

Sole Agency for U.S.A.: Interscience Publishers, Inc. — New York

NORTH-HOLLAND PUBLISHING COMPANY - AMSTERDAM

Send your order to your bookseller or directly to us

Scintillators in 5 forms

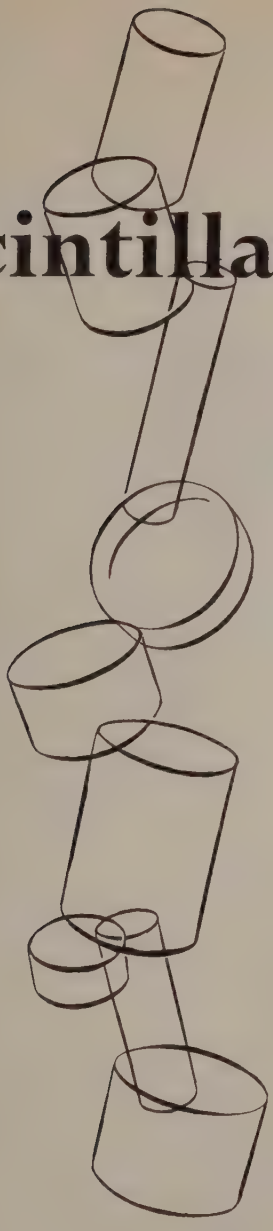

Scintillators in five forms are now available from Nash and Thompson Ltd.

CRYSTALS

Anthracene, Stilbene, Diphenylacetylene, in discs and cylinders.

PLASTICS

N.11 and N.11-X-ray, high sensitivity, high transmission polyvinyl toluene based.

LIQUIDS

Ready made, sealed in glass containers to your specification, or as scintipaks.

SCINTIPAKS

Accurately mixed dry constituents sealed in polythene envelopes, ready for dissolving in a suitable solvent as required.

POWDERS

Scintillation purity chemicals for crystal growing experiments, and the manufacture of special scintillators.

Meet Nash and Thompson on the S.I.M.A. Stand at the 'Atoms for Peace' Exhibition, Geneva, September 1st-14th, 1958.

Write or telephone for full information to

Nash and Thompson *LTD*

OAKCROFT ROAD · CHESSINGTON · SURREY · ENGLAND
ELMBRIDGE 5252

WHG/NT64

INTERNATIONAL

advertise
YOUR NUCLEAR PRODUCTS IN

sell
YOUR NUCLEAR PRODUCTS

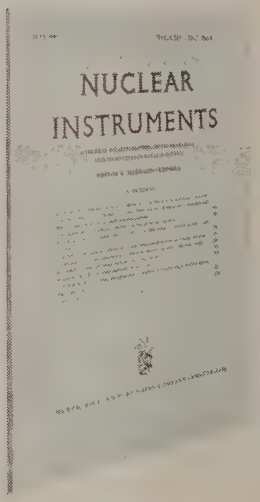

reap
YOUR NUCLEAR SALES
REWARDS

world wide
KEY NUCLEAR MANAGEMENT
NUCLEAR SCIENTISTS
NUCLEAR ENGINEERS
NUCLEAR PRODUCTION
PERSONNEL

SUBSCRIBE TO

you reach
THE WHOLE
NUCLEAR SALES WORLD IN

Entirely international in scope Nuclear Instruments is the one nuclear scientific journal that has an established subscription clientele through-out the whole world-where-ever nuclear men are at work—they want your nuclear products—they need your nuclear products—advertise in Nuclear Instruments and tell them WHAT – HOW – WHERE they can get your nuclear products

GO INTERNATIONAL WITH YOUR SALES PROGRAM TODAY WRITE

WILLIAM F. BAARS - ADVERTISING MANAGER NORTH-HOLLAND PUBLISHING COMPAI

P.O. BOX 103 – AMSTERDAM, HOLLAND

INTERNAIICONAL

NUCLEAR INSTRUMENTS 3 (1958) 1–16; NORTH-HOLLAND PUBLISHING CO. – AMSTERDAM

ATOMIC BEAM RESONANCE APPARATUS WITH SIX-POLE MAGNETS FOR RADIOACTIVE ISOTOPES

INGVAR LINDGREN

Institute of Physics, University of Uppsala, Uppsala

Received 20 January 1958

The construction of an atomic beam resonance apparatus with focusing six-pole magnets for measurements of spins and magnetic moments of radioactive nuclei is reported. The main features are similar to those of the apparatus of Hamilton, Lemonick, and Pipkin†. The principles of the design and of maximizing the intensity are discussed. The effective solid angle, averaged over the velocity distribution of the beam, has been calculated to be about 3×10^{-4} steradians in a typical case, which is one order of magnitude larger than can be obtained by the conventional method. The apparatus has been used for measurements on four radioactive bismuth isotopes, which will be reported elsewhere.

1. Introduction

There is now a great interest in the determination of spins and magnetic moments of nuclei in the ground state, especially for radioactive isotopes. Among the methods used for stable nuclei, only the atomic beam method has been employed to a great extent for radioactive nuclei. Here the radioactivity is frequently utilized for the detection and the method can therefore by very sensitive.

The majority of the nuclear spins and magnetic moments of stable isotopes have now in fact been measured. So far, however, only relatively few of the radioactive isotopes have been investigated, even if the number of measured spins and magnetic moments is now rapidly increasing.

The first measurement on a radioactive isotope by the atomic beam method was made by Zacharias[1]) in his well-known experiment with K^{40} in 1942. He then introduced the so called "flop-in" technique which has been used ever since in practically all atomic beam investigations of radioactive isotopes. Davis, Nagle, and Zacharias[2]) in 1948–49 used this technique in measurements on Na^{22}, K^{40}, Cs^{135} and Cs^{137} and Jaccarino, Bederson and Stroke[3]) in 1952 on Cs^{134}. In 1951–52 Bellamy and Smith[4]) made measurements on Na^{24}, K^{42}, Rb^{86}, Cs^{131}, and Cs^{134}, the first experiments with the radioactive deposition technique.

During the last few years the work on radioactive isotopes has been intensified. In 1954 Hamilton, Lemonick, and Pipkin[5,6]) started to work with a focused atomic beam, achieved with six-pole magnets, in order to get higher intensity. They first measured Cu^{64}, Ag^{111}, Au^{198}, and Au^{199} and later Hamilton *et al.*[7]) have studied As^{76} and some other Cu, Ag, and Au isotopes. The Berkeley group, Hubbs, Nierenberg, Silbsee, Shugart, Sunderland *et al.*[8]), has

† The author is much indebted to Professor D. R. Hamilton and Dr. A. Lemonick for having submitted some data of their apparatus prior to publication.

[1]) J. R. Zacharias, Phys. Rev. **61** (1942) 270.

[2]) L. Davis Jr., D. E. Nagle and J. R. Zacharias, Phys. Rev. **76** (1949) 1068.

[3]) V. Jaccarino, B. Bederson and H. H. Stroke, Phys. Rev. **87** (1952) 676.

[4]) E. H. Bellamy and K. F. Smith, Phil. Mag. **44** (1953) 33

[5]) A. Lemonick, F. M. Pipkin and D. R. Hamilton, Rev. Sci. Instr. **26** (1955) 1112.

[6]) A. Lemonick and F. M. Pipkin, Phys. Rev. **95** (1954) 1356; R. L. Christensen, D. R. Hamilton, A. Lemonick, F. M. Pipkin, J. B. Reynolds and H. H. Stroke, Phys. Rev. **101** (1956) 1389.

[7]) R. L. Christensen, H. G. Bennewitz, D. R. Hamilton, J. B. Reynolds and H. H. Stroke, Phys. Rev. **107** (1957) 633; D. R. Hamilton, Report at the Third Molecular Beam Conference at Brookhaven (November 1957).

[8]) J. C. Hubbs, W. A. Nierenberg, H. A. Shugart, H. B. Silsbee, R. J. Sunderland *et al.*, Phys. Rev. **104** (1956) 757

measured a number of spins and magnetic moments of cyclotron-produced isotopes of Rb and Cs and lately some spins of isotopes of Ga, Tl, Ag, Au, Br, and I and of the transuranic elements Np, Pu, and Am[9]). Radioactive isotopes have during this time also been investigated by Gilbert and Cohen[10]) (Cs^{134m}), Goodman, Wexler *et al.*[11]) (Cs^{134m}, In^{113m}, In^{114m}, In^{116m}), Smith[12]) (Bi^{210}), Nutter[13]) (In^{116m}), Woodgate and Hellwarth[14]) (Ag^{111}), and Sherwood[15]) (I^{128}).

Almost all radioactive isotopes investigated so far by atomic beam methods have an electronic angular momentum $J = 1/2$. Only a few elements with half-integral J greater than 1/2 have been studied, and, as far as we know, only one isotope with even atomic number has been investigated, namely Pu^{239} by Hubbs *et al.*[9]). Especially in this latter group of elements there is a large number of new isotopes that could be studied with the atomic beam technique.

2. The Beam Resonance Method

The molecular beam resonance method, introduced by Rabi *et al.*[16]) in 1938, was first applied to beams of non-paramagnetic molecules in order to measure nuclear magnetic moments by their direct interaction with an external field[17]). Later, this method was also applied to paramagnetic atoms by Kusch, Millman, and Rabi[18]). In this case the transitions take place between certain hyperfine structure (hfs) levels of the atoms and the nuclear properties have then to be calculated from the hfs.

In the original arrangement of the resonance apparatus, the gradients of the deflecting fields (the "A" and "B" fields) are oppositely directed. The beam is then normally refocused on the detector and the intensity reaches a minimum at resonance ("flop-out"). In the opposite arrangement, ("flop-in"), the gradients of the A and B magnets are parallel and the beam is refocused at resonance.

With the flop-out technique, all transitions that result in a change of the effective magnetic moment at strong fields can, in principle, be observed. With the flop-in technique, however, the refocusing condition can be fulfilled only for a certain change of the effective moment and the number of observable transitions is therefore in general reduced. At flop in, the magnetic fields are usually such that the effective moment should have the same magnitude but opposite sign in the A and B fields.

The flop-in technique is, of course, very suitable for isotopes that can only be obtained in small amounts at low concentrations. In practically all atomic beam work on radioactive isotopes this method has been employed.

In most of the radioactive atomic beam works the radioactivity itself is utilized for the detection. The atoms are here collected on a "button", which can be removed from the apparatus, and the deposited activity is measured. The activity is determined as a function of the applied frequency point by point.

It is, of course, particularly important in the radioactive work to get a high luminosity of the apparatus in order to make possible the use of weaker sources. A great increase in intensity can be obtained by space focusing the beam. This can be done as shown by Hamilton, Lemonick and Pipkin[5]), if the conventional A and B dipole

and 1380; Phys. Rev. **105** (1957) 1928; Phys. Rev. **107** (1957) 189 and 723; H. A. Shugart and E. Lipworth, Reports at the Third Molecular Beam Conference at Brookhaven (November 1957).

[9]) J. C. Hubbs, R. Marrus, W. A. Nierenberg and J. L. Worcester, Bull. Am. Phys. Soc. **II, 2** (1957) 316; J. C. Hubbs and W. A. Nierenberg, Report at the Third Molecular Beam Conference at Brookhaven (November 1957).

[10]) D. A. Gilbert and V. W. Cohen, Phys. Rev. **97** (1955) 243; Phys. Rev. **98** (1955) 1194.

[11]) L. S. Goodman and S. Wexler, Phys. Rev. **99** (1955) 192; Phys. Rev. **100** (1955) 1245 and 1796; W. Childs and L. S. Goodman, Bull. Am. Phys. Soc. **II, 1** (1956) 342.

[12]) K. F. Smith, Report by C. S. Wu at the Glasgow Conference on Nuclear Physics, 1954 (Pergamon Press, 1955).

[13]) B. P. Nutter, Phil. Mag **1** (1956) 587.

[14]) G. K. Woodgate and R. W. Hellwarth, Proc. Phys. Soc. A **69** (1956) 581.

[15]) J. E. Sherwood, Report at the Third Molecular Beam Conference at Brookhaven (November 1957).

[16]) I. I. Rabi, J. R. Zacharias, S. Millman and P. Kusch, Phys. Rev. **53** (1938) 318.

[17]) I. I. Rabi, S. Millman, P. Kusch and J. R. Zacharias, Phys. Rev. **55** (1939) 526.

[18]) P. Kusch, S. Millman and I. I. Rabi, Phys. Rev. **57** (1940) 765.

magnets are replaced by six-pole magnets. The focusing properties of the six-pole field and the principal arrangement of a resonance apparatus with such fields will be described in section 4.

3. Calculation of Nuclear Moments from the Atomic Hyperfine Structure

A short review of the well-known theory of hfs will be given in this paragraph and a few formulas developed, which are convenient in calculating the nuclear moments from the resonance frequencies.

The interaction between the nuclear magnetic moment, the atomic field and an external magnetic field (**B**) can be written

$$\mathrm{H} = ha\,\mathbf{I}\cdot\mathbf{J} - \frac{\mu_J}{J}\,\mathbf{J}\cdot\mathbf{B} - \frac{\mu_I}{I}\,\mathbf{I}\cdot\mathbf{B}\,,$$

where **I** and **J** are the nuclear and electronic angular momentum vectors, μ_I and μ_J the corresponding magnetic moments and a the magnetic dipole interaction constant. At very weak external fields, **I** and **J** are tightly coupled to $\mathbf{F} = \mathbf{I} + \mathbf{J}$ and the energy becomes approximately

$$W_{F,m} = \frac{ha}{2}\,C - \\ - \frac{\mu_J}{J}\,\frac{F\,(F+1) - I\,(I+1) + J\,(J+1)}{2\,F\,(F+1)}\,mB - \\ - \frac{\mu_I}{I}\,\frac{F\,(F+1) + I\,(I+1) - J\,(J+1)}{2\,F\,(F+1)}\,mB\,, \quad (1)$$

where $C = F\,(F+1) - I\,(I+1) - J\,(J+1)$ and m is the magnetic quantum number for F. In this region the splitting between the levels is proportional to the field strength (the Zeeman region). It is seen from (1) that if J and μ_J are known, the nuclear spin can be obtained from the resonances at very weak fields (the term containing μ_I can be neglected).

In the special case of $J = 1/2$ the energy levels can be given an exact analytic form by the well-known Breit-Rabi formula,

$$W_{F,m} = -\frac{\Delta W}{2\,(2\,I+1)} - \frac{\mu_I}{I}\,B\,m \pm \\ \pm \frac{\Delta W}{2}\left[1 + \frac{4\,m}{2\,I+1}\,x + x^2\right]^{1/2}\,, \quad (2)$$

where $x = (-\mu_J/J + \mu_I/I)\,B/\Delta W$ and $\Delta W = ha\,(I + 1/2)$ is the energy difference between the states $F = I + 1/2$ and $F = I - 1/2$ at zero field. The upper sign in (2) is used for $F = I + 1/2$, (see fig. 1). The quantity $|\Delta W|/h = \Delta\nu$ is usually called the hfs separation. When the nuclear spin has been determined at weak fields, the hfs separation can be obtained at intermediate fields by means of (2).

With the conventional flop-in arrangement for $J = 1/2$, only one transition can be observed at low frequencies, since the two states involved should have strong field moments of opposite sign. This transition is $F = I + 1/2$, $m = \mp\,(I - 1/2) \longleftrightarrow m = \mp\,(I + 1/2)$, where the upper sign is valid if the nuclear magnetic moment is positive. In fig. 1 this transition is indicated with an arrow. The frequency for this particular transition is

$$\nu = \frac{\Delta\nu}{2}\left[\sqrt{1 - 2\,\frac{2\,I-1}{2\,I+1}\,|\,x\,| + x^2} - (1 - |\,x\,|)\right] \mp \\ \mp \frac{\mu_I}{hI}\,B\,,$$

where the upper sign is to be used if the electronic g-value, $g_J = -\mu_J/\mu_0 J$, is positive (μ_0 is the Bohr magneton).

For I and J greater than 1/2 there may also be an electric quadrupole interaction and omitting higher-order interaction the Hamiltonian can be written†

$$H = -\frac{\mu_J}{J}\,\mathbf{J}\cdot\mathbf{B} - \frac{\mu_I}{I}\,\mathbf{I}\cdot\mathbf{B} + ha\,\mathbf{I}\cdot\mathbf{J} + \\ + hb\,\frac{\frac{3}{2}\,\mathbf{I}\cdot\mathbf{J}\,(2\,\mathbf{I}\cdot\mathbf{J}+1) - I\,(I+1)\,J\,(J+1)}{2\,I\,(2\,I-1)\,J\,(2\,J-1)}\,, \quad (3)$$

where b is the electric quadrupole interaction constant. The energy levels are in this case most simply calculated by the perturbation method. The energy level diagram for an atom with $J = 3/2$ is shown in fig. 2.

In calculations of the energy levels at weak fields by the perturbation method, the first two terms of (3) are regarded as the perturbation.

† See, for example, N. F. Ramsey, Molecular Beams, Oxford University Press, London (1956) p. 272.

The first-order energy term then becomes identical with the last two terms of (1) and the second-order energy term†

$$W''_{F,m} = (g_J - g_I)^2 (\mu_0 B)^2 \times$$
$$\times \left[\frac{(F, m \mid J_z \mid F-1, m)^2}{W^0_F - W^0_{F-1}} - \frac{(F, m \mid J_z \mid F+1, m)^2}{W^0_{F+1} - W^0_F} \right], \quad (4)$$

and the separations become

$$\Delta\nu_F = \frac{1}{h} (W^0_F - W^0_{F-1}) = aF + \tfrac{3}{2} bF \times$$
$$\times \frac{F^2 - I(I+1) - J(J+1) + 1/2}{I(2I-1)J(2J-1)}. \quad (5)$$

The quadrupole interaction term of (5) is often of the same order of magnitude as the dipole term. Therefore, at least two zero-field separations must be determined in order to obtain the interaction constants. As can be seen from fig. 2, at least two transitions at different F values can for $J \geq 3/2$ be observed at low frequencies with a flop-in arrangement of the conventional type. These transitions are indicated with arrows in the figure. Generally the observable transitions for half-integral J take place between the m values $\mp (F - J - 1/2)$

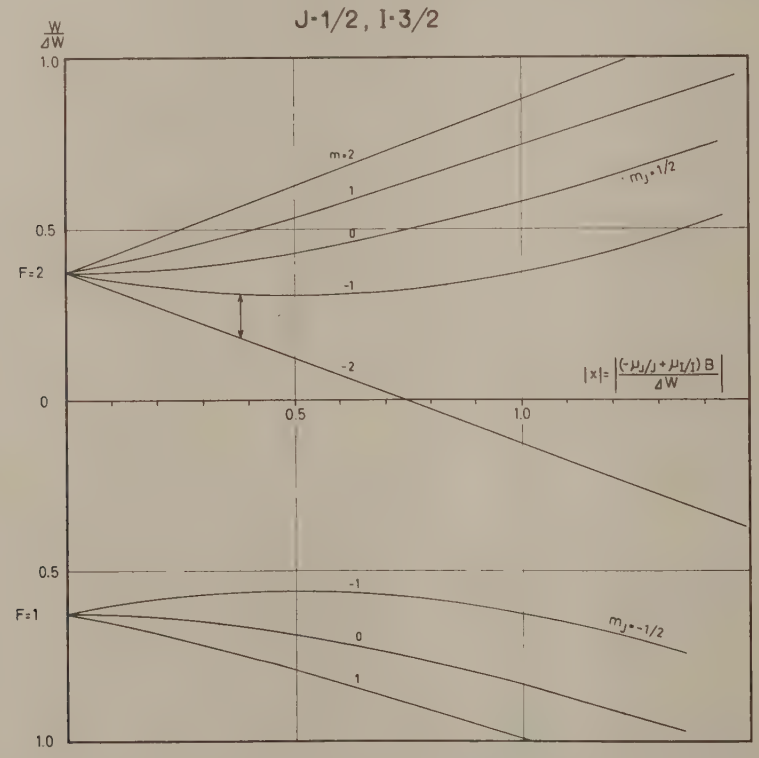

Fig. 1. The variation with the magnetic field of the energy levels of an atom with electronic angular momentum $J = 1/2$ and nuclear angular momentum $I = 3/2$. For negative nuclear magnetic moment the sign of m and m_J is reversed.

where $(F, m \mid J_z \mid F', m')$is the matrix element of J_z (the component of $\mathbf{J}$ in the field direction) in the F, m representation and W^0_F is the energy of the state F at zero field.

The energy levels at zero field are

$$W^0_F = \frac{1}{2} ha\, C + hb\, \frac{\frac{3}{4} C(C+1) - I(I+1)J(J+1)}{2I(2I-1)J(2J-1)}.$$

† See, for example, E. U. Condon and G. H. Shortley, Theory of Atomic Spectra, Cambridge University Press, Cambridge, England (1935).

and $\mp (F - J + 1/2)$, where the upper sign is valid if μ_I is positive.

The nuclear magnetic moment can be obtained from the dipole interaction constant a, if the atomic magnetic field at the nucleus is known.

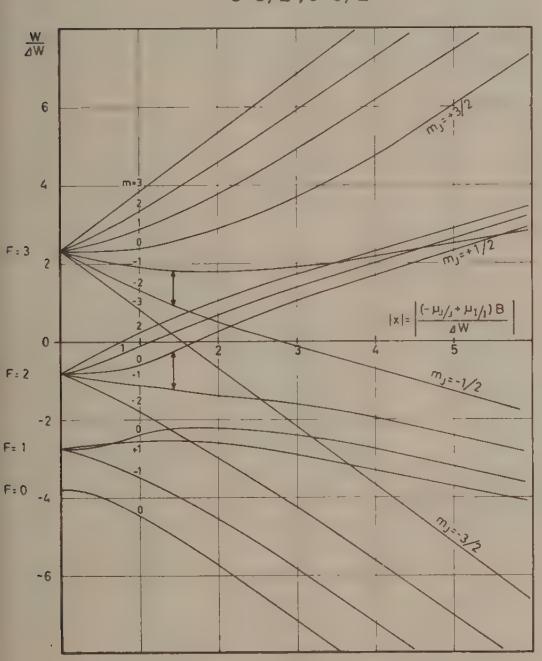

Fig. 2. The variation with the magnetic field of the energy levels of an atom with electronic angular momentum $J = 3/2$ and nuclear angular momentum $I = 3/2$, (from L. Davis, B. T. Feld, C. W. Zabel and J. R. Zacharias, Phys. Rev. **76** (1949) 1076). For negative nuclear magnetic moment the sign of m and m_J is reversed.

But this field can, in general, only be roughly estimated so that no accurate determination of the moment can be made in this way. If, however, the magnetic moment and the dipole interaction constant are known for a different isotope of the same element most of this uncertainty can be eliminated. If the nucleus is regarded as a point dipole the well-known Fermi-Segré formula gives

$$\frac{\mu_1}{\mu_2} = \frac{a_1 I_1}{a_2 I_2} .$$

The relation is valid if the hfs anomaly is neglected. This effect is usually less than one percent. In a similar way the electric quadrupole moment can be determined from the quadrupole interaction constant b. Most of the moments of radioactive nuclei are determined in this way by comparison with the stable isotopes.

4. Six-Pole Focusing. Principles of Operation

The possibility of focusing neutral particles by means of their magnetic moments in a magnetic multi-pole field was first pointed out by Friedburg and Paul[19]) and Korsunskii and Fogel[20]). The principles of this type of focusing will be given briefly here.

The force acting on a particle with the magnetic energy W is

$$F = -\operatorname{grad} W = \mu_{\text{eff}} \cdot \operatorname{grad} B , \qquad (6)$$

where $\mu_{\text{eff}} = -\mathrm{d}W/\mathrm{d}B$ is the effective magnetic moment.

In a magnetic $2n$-pole field the magnetic potential is in cylindrical coordinates (r, φ, z)

$$\Phi = \text{const.} \cdot r^n \cos n\varphi .$$

The field gradient is then

$$\operatorname{grad} B = \text{const.} \cdot r^{n-2} \hat{\mathbf{r}} ,$$

where $\hat{\mathbf{r}}$ is the unit vector in the direction of the

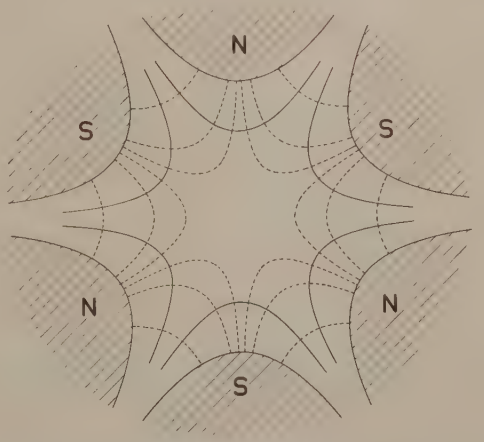

Fig. 3. The field- and potential lines in a six-pole field. The field lines are dashed.

[19]) H. Friedburg and W. Paul, Naturwiss. **38** (1951) 159.
[20]) M. I. Korsunskii and Ya. M. Fogel, J. Exp. Theor. Phys. (USSR) **21** (1951) 25 and 38.

radius. Therefore, the force is converging if μ_{eff} is negative and diverging if μ_{eff} is positive.

In a six-pole field ($n = 3$) the magnetic potential becomes $\Phi = \text{const.} \cdot r^3 \cos 3\varphi$, and the equipotential surfaces have the equation (see fig. 3)

$$r = \text{const.} \cdot (\cos 3\varphi)^{-1/3} .$$

The gradient and the force are then

$$\text{grad } B = \text{const.} \cdot r\hat{\mathbf{r}} \quad \text{and} \quad \mathbf{F} = \text{const.} \cdot \mu_{eff} r\hat{\mathbf{r}} .$$

is usually distributed over a wide range, which gives an appreciable "chromatic" aberration. In an atomic beam resonance apparatus, this difficulty can be partially overcome by using one converging and one diverging lens. This arrangement, which was introduced by Hamilton *et al.*[5,6]), has been used in our case, and the principles of operation of this type of apparatus are briefly the following.

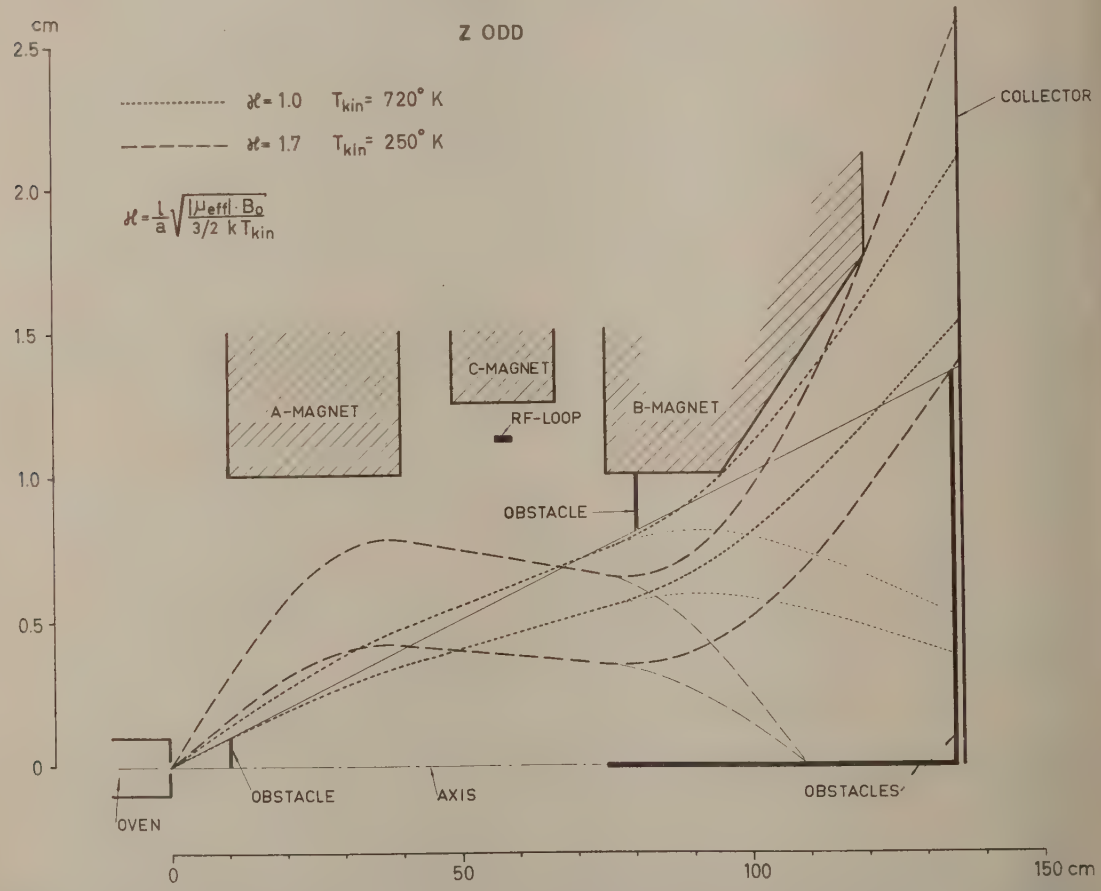

Fig. 4. Calculated beam trajectories for atoms with odd atomic number. The heavier curves represent atoms with different sign of the effective magnetic moment in the A and B field. The weaker lines represent atoms which have not undergone any transition in the C field.

The particles are elastically bound to the axis if $\mu_{eff} < 0$, and particles emitted from a point on the axis under small angles and with uniform velocity are actually focused to a point on the axis. In an atomic beam, however, the velocity

Fig. 4 shows the shape of the magnets, used in our case, and some beam trajectories for atoms with odd atomic number. It is supposed that the atoms have $\mu_{eff} < 0$ in the A magnet and are thus there deflected towards the axis.

If there is a transition in the C field to a state with $\mu_{eff} > 0$ at strong fields, the beam deverges in the B field. It is assumed that the magnitude of the effective moment is the same in the A and B fields. The transition occurs between $m_J = +1/2$ and $m_J = -1/2$, which, of course, is possible only for atoms with odd atomic number.

As can be seen in fig. 4, there are three obstacles with the edges on a conical surface with atoms that have undergone a transition from negative to positive strong field moment can reach the detector. All other atoms are stopped at the obstacles or at the walls of the apparatus. It is assumed here, that the oven hole is point sized and that the scattering in the apparatus can be neglected.

Since the intensity at the detector has a maximum at resonance, this arrangement is of

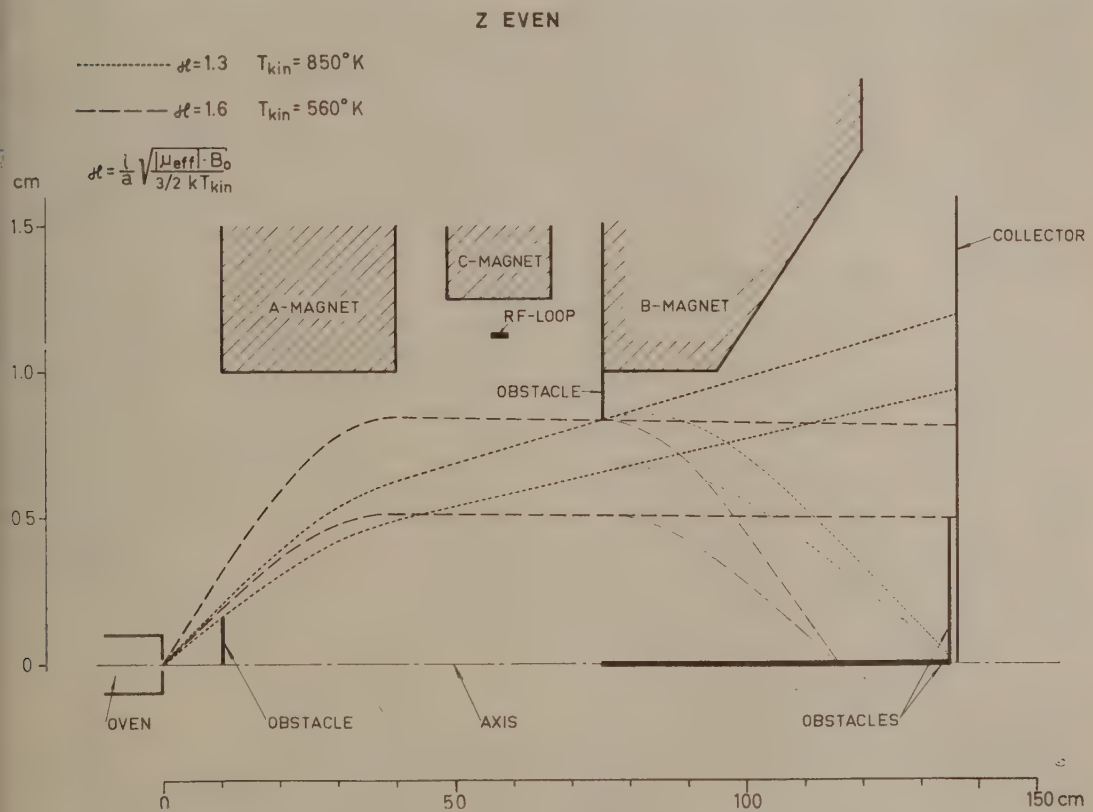

Fig. 5. Calculated beam trajectories for atoms with even atomic number. The heavier curves represent atoms with negative effective moment in the A field and zero moment in the B field.

the top at the oven hole. The first obstacle is a small disk on the axis at the entrance of the A magnet, the second one is ring-shaped and placed near the entrance of the B magnet and the third is a disk placed in front of the detector. There is also an obstacle along the axis of the B magnet, in order to prevent atoms from crossing the axis. It is easily realized that only those the flop-in type. In the flop-in arrangement in a conventional apparatus of the Rabi type, the atoms are focused on the axis at resonance. This is not possible in a six-pole apparatus, since here the gradient is always directed outwards. One difficulty with this arrangement is that the intensity is spread over a rather large area. But in the work with radioactive isotopes, where the

deposition technique is used, the large detector is not so disadvantageous.

The arrangement described above is, as mentioned, only applicable to elements with odd atomic number. For elements with even atomic number it is possible to utilize transitions between $m_J = \pm 1$ and $m_J = 0$ in a flop-in experiment. Such an arrangement is shown in fig. 5. There it is assumed that $\mu_{eff} < 0$ in the A field and $\mu_{eff} = 0$ in the B field. The atoms are then focused in the A field but not affected by the B field. The atoms that do not undergo any transition are focused also in the B field. The obstacles are in this case arranged in such a way that atoms touching the first two obstacles and not undergoing any transition are also touching the edge of the third obstacle.

5. Calculation of Intensity. Principles of Design

The luminosity (solid angle) of the apparatus is calculated in the following way. The beam trajectories are calculated for different velocities (v) and emission angles (α), (see fig. 4 and 5). The solid angle for which the atoms reach the detector at resonance is determined for different values of v and integrated over the velocity distribution of the beam, giving an "effective" solid angle. The intensity is then the same as in a hypothetical piece of apparatus with a monochromatic beam and a useful angle equal to the effective solid angle.

The trajectories can easily be calculated if the six-pole magnets have cylindrical pole faces (i.e. if the cross section is independent of z), in which case the trajectories are trigonometric or hyperbolic curves.

If the field strength at the pole tops, lying on a circular cylinder with radius a, is B_0, then the field strength at a distance r from the axis is $B = (B_0/a^2)r^2$. The gradient is then grad $B = (2\,B_0/a^2)r\hat{\mathbf{r}}$, and the force acting on the atoms, from (6),

$$\mathbf{F} = \frac{2\,\mu_{\text{eff}} \cdot B_0}{a^2} r\hat{\mathbf{r}} .$$

If the atoms travel near the axis, the velocity in the z direction is approximately equal to the total velocity v. Then the equation of motion becomes

$$\frac{\mathrm{d}^2 r}{\mathrm{d}z^2} - \frac{2\,\mu_{\text{eff}} \cdot B_0}{m\,v^2\,a^2}\, r = 0 ,$$

where m is the mass of the atoms. If the dimensionless variables $\rho = r/a$ and $\zeta = z/l$, where l is a unit length, are substituted and the parameter

$$\varkappa = \frac{l}{a}\sqrt{\frac{|\,\mu_{\text{eff}}\,|\,B_0}{m\,v^2/2}} \tag{7}$$

is introduced, the equation becomes

$$\frac{\mathrm{d}^2\rho}{\mathrm{d}\zeta^2} \mp \varkappa^2\rho = 0, \qquad \begin{matrix} -\text{ if } \mu_{\text{eff}} > 0 \\ +\text{ if } \mu_{\text{eff}} < 0 \end{matrix} .$$

The trajectories are trigonometric curves if $\mu_{eff} < 0$ and hyperbolic curves if $\mu_{eff} > 0$. It is here assumed that the effective magnetic moment is constant, i.e. the fields are strong enough to decouple **I** and **J** completely. The shape of the trajectories is independent of the emission angle α, as long as the latter is small, and only dependent on the parameter $\varkappa$.

If the magnets are "shaped", so that the pole faces are no longer cylindrical, the calculation of the trajectories is more complicated. In order to give a good six-pole field the pole faces should be equipotential surfaces. In practice, however, the iron is saturated so that the field strength is approximately constant at the surface. If the equation of the pole tops is $\rho_0 = R(\zeta)$, the equation of motion becomes

$$\frac{\mathrm{d}^2\rho}{\mathrm{d}\zeta^2} \mp \frac{\varkappa^2}{R\,(\zeta)^2}\,\rho = 0 .$$

If $R(\zeta)$ is a linear function, the solution can be given an exact analytic expression. For $R(\zeta) = (1 + k\zeta)$ the solution has the form

$$\rho = (1 + k\zeta)^n, \qquad n = \frac{1}{2}\,(1 \pm \sqrt{1 \pm 4\,\varkappa^2/k^2}) .$$

Fig. 4 shows the beam trajectories for two different values of $\varkappa$ in the arrangement for odd atomic numbers. The trajectories are given for the smallest and the largest emission angles for which the atoms reach the detector at resonance. The useful solid angle Ω is given in fig. 6 as a function of $\varkappa$. The unit length l has arbitrarily been taken to be the distance from the oven to the exit of the A magnet. The $\varkappa$ value corresponds

to a kinetic temperature, T_{kin}, defined by $\frac{1}{2} mv^2 = \frac{3}{2} kT_{kin}$.

The solid angle is then integrated over the velocity distribution of the beam. In an atomic beam, produced in an oven with a Maxwellian distribution, the velocity distribution is

$$\frac{dN}{N} = 2 \left(\frac{v}{v_0}\right)^3 e^{-(v/v_0)^2} d\left(\frac{v}{v_0}\right) = \\ = 2 \left(\frac{\varkappa_0}{\varkappa}\right)^5 e^{-(\varkappa_0/\varkappa)^2} d\left(\frac{\varkappa}{\varkappa_0}\right),$$

where $v_0 = (2\,kT/m)^{1/2}$ is the most probable velocity in the oven and $\varkappa_0$ is the corresponding $\varkappa$ value,

$$\varkappa_0 = \frac{l}{a} \sqrt{\frac{|\,\mu_{eff}\,|\,B_0}{m\,v_0^2/2}} = \frac{l}{a} \sqrt{\frac{|\,\mu_{eff}\,|\,B_0}{kT}} . \qquad (8)$$

T is the oven temperature.

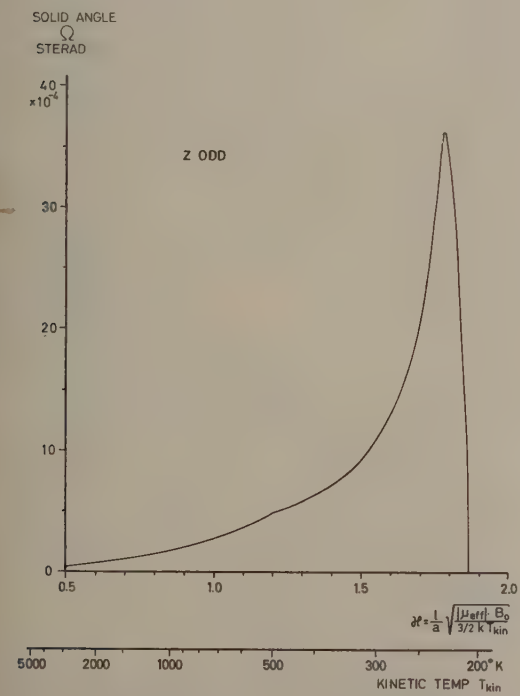

Fig. 6. The useful solid angle versus the parameter $\varkappa$ for odd atomic number. The scale of the kinetic temperature is valid for $|\,\mu_{eff}\,| = 1$ Bohr magneton and $B = 1$ Wb/m².

The integrated or effective solid angle is, besides the geometry of the apparatus, only dependent on the parameter $\varkappa_0$. If the effective solid angle is denoted by Ω_{eff} and the corresponding solid angle in the dimensionless $\rho\zeta$ space by ω_{eff}, the following relation is obtained

$$\Omega_{eff} = \left(\frac{a}{l}\right)^2 \omega_{eff}\,(\varkappa_0) = \frac{\omega_{eff}\,(\varkappa_0)}{\varkappa_0^2} \cdot \frac{|\,\mu_{eff}\,|\,B_0}{kT} . \qquad (9)$$

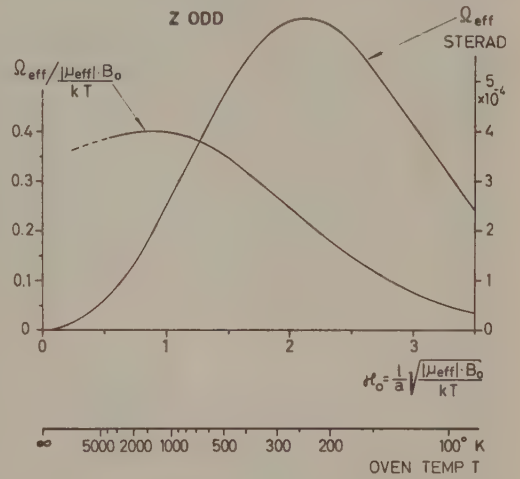

Fig. 7. The effective solid angle (Ω_{eff}), integrated over the velocity distribution, and the quantity $\Omega_{eff} \Big/ \frac{|\,\mu_{eff}\,|\,B_0}{kT}$ versus the parameter $\varkappa_0$ for odd atomic number. The temperature scale is valid for $|\,\mu_{eff}\,| = 1$ Bohr magneton and $B = 1$ Wb/m².

From (9) it can be seen that, in looking for the optimum geometry of the apparatus, one should maximize the quantity

$$\frac{\omega_{eff}}{\varkappa_0^2} = \Omega_{eff} \Big/ \frac{|\,\mu_{eff}\,|\,B_0}{kT}$$

for the conditions of operation that occur most frequently. Then, to find the best conditions of operation for a given apparatus one should maximize ω_{eff} (or Ω_{eff}).

The effective solid angle Ω_{eff} and the quantity

$$\Omega_{eff} \Big/ \frac{|\,\mu_{eff}\,|\,B_0}{kT}$$

are given in fig. 7 as functions of the parameter $\varkappa_0$. The latter function has a flat maximum of about 0.40 for $\varkappa_0 \approx 1$. The ratio l/a has been determined so that this $\varkappa_0$ value corresponds to a suitable value of $|\,\mu_{eff}\,|\,B_0/kT$; $l/a = 40$ and $B_0 = 1$ Wb/m², $|\,\mu_{eff}\,| = 1$ Bohr magneton and

$T = 1000°$ K gives $\varkappa_0 \approx 1.03$ and the effective solid angle

$$\Omega_{\text{eff}} \approx 2.7 \times 10^{-4} \text{ steradians} .$$

It is usually not possible to get a high field strength enough to reach the maximum of the Ω_{eff} curve. Therefore the field strength should be as high as possible, and near the maximum of

$$\Omega_{\text{eff}} \Big/ \frac{|\mu_{\text{eff}}| B_0}{kT}$$

the intensity varies as $|\mu_{eff}| B_0/kT$.

Fig. 5 shows some beam trajectories in the arrangement for even atomic numbers. The useful solid angle (Ω) varies with the parameter

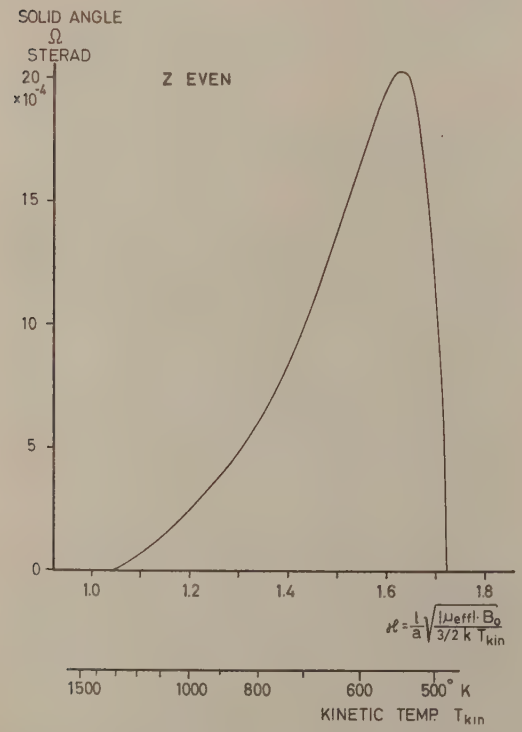

Fig. 8. The useful solid angle versus the parameter $\varkappa$ for even atomic number. The scale of the kinetic temperature is valid for $|\mu_{eff}| = 2$ Bohr magnetons in the A field and $B = 1$ Wb/m².

$\varkappa$ in this case as shown in fig. 8. The effective solid angle Ω_{eff} and

$$\Omega_{\text{eff}} \Big/ \frac{|\mu_{\text{eff}}| B_0}{kT}$$

are given in fig. 9. For $|\mu_{eff}| = 2$ Bohr magnetons in the A field, $B_0 = 1$ Wb/m² and $T = 1000°$ K the effective solid angle is about 2.7×10^{-4} steradians, or just about the same as in the previous case.

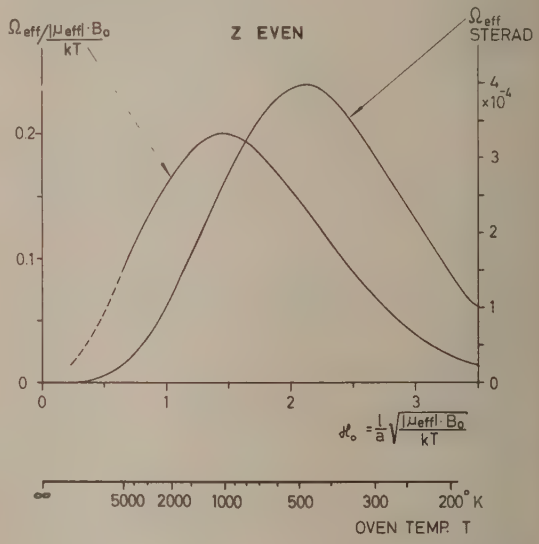

Fig. 9. The effective solid angle (Ω_{eff}) and $\Omega_{\text{eff}} \Big/ \frac{|\mu_{\text{eff}}| B_0}{kT}$ versus the parameter $\varkappa_0$ for even atomic number. The temperature scale is valid for $|\mu_{eff}| = 2$ Bohr magnetons in the A field and $B = 1$ Wb/m².

6. Experimental Arrangement

Fig. 10 is a photograph of the atomic beam apparatus and fig. 11 shows a schematic cross-section.

6.1. THE VACUUM SYSTEM

In contrast to almost all atomic beam set-ups now in use this apparatus has the magnets outside the vacuum chamber and the beam passes through the magnets in a narrow tube. The vacuum chamber, which is mainly of brass, consists of three sections, an oven section, a main section, and a separating section. The main section is divided into two parts, one at each side of the magnets. The separating section is used for reducing the leakage into the main chamber from the poorer vacuum in the oven chamber. The tube through the magnets, which has a smallest diameter of 2 cm and a length of

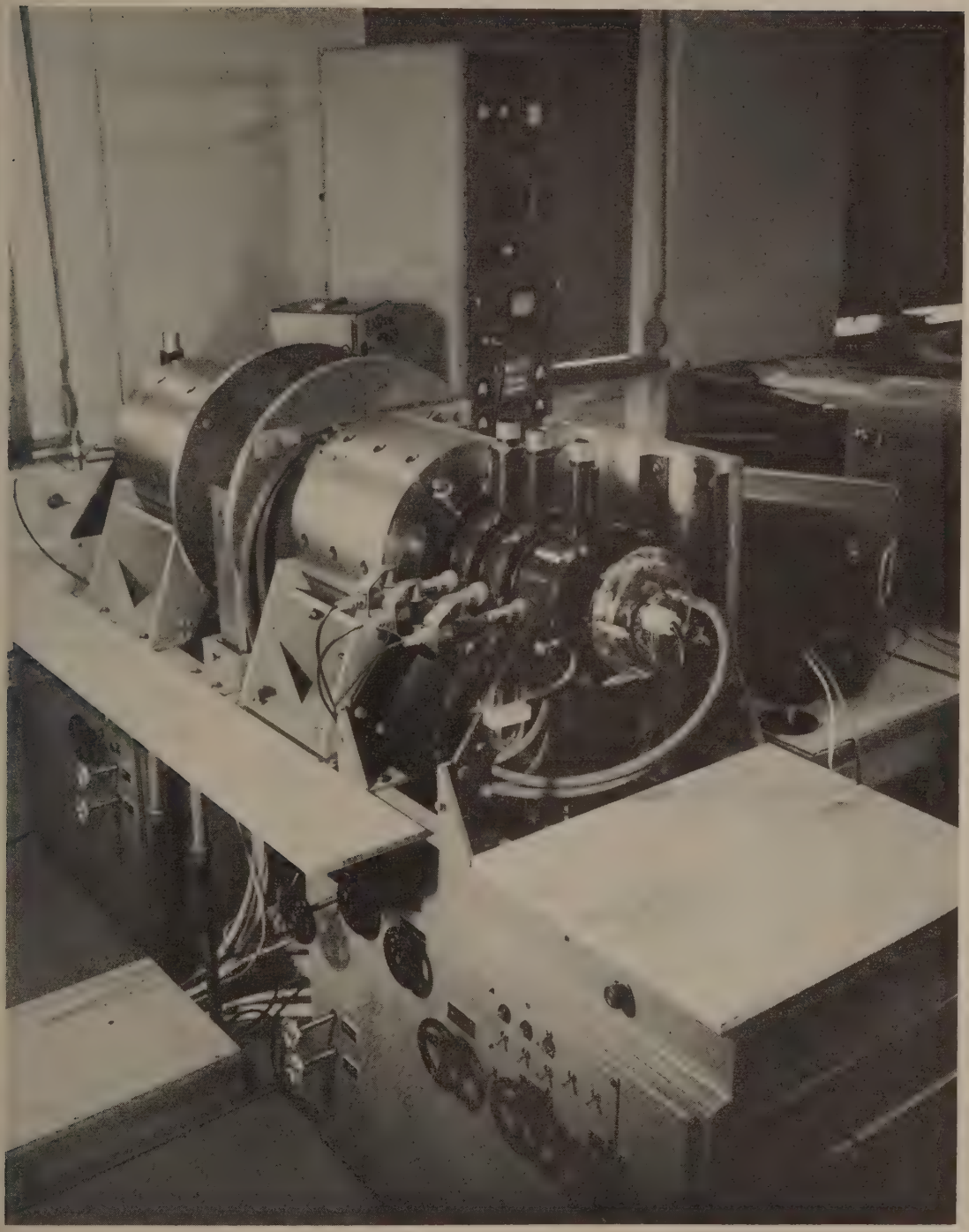

Fig. 10. A photograph of the atomic beam apparatus.

120 cm, is made of copper, except for the part through the C magnet which is made of glass. With this arrangement also the rf-loop can be

muth is made of molybdenum, is cylindrical with a diameter of about 10 mm. The beam comes out of the oven through a long channel

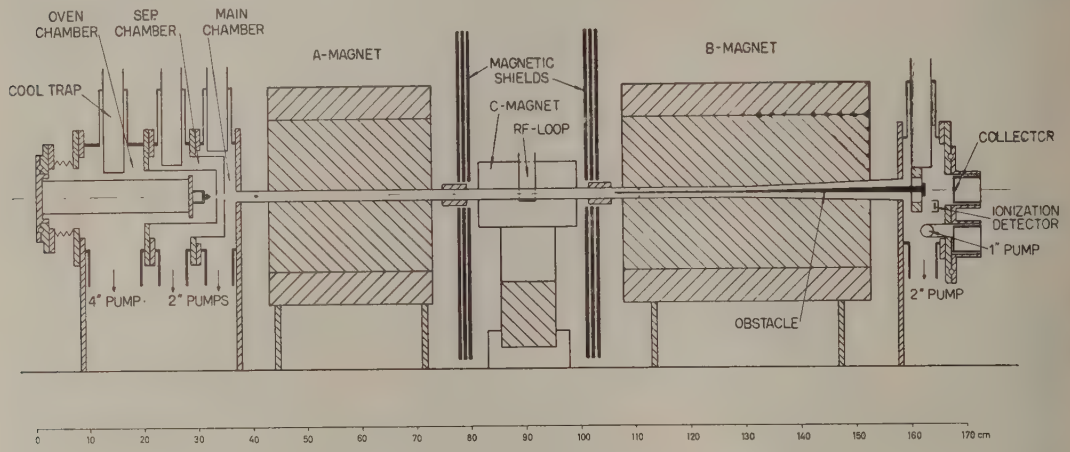

Fig. 11. Schematic cross-section of the apparatus.

placed outside the tube. The connections between the copper and glass tubes are made with simple "O"-ring seals.

The oven chamber is evacuated with a 4″ oil diffusion pump, the separating chamber with a 2″ pump and the main chamber with two 2″ pumps.

The pressure is measured with a cold cathode ionization gauge of the Penning type, operating at 2000 volts. The vacuum obtained in the main chamber is better than 5×10^{-7} mm Hg with liquid air in the cool traps. In the separating and oven chambers the vacuum is, when the oven is in use, of the order of 10^{-6} and 10^{-5} mm Hg, respectively. The vacuum is good enough for the beam to traverse the whole apparatus without any observable loss in intensity.

6.2. THE OVENS

The oven chamber contains two ovens, the main oven for the radioactive substance and the calibration oven (fig. 12). The calibration oven is used for determination of the field strength in the C field with the aid of a known substance, usually ordinary potassium.

The main oven, which in the work with bis-

about 8 mm long and 0.5 mm wide. The use of a long channel conserves the radio-active material, since the intensity at large emission angles is reduced. The oven is supported by a molybdenum ring with three edges, which is fixed with

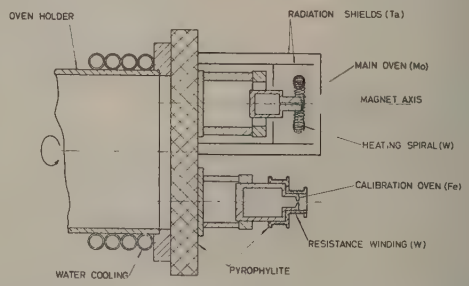

Fig. 12. The oven arrangement. The ovens are exchanged by rotating the oven holder around its horisontal axis.

three molybdenum rods at an insulating plate of pyrophylite. The heat conduction from the oven to the water-cooled oven holder is then relatively small.

The main oven is heated by radiation and electron bombardment from a wolfram spiral in front of the oven. This arrangement gives a higher temperature to the front of the oven and prevents the channel from clustering. Around

the oven there is a double radiation shield of tantalum.

The temperature of the main oven is measured with a Pt- PtRh thermo-couple in the back of the oven. The temperature can be stabilized with a temperature regulator, which switches the high voltage on and off. The emission current needed for a temperature of 1000° C is of the order of 50–100 mA at 500 volts.

The calibration oven is made of iron and heated by a resistance winding of wolfram around the oven. Both ovens are fixed at a plate of baked pyrophylite. By rotating the oven holder around its horizontal axis the two ovens can easily be exchanged.

6.3. THE SIX-POLE MAGNETS

Fig. 13 shows a section of the six-pole magnets and the pole tops. The material in the magnets is a very pure iron, REMA†. The pole tops are lying on a circular cylinder with a radius of 1 cm, except in the second half of the B magnet, where the tops lie on a conical surface with a radius of 1.75 cm at the exit of the B magnet. The length of the A and B magnets is 30 and 45 cm, respectively, and the outer diameter is 40 cm.

Three of the poles in each magnet are wound with twenty turnes of copper tubes and the coils are all in series. The magnets can be excited with a current of 500 amps at 75 volts from a motor-generator. However, the magnets are almost saturated at 300 amps. The maximum field strength at the pole tops has been calculated to be about 10 000 gauss††. The windings are cooled with distilled water, pressed through the tubes by a pump at a pressure of 10 atm and cooled in a heat exchanger. For the water-cooling the windings are divided into twelve parallel coils.

Without stabilization the drift of the current in the six-pole magnets often cause a drift of the C-field during a run corresponding to 10–20 kc/s in the K^{39}-line. This drift is not troublesome for spin determinations, but for accurate moment measurements the six-pole current had to be stabilized. The stabilization is made by means of

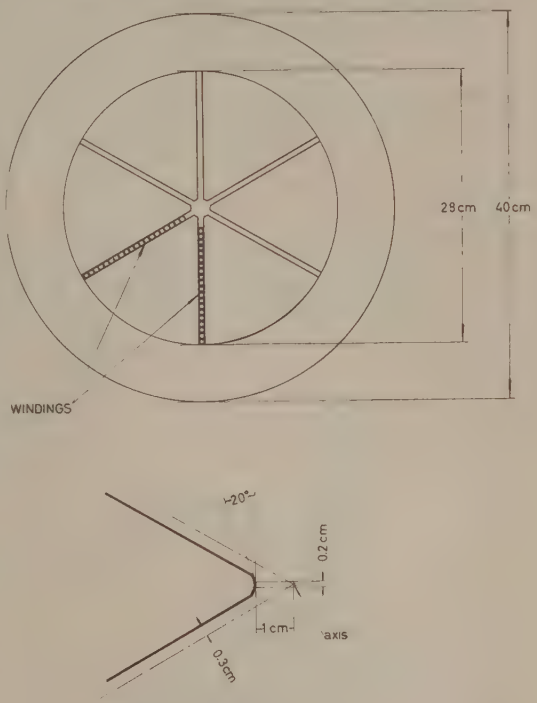

Fig. 13. Schematic cross-section of the six-pole magnets and of the pole tops.

an electronic feed-back system which directly regulates the current in the field windings of the main generator.

6.4. THE C FIELD AND THE RADIO-FREQUENCY SYSTEM

The C magnet is also made of REMA iron and is of conventional design with a single yoke. The pole pieces are 18 × 12 cm and the air gap 2.5 cm. The rf-loop is, as mentioned before, applied outside a glass tube, and consists of a single turn of copper sheet. The optimum length of the loop seems to be about 1.5 cm, and the line width obtained with this loop is about 35 kc/s, which is close to the theoretical value.

The rf power is supplied from two Marconi generators. For low frequencies (up to 12 Mc/s) a video oscillator, type TF 885 A/1, is used, which has an output of 30 volts (convenient for

† Delivered by Fagersta Bruk, Fagersta, Sweden.

†† These calculations were kindly performed by Dr. Dreyfus, ASEA.

producing multiple quantum transitions). For high frequencies a singal generator, type TF 801 B/1, is used, which has about 3 volts output from 12 to 470 Mc/s. The loop is tuned by two condensors at high frequencies. The frequency is measured with a Schomandl frequency meter, type FD 1, which has an accuracy of 1 part in 10^6.

6.5. THE DETECTOR

The calibration material is detected by means of a conventional surface ionization detector of wolfram. The ion current is measured with a direct current amplifier with a sensitivity of 10^{-13} amps†.

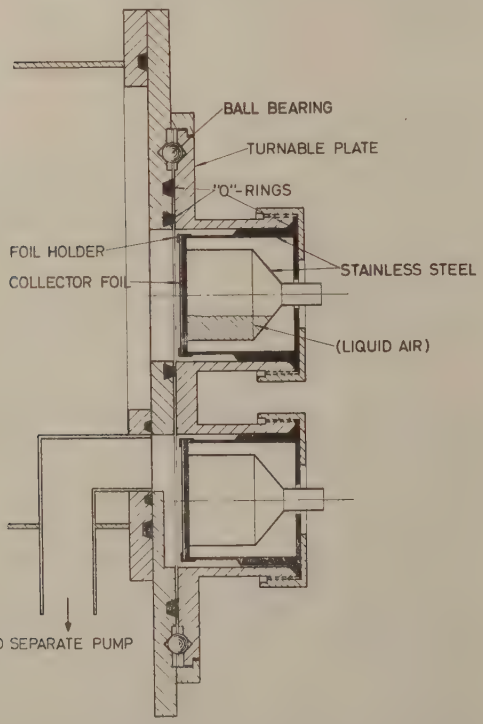

Fig. 14. The collector arrangement. The collectors are exchanged by rotating the plate.

As mentioned before, the radioactive beam is deposited on a collector, which is removed from the apparatus and measured in a counter. The collector consists of a metal foil with carbon deposited on the surface by means of a paraffin-oil flame. In the work with bismuth this surface has turned out to be very efficient and has a higher sticking coefficient than a clean metal surface, even if the latter is cooled with liquid air. It is also easy to get the deposit reproducible.

Fig. 14 shows the collector arrangement in detail. While one of the collectors is being exposed, the other can be taken out and counted and be replaced by a new one. The very small volume containing the second collector is evacuated by a separate 1″ diffusion pump. When the exposure of the first collector is finished sufficiently good vacuum has been obtained so that the collector holder can be turned round and a new exposure take place immediately.

The collectors are counted in a well shielded counter with a scintillation crystal or a GM tube. For the investigation of neutron-deficient bismuth isotopes a thin crystal has been used for detection of the X-rays. The pulses are selected by a conventional single-channel pulse height analyzer.

Since the collectors are rather large, about 5 cm in diameter, the collector foils are folded in order to allow the use of a smaller crystal. This procedure can be used without any loss in reproducibility.

6.6. MEASUREMENTS

Typical resonance curves are given in fig. 15, which shows the $\Delta F = \pm 1$ transitions for K^{39} at a very weak field. The transitions $m = \pm 1 \leftrightarrow m = 0$ have a line width of about 35 kc/s, which is quite close to the theoretical value for a loop length of 1.5 cm. The double line in the middle is the field-independent line $m = 0 \leftrightarrow m = 0$. The rf loop is arranged to produce the oscillatory field mainly perpendicular to the static field, which would induce π-transitions ($\Delta m = \pm 1$). However, the stray fields at the ends of the loop are strong enough to induce σ-transitions ($\Delta m = 0$). The line shape is in agreement with calculations by Woodgate and

† The amplifier has been designed by Dr. C. Reuterswärd at this Institute (Ark. f. Fysik **10** (1956) 501).

Hellwarth[21]). The upper curves of fig. 15 represent the field-independent line at two different field strengths. The half-width of the whole line is about 20 kc/s. This line is narrower than the π-lines, because it is field-independent and consequently not broadened by inhomogeneities. The minimum between the two peaks directly gives the hfs separation (with a small correction for the quadratic effect), which has been determined to be

$$\Delta\nu = 461.720 \pm 0.001 \text{ Mc/s} .$$

This result is in good agreement with recent measurements[22]).

The apparatus has also been used to measure the spins of four bismuth isotopes[23]), which will be reported in more detail elsewhere[24]). A typical

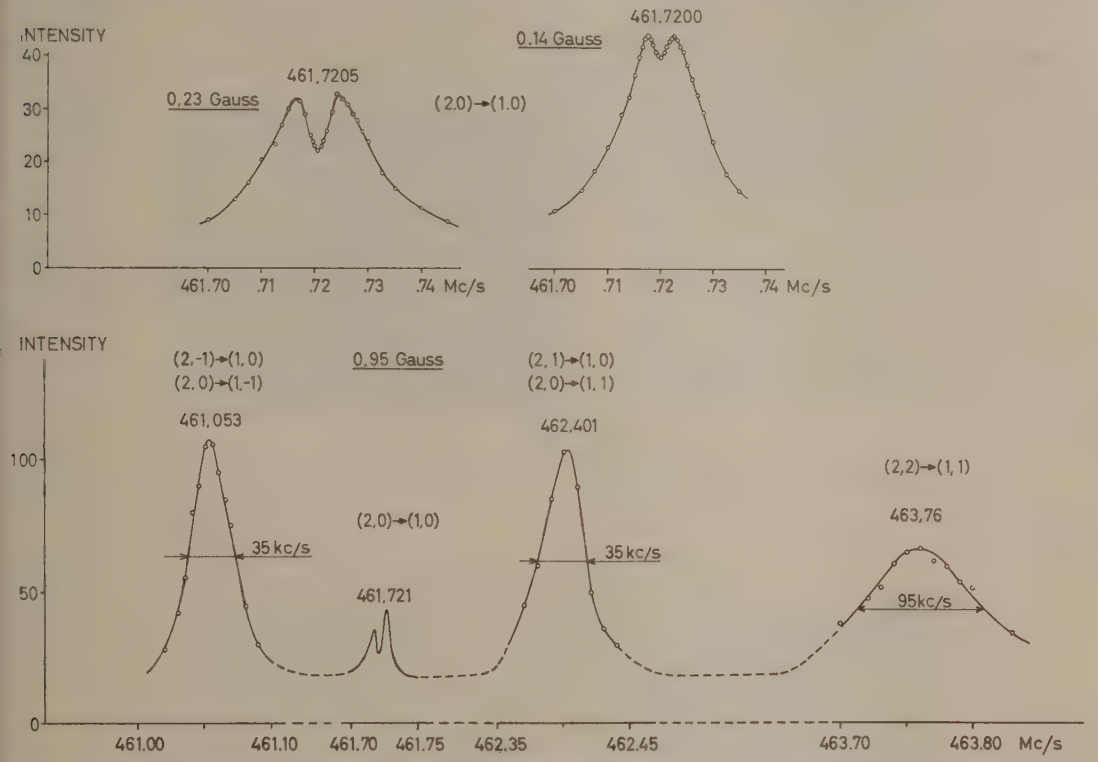

Fig. 15. $\Delta F = \pm 1$ transitions of K^{39} at a very weak field. The two upper curves represent the field-independent line $m = 0 \rightarrow m = 0$ at two different fields.

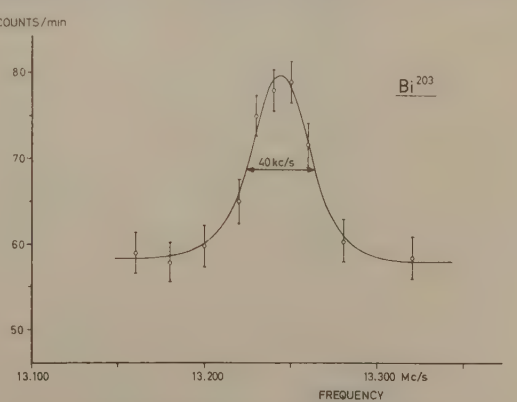

Fig. 16. A typical resonance curve of radioactive bismuth.

[21]) G. K. Woodgate and R. W. Hellwarth, Proc. Phys. Soc. A 69 (1956) 588.

[22]) G. Gould, Report at the Second Molecular Beam Conference at Brookhaven (October 1956).

[23]) I. Lindgren and M. Johansson, Report at the Third Molecular Beam Conference at Brookhaven (November 1957).

[24]) M. Johansson and I. Lindgren, being published in "Nuclear Physics".

resonance curve is shown in fig. 16. These measurements are now being continued in order to determine the hfs interaction constants and the magnetic moments.

7. Acknowledgements

The author wishes to express his gratitude to Professor Kai Siegbahn for initiating this project and for his interest throughout the work. He is also much indebted to Professor W. Paul, Bonn, whose laboratory he visited for two months, to Ingenjör L. Eriksson for his valuable help with the mechanical design, to Fil. kand. C. M. Johansson for his assistance at the final stages of construction, and to Fil. lic. Evelyn Sokolowski for correcting the English.

This work has been supported by the Swedish Atomic Committée and U.S. Air Force Research and Development Command.

NEW ANTON PROCESSES AND TECHNIQUES IMPROVE NEUTRON DETECTOR RELIABILITY, RUGGEDNESS AND HIGH TEMPERATURE CHARACTERISTICS

Basic development work for the military and AEC plus years of continuous production of BF_3 Proportional Counters and Compensated Ionization Chambers result in the widest variety of commercially available detectors from Anton.

- Rugged, unitized electrode structure enables the chamber to operate in any position, withstand shock and vibration conditions present during propulsion reactor operation.
- All-ceramic insulation to permit high temperature operation impossible to achieve with conventional plastic insulators.
- Magnesium-Aluminum alloy electrodes contained in an all-welded aluminum envelope.
- Electrically compensated...guard ring design.
- Flake-proof B^{10} coated electrodes.
- Longer life and greater electrical stability assured by advanced mechanical design that permits evacuation and processing at high temperatures.

Operational Data

1. Operating thermal neutron flux range:
   2.5×10^2 to 2.5×10^{10} neutrons/cm²/sec.
2. Thermal neutron sensitivity:
   4×10^{-14} amps/unit neutron flux
3. Gamma sensitivity:
   3×10^{-11} amps/R/hour
4. HN connectors in circular array for easy connection to commercially available HN type cable fittings. Mate with Amphenol 82-38 (MIL-UG 59 A/U or equal)
5. Overall dimensions:
   3-1/8 ± 1/16" dia. x 23-3/4 ± 1/4" long
6. Sensitive length:
   14-1/16" approximate

A wide range of improved neutron proportional counters is available with a variety of all-welded cathode materials (stainless steel, aluminum). In addition to standard catalog items, sizes can be supplied ranging from ¼" dia. x 1" long to 2" dia. x 30" long. Minimum wall thickness for Al is 0.010"; stainless steel minimum is 0.002". Connectors can be supplied per your specification.

High temperature operation of Anton neutron detectors is made possible by the use of thermally matched seal components . . . high temperature ceramic insulators . . . unique processing and seasoning . . . restriction to high temperature organic moderators where needed.

Multi-element, high sensitivity counters encased in super Dylan moderators can be supplied from production to provide thermal and intermediate neutron sensitivity up to 45 counts/neutron/cm².

Fills and pressures are available up to 2 atmospheres. A closely supervised gas purification system allows versatile application of spectroscopically pure normal (18% B^{10}), depleted (10% B^{10}) or enriched (96% B^{10}) Boron Trifluoride fills. Special zone temperature controlled muffle furnaces provide the most uniform method of Boron coating available to date.

Uniform, stable characteristics are assured from tube to tube. High temperature, high vacuum outgassing techniques are used for all components. The metal to ceramic seals are permanently fused and the exhaust tip is concealed. All parts are processed by patented methods to make them extremely resistant to the corrosive effects of BF_3. The insulators are precision molded, mechanically rugged and chemically inert.

Ruggedness and non-microphonism are assured by the incorporation of an Anton developed "no-spring" anode suspension (Pat. Pend.). This maintains the wire taut even when the tube is subjected to the severe impact shock and vibration experienced by equipment used for propulsion reactor control and monitoring, geological survey, oil well logging and similar applications.

Prompt delivery may be expected! Anton Laboratories maintains modern tube filling stations and a complete chemical laboratory for the production of neutron detectors and specialized fills. These plus Anton's machine shop and tube processing facilities assure early delivery of stock and special neutron detectors.

Send for FREE DATA about compensated chambers as well as other neutron counting devices. Investigate Anton's new, low-cost neutron counter price schedule. Write DEPT. NTN.

ANTON ELECTRONIC LABORATORIES, INC.

A subsidiary of United States Hoffman Machinery Corporation

1226 FLUSHING AVE., BROOKLYN 37, N. Y.

Brown, Boveri & Co., Ltd., Baden (Switzerland)

Representatives in most countries

NUCLEAR INSTRUMENTS 3 (1958) 17–24; NORTH-HOLLAND PUBLISHING CO. – AMSTERDAM

STATISTICAL SPREAD IN PULSE SIZE OF THE SCINTILLATION SPECTROMETER

A. BISI and L. ZAPPA

Istituto di Fisica Sperimentale del Politecnico, Milano

Received 15 February 1958

The results of an experimental investigation concerning the statistical spread of the pulse sizes of the scintillation spectrometer are reported. It was found that for γ-ray energies lower than 800 keV the measured half-width η of the lines fit strictly the relation $\eta^2 = \alpha + \beta/E$ where the two constants α and β vary slightly from one spectrometer to another. At higher energies the half-widths appear to be considerably smaller than predicted from the previous relation. That is due to the fact that at the high energies the γ-rays are absorbed in the phosphor not only by photoelectric effect, but any combination of processes by which the γ-ray is completely absorbed, can happen. All the experimental results are compared with statistical predictions.

1. Introduction

It is well known that the scintillation spectrometer has acquired importance in recent years as a powerful tool in nuclear spectroscopy investigations. The greater part of the information on the disintegration schemes accumulated until now, was obtained with the help of scintillation spectrometry. A comparison of the scintillation method for the detection of γ-rays with the crystal diffraction method and with the external conversion magnetic spectrometry, gives a picture of the advantages and disadvantages of each. In particular the scintillation spectrometer is characterized by a high detection efficiency and a low energy resolution. Although the detection efficiency has been extensively studied, comparatively little information on the energy resolution exist, and, moreover, as pointed out by Breitenberger[1]), even those known data do not lend themselves to comparison with theoretical predictions.

We are reporting here the results of our experimental investigation concerning the statistical spread of the pulse sizes of the scintillation spectrometer, preceded by a brief summary of the arguments underlying the pulse formation in a scintillation spectrometer. The reader is referred to the exhaustive paper of Breitenberger[1]) for theoretical treatment and nomenclature.

The spectrometer was in most cases assembled in its most current version, i.e. NaI (Tl) crystal ($1\frac{1}{2}''$ diameter, $1''$ thick) optically coupled with a phototube (photocathode diameter $1\frac{1}{2}''$). The response of several scintillators and photomultipliers was investigated as a function of the γ-ray energy.

2. Instrumental Line

The energy resolution of the γ scintillation spectrometer is affected by various factors which can be clarified by considering the formation of a pulse.

The pulse starts with the loss of energy to the scintillator by photoelectrons or Compton recoil electrons. Only a part of the energy lost is stored in the fluorescence centers and then converted into light quanta. A fraction of the emitted quanta escapes from the phosphor into the light guide, the remainder being self-absorbed in the phosphor. Some quanta are then lost by absorption and reflection in the light guide and only a part (a fraction f) reaches the photocathode; a few of these give rise to photoelectrons (a fraction p). Furthermore, some photoelectrons are lost in the region between the photocathode and the first dynode, the remainder (a fraction c) initiates the secondary avalanches from which originate the observed output pulse.

[1]) E. Breitenberger, Progress in Nuclear Physics 4 (1955) 56.

The above process, covering the interval up to the arrival of photoelectrons to the first dynode, is called "photon transfer"; it takes place with a transfer efficiency $T = e\,f\,p\,c$. It must be pointed out that every stage of the photon transfer and the production of the secondary avalanche, are governed by a law of chance. Consequently the output pulse sizes are statistically spread around their average value to give the so-called "instrumental line".

A closer examination of the phenomenon reveals that the four stage factors (e, f, p, c) are not instrumental constants of a given scintillation spectrometer, and that they are mutually interdependent. There are connections between e, f, p, c, as a consequence of the varying region of photon emission, of the varying spatial and chromatic distribution of light quanta and of the photocathode inhomogeneities. For that reason one is obliged to consider only the whole factor T and not the stage factors separately.

As the transfer efficiency is different between one photon and another of an individual scintillation, we must deal, for a correct treatment, with the average value T_i of the transfer efficiencies over the photons of each individual scintillation. Recalling further, that the average T_i varies from one scintillation to another as a consequence of the fact that successive scintillations occur in different points inside the phosphor, the average of T_i, $\overline{T}$ must be taken over the different scintillations. The overall parameter $\overline{T}$ so defined, describes correctly the photon transfer. Obviously the statistical spread of T_i around $\overline{T}$ are described by the relative variance (relative square standard deviation) v_T.

As far as concerns the secondary electron avalanches, it has already been mentioned that the multiplication process, statistical in nature, contributes somewhat to the width of the instrumental line. It is necessary to distinguish between the average tube gain $\overline{G}$ and the average tube gain including aftereffects, $\overline{M}$. The first is defined as the average number of secondaries arriving at the multiplier anode due to the incidence of one photoelectron at first dynode, that is

$$G = \overline{m}_1\,\overline{m}_2 \ldots \overline{m}_n$$

where $\overline{m}_i$ (gain of the i-th dynode) is the average number of secondaries produced by one electron incident on the i-the dynode, that arrive on the next dynode. The average $\overline{M}$ is defined by taking into account the fact that a secondary electron avalanche is always accompanied by parasitic phenomena leading to a delayed emission of electrons from the photocathode or from the dynodes. The afteremission processes are due to various causes among which ion feedback, light feedback, field emission on cathode or dynodes. Owing to the fact that the greater contribution to the afterpulses is given by the cathode, it is assumed in a first approximation that a photoelectron released from the cathode is followed by A afterelectrons so that the tube gain including aftereffects is

$$\overline{M} = (1 + \overline{A})\,\overline{G}\,. \tag{1}$$

Eq. (1) obviously implies that the collecting time constant at the phototube anode is so large that the primary and afterpulses are added up; it can be shown that the relative variance v_m of tube gain M is given by:

$$v_M = \frac{v_T}{1 + \overline{A}} + v_A \frac{\overline{A}^2}{(1 + \overline{A})^2}$$

where v_G and v_A are respectively the relative variance in the tube gain G (without aftereffects) and in the number of the A afterelectrons.

From what has been stated in this section, one should deduce that the spread in pulse size of the scintillation spectrometer is due to the following two causes: (a) varying transfer efficiency; (b) varying tube gain. However it must not be forgotten that the number X of photons produced by monoenergetic γ-rays fluctuates about its average value $\overline{X}$. In the next section, therefore, we must take into account, even the relative variance of X.

3. Instrumental Line Width

When the preceding considerations are assembled quantitatively, it is possible, by using the probability generating functions, to express easily the relative variance v_Q of the total number of electrons

$$Q = X\,T\,M$$

arriving at the anode of the photomultiplier due to the absorption of monoenergetic γ-rays in the phosphor. The number Q, obviously proportional to the output pulse size, fluctuates about its average value $\overline{Q} = \overline{X}\,\overline{T}\,\overline{M}$ with the relative variance:

$$v_Q = v_T + (1 + v_T)\,(v_X - 1/\overline{X}) + (1 + v_M)/\overline{X}\,\overline{T}. \quad (2)$$

Eq. (2) will be the basic relation for the discussion of our experimental results. To this end, it is convenient to rewrite it by taking into account the following points: (a) the relative variance v_Q is numerically equal to the relative variance in the measured pulse size if it is assumed that extraneous sources of amplitude fluctuation are rendered negligible; (b) the value of $\overline{X}$ is proportional to the energy E of the γ-ray absorbed in the phosphor; (c) the line shape is very nearly gaussian, as will be seen in the next section. One obtains:

$$\eta^2 = \alpha + \beta/E \quad (3)$$

where $\eta^2 = 2\sqrt{2 \ln 2}\, v_Q = 5.56\, v_Q$ is the relative square full width of a gaussian line at half maximum (the square of the so-called "half-width"); α and β are two constants. In the case of normal scintillation variance ($v_X = 1/\overline{X}$), the constant α is reduced to

$$\alpha = 5.56\, v_T$$

and the constant β to

$$\beta = 5.56\,(1 + v_M)\, K/\overline{T}$$

where K is the energy expended in producing a photon.

4. Instrumental Apparatus

In the present investigation we have employed a group of various scintillation spectrometers by assembling 6292 Du Mont photomultipliers with NaI (Tl) crystals, ($1\frac{1}{2}''$ diameter and $1''$ thickness), cylindrical in shape and occasionally of different sizes and shapes (see table 2). The scintillators are different in origin as well as in preparation and mounting. Some of them were supplied by the Harshaw Chemical Company both as mounted and as unmounted crystals; some were supplied by the Quartz and Silice Society as mounted crystals. The Harshaw unmounted crystals which forthwith will be briefly mentioned as H.u. crystals, were prepared and mounted as follows. All surfaces of the dry crystal were grinded on 120 coarse grinding paper in a dry box having a relative humidity less than 10%. The crystal was next optically coupled to a flat glass disc with DC200 silicone oil (10^6 centistokes); powdered magnesium oxide previously dried in an oven was pressed between the crystal and a thin Al tube sealed onto the glass disc. A thin Al reflector (25 mg/cm² thick) was placed on the top surface of the crystal and sealed onto the Al tube. Although a slight improvement in resolution is reported[2]), no light pipe was used, so as to reproduce the usual operational conditions in spectrometrical works were backscattering effects are undesiderable.

The photomultiplier was operated by a precision regulated high-voltage supply[3]) which shows a drift of not more than 0.01% for a period of hours. The collecting time constant at the photomultiplier anode was of some microseconds so that the afterpulses and primary pulses are added up.

The amplifying chain was of the conventional type and consisted of a cathode follower, a pulse shaper and a Mod. 100 amplifier[4]). The pulse size distribution was analyzed with a 10 channel fast pulse analyzer[5,6]), accepting pulses as high as 60 volts. The channel width, constant for all channels, can be set equal to 0.5 ,1 and 2 volts.

5. Extraneous Sources of Line Width

It was assumed, in connection with eq. (3) that extraneous sources of line width are rendered negligible, although in practice it is difficult to attain this situation. Care was taken in our investigation to minimize these extraneous sources; some comments on this matter can be given as follows:

[2]) P. R. Bell, in Beta and Gamma-ray Spectroscopy, edited by K. Siegbahn (North-Holland Publ. Comp. Amsterdam, 1955) p. 133.

[3]) W. A. Higinbotham, Rev. Sci. Instr. **22** (1951) 429.

[4]) W. C. Elmore and M. Sands: Electronic Experimental Techniques (Mc Graw-Hill Book Company, Inc. New York, 1949) p. 165.

[5]) E. Gatti, Nuovo Cimento **11** (1954) 153.

[6]) S. Colombo, C. Cottini and E. Gatti, Nuovo Cimento **5** (1957) 748.

(a) It is known that the operation of the phototube with the focusing electrode at a potential near that of first dynode is characterized also by a good uniformity of response over the entire cathode area. The influence of the operation of the focusing electrode on the line width was investigated by varying the voltage between this electrode and the photocathode for a set of voltages between the photocathode and the first dynode. The curve shown

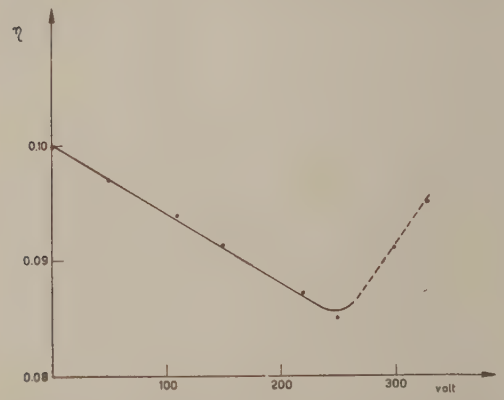

Fig. 1. Energy resolution as a function of the voltage between the focusing electrode and the photocathode (at 661 keV energy).

in fig. 1 is typical and suggests operating the phototube with the focusing electrode at the potential of the first dynode. As regards the voltage across the whole phototube, satisfactory results were obtained by keeping the voltage between cathode and first dynode equal to 250 volts and the voltage for each succeeding dynode stage equal to 80 volts. These values however are not too critical. No influence on line width was found to be due to the voltage drop from photocathode to anode.

(b) Space charge effects in photomultipliers, if present, can affect the line width. They reveal themselves also by causing a non-linearity of response to increasing particle energies. In our experiments the linearity of response was checked by calibrating the γ spectrometer with γ-rays of known energies.

(c) The influence of the earth's magnetic field was studied by equipping the photomultipliers with Mu-metal shields. We found that the earth's magnetic field affects to some extent the pulse height but not the line width.

(d) Fast fluctuations in the supply voltage, that is, fluctuations arising when the pulse spectrum is being recorded, can alter the tube gain $\overline{M}$. If the tube gain, being a function of the tube overall voltage V, varies like V^a, the resulting increase in relative half width is

$$5.56\, a^2\, v_V \qquad (4)$$

where v_V is the relative variance of V. In our case, as we found that $a = 8$ and $v_V \approx 10^{-8}$, the term (4) is negligible compared with the constant α ($\alpha \approx 5 \times 10^{-3}$, see next section) and so the fluctuations in the voltage supply do not contribute to the line width.

(e) The drifts of the whole electronic equipment (amplifier and pulse analyzer) were checked with the help of a pulse generator and found negligible for a period of hours. It is emphasized also that the counting time was always less than five minutes.

(f) The effect of the finite channel width on the energy resolution was investigated by registering the high energy photoelectric peaks ($\geq$ 0.8 MeV) with different channel width (2.0, 1.0, 0.5 volts). The lines recorded by using 1.0 volt channel width do not appear enlarged by the analyzer.

6. Energy Resolution

The γ-rays utilized in this investigation arised from the disintegration of radioactive nuclei characterized by simply decay scheme. Their energies together with the disintegrating nuclei and the decay modes are listed in table 1. The lowest energy radiations are KX-rays characteristic respectively of Ag arising from K electron capture of ^{109}Cd and from K internal conversion of the 87 keV γ-ray present in the decay, and of Ba arising from K internal conversion of the 661 keV γ-ray of ^{137}Cs.

The quoted energies are the weighted mean of the $K\alpha_1$ and $K\alpha_2$X-rays energies. It should be pointed out that the energy difference between $K\alpha_1$ and $K\alpha_2$X-rays is much lower than the

energy spread due to statistical fluctuations. The two peaks at the highest energies were obtained by using the summation method:

TABLE 1

Isotope	Mode of decay	γ Energy (MeV)	K_αX-energy (keV)
^{109}Cd	E.C., γ		22.10
^{137}Cs	β^-, γ		32.07
RaD	β^-, γ	0.0467	
^{109}Cd	E.C., γ	0.0875	
^{139}Ce	E.C., γ	0.166	
^{203}Hg	β^-, γ	0.279	
^{22}Na	β^+, γ	0.511	
^{137}Cs	β^-, γ	0.661	
^{54}Mn	E.C., γ	0.835	
^{22}Na	β^+, γ	1.277	
^{22}Na	β^+, γ	1.79 (summation peak)	
^{60}Co	β^-, γ	2.49 (summation peak)	

when the active source is located sufficiently near the scintillator, two time coincident γ-rays are detected simultaneously with appreciable efficiency. In this case the energy absorbed in the crystal is equal to the sum of the energies of the two γ-rays.

The possibility of fitting the pulse shapes with gaussian curves was analyzed by plotting in a semilogarithmic scale the counting rate against the square of the ratio between the distance from the center of the peak and the standard deviation. As can be seen from fig. 2, where some example are reported, the pulse size distributions produced by the investigated radiations can be fitted with gaussian curves, at least in an interval of about $\pm$ 2.5 standard deviations. Therefore in deducing the relative variance of a line we are justified to utilize the relation

$$v_Q = \eta^2/5.56 .$$

The dependence of the half-width of the photoelectric peaks on the energy of the γ-rays was investigated, by plotting, as shown in fig. 3, which is a typical one, their squares against the reciprocal energy $1/E$, as suggested by eq. (3). The measured values fit strictly a straight line down to about 0.800 MeV in a very good agreement with theoretical predictions. From the straight line, after extrapolation to infinite pulse height, we obtain the two constants α and β:

$$\alpha = 4.50 \times 10^{-3}$$
$$\beta = 1.57 \times 10^{-3} .$$

That is, for normal scintillation variance, the constants

$$v_T = 8.1 \times 10^{-4}$$
$$(1 + v_M)\, K/\bar{T} = 2.82 \times 10^{-4} .$$

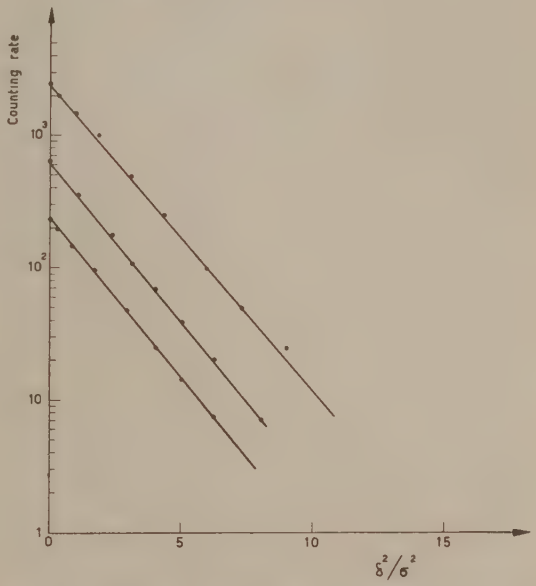

Fig. 2. Probe of the gaussian shape of instrumental lines. Counting rate are plotted in a semilogaritmic scale against the square of the ratio between the distance from the center of the peak δ and the standard deviation σ. The straight lines refer respectively to the 22.1 keV, 661 keV and 2.49 MeV peaks (from top to bottom).

All our scintillation spectrometers were studied as indicated above and the two mentioned constants were deduced in each case. Tables 2 and 3 summarize the obtained results; in particular table 2 reports the data relative to eight different scintillators coupled with the same photomultiplier and table 3 the data relative to six different photomultipliers coupled with the same scintillator.

We turn, now, our attention to the points which in the plot of fig. 3 lie under the extrapolated portion of the straight line. This fact is

TABLE 2

Crystal (phototube 1)	$v_T \times 10^4$	$(1 + v_M) \times K/\overline{T} \times 10^4$
1 (H.u)	8.10	2.82
2 (H.u.)	10.45	2.37
3 (Q.S.)	9.35	2.43
4 (Q.S.)	10.25	2.35
5 (H.)	12.60	2.70
6 (H.)	12.20	2.63
7 (H.u. cubic $1'' \times 1''$)	11.85	3.11
8 (H.u. Cil. $\frac{1}{2}'' \times \frac{1}{2}''$)	13.50	3.45

TABLE 3

Phototube (crystal 1)	$v_T \times 10^4$	$(1 + v_M) \times K/\overline{T} \times 10^4$
1	8.10	2.82
2	7.69	3.44
3	10.25	3.74
4	8.63	3.00
5	10.85	2.91
6	9.60	3.16

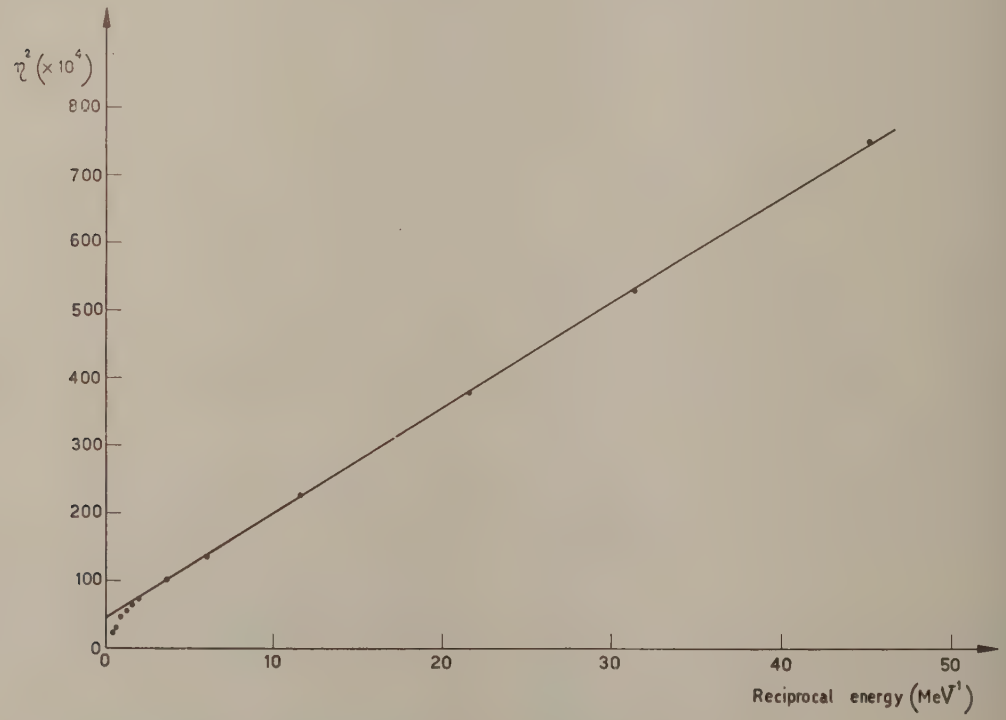

Fig. 3. Square half-width as a function of the reciprocal energy.

not due to space charge effect, as should appear at first glance, by reason of the response linearity of our spectrometer. In order to give a semiquantitative account of the observed effect, we can examine the following ideal case. Let E_1 and E_2 be the energies of two quanta which are simultaneously absorbed in the crystal by photoelectric processes, giving rise to a peak of energy $E = E_1 + E_2$; if we assume that the two events are statistically independent, the relative half width η of the observed peak can be calculated according to eq. (3). A short calculation yields:

$$\eta^2 = \alpha \left\{ 1 - \frac{2\,E_1E_2}{(E_1 + E_2)^2} \right\} + \frac{\beta}{E_1 + E_2} . \qquad (5)$$

From eq. (5) it can be seen that the width of the summation peak is smaller than the width of a photoelectric peak due to the absorption in the crystal of only one γ-ray of energy $E_1 + E_2$;

particularly when $E_1 = E_2$, η^2 reaches the minimum value

$$\eta^2_{\min} = \frac{\alpha}{2} + \frac{\beta}{2\,E_1} .$$

The same argument holds true for one high energy quantum absorbed in the crystal; as in the NaI (Tl) scintillators the pulse height per MeV is nearly independent of energy, any combination of processes by which the γ-ray is completely absorbed in the phosphor produces the same pulse height. In particular a photoelectric event and a Compton scattering followed by a photoelectric process produce the same pulse height. However as far as concerns the pulse formation we must consider that in the first case one deals with a photoelectron of energy E, in the second case with a Compton electron of energy E_1 and a photoelectron of energy $E - E_1$. Obviously the Compton and the photoelectrons are absorbed in different regions of the phosphor: therefore this process simultates the above mentioned ideal case. It must only be noted that, for a given energy of the incident quantum, E_1 is not constant but smeared, as a consequence of the angular distribution in Compton effect. As a first approximation we interpret the experimental results at high energies by using eq. (5) with E_1 representing the average energy of the Compton electron, and considering that a fraction of pulses under the peak at energy E, arises from photoelectric effect. The ratio of the pulses of maximum size (peak) to all pulses produced (total) for a $1\frac{1}{2}$ inches diameter and 1 inch thickness crystal totgether with the ratio of peak to total if no multiple processes occurred, was taken from Bell[2]).

TABLE 4

Energy (MeV)	η^2 [eq. (3)]	$\eta^2_{\text{predicted}}$	$\eta^2_{\text{observ.}}$
0.511	75.6×10^{-4}	72.0×10^{-4}	72.0×10^{-4}
0.661	68.7×10^{-4}	64.0×10^{-4}	65.0×10^{-4}
0.835	62.8×10^{-4}	57.5×10^{-4}	57.0×10^{-4}
1.28	57.2×10^{-4}	51.2×10^{-4}	50.0×10^{-4}
1.79	54.0×10^{-4}	32.1×10^{-4}	30.5×10^{-4}
2.49	51.3×10^{-4}	25.7×10^{-4}	25.0×10^{-4}

The interpretation of the widths of the peaks at 1.79 and 2.49 MeV energy which are in origin "true" summation peaks, is a pure matter of calculation.

Table 4 summarizes the measured values and the ones predicted according to the previous argument.

7. Discussion

As conclusions of our measurements a few comments may be made:

(a) Our experimental line widths vary with the energy of the γ-rays in strict agreement with the theoretical predictions leading to the eq. (2). The anomalous trend at highest energies is not fundamental in character. It can be explained by the same equation.

(b) As shown in tables 2 and 3 and according to the predictions, the two constants α and β are dependent on the scintillation spectrometer. It is very likely that the phototube and the phosphor contribute about equally to the constant α: in effect the spreads of the α values ($\approx 5.6\%$) obtained by coupling the same phosphor to various phototubes are nearly equal to these obtained by coupling the various scintillators $1'' \times 1\frac{1}{2}''$ to the same phototube ($\approx 6.5\%$). A different trend is shown by the β values; the observation of their spreads indicates that the β constant seems to be affected more by the phototubes than by the phosphor. In the same cases illustrated above, the spreads are respectively 5.8% and 3.1%. These statements, of course, must be taken with caution: it must not be forgotten that the performance of the spectrometer is dependent on the overall parameter T and on the gain M. Moreover the number of spectrometers investigated is too small for statistical conclusions.

(c) In the case of normal scintillation variance ($v_X = 1/\bar{X}$) the constant α is reduced to $5.56\ v_T$. It was calculated by Breitenberger[1]) that for a perfectly transparent crystal, optically coupled to a perfectly homogeneous photocathode, the relative variance v_e of the photon escape probility throughout the crystal, is nearly:

$$v_e \approx (1 - \varrho)^2\, \sigma^2_{\frac{1}{T}}$$

where $\sigma_{\bar{r}}$ (about 0.15 for a cube as well as for a short cylinder) is the variance of the mean number of reflections undergone by a photon, and ρ indicates the reflectivity of the faces of the crystal. Our measurements would lead, in the extreme assumption that the crystal alone contributes to the relative transfer variance, to a reflectivity ranging from 92% to 93%. These values are reasonably close to the reflectivity of magnesium oxide. The same considerations show that all investigated crystals are flawless.

Finally, in the opposite extreme assumption that the photocathode inhomogeneities alone contribute to the relative variance v_Q, our results would indicate that point-to-point variations of the photocathode sensitivity amount to about $\pm$ 10%.

Our best thanks are due to Professor G. Bolla for his kind interest in this work.

NUCLEAR INSTRUMENTS 3 (1958) 25–26; NORTH-HOLLAND PUBLISHING CO. – AMSTERDAM

IMPROVED NaI SCINTILLATION SPECTROMETER FOR THE STUDY OF CONTINUOUS X-ray SPECTRA

G. HETTINGER and N. STARFELT

Radiation Physics Department, University of Lund, Lund

Received 3 February 1958

The K X-ray escape fraction of a NaI scintillation spectrometer is essentially reduced by letting the collimated X-rays to be studied enter through a narrow well in the crystal.

The pulse-height distribution produced in a NaI(Tl) scintillation spectrometer by monoenergetic X-rays of energies below a few hundred keV is fairly simple. At these energies the well-known Compton electron tail is negligible for all but the very smallest crystals. There is, however, one complication caused by the fact that the photoelectric absorption processes in the crystal quite probably occur very close to the entering surface. Therefore the K X-rays emitted after photoelectric absorption in iodine atoms have a considerable chance of escaping from the crystal, giving rise to the so-called K X-ray escape peak displaced 29 keV below the photopeak. At an X-ray energy of 33 keV this escape peak is 30% of the photopeak, the value decreasing with increasing energies, and reaching 1.3% at 150 keV[1–6]).

In the study of pure line-spectra the K X-ray escape does not, in most cases, give rise to any difficulties but it considerably complicates the analysis of the pulse height distribution caused by a continuous X-ray spectrum. It would therefore be of great value if this effect could be avoided or at least its magnitude decreased. The way of doing this when the X-rays to be studied are collimated to a narrow beam is to let the beam enter the crystal through a narrow well as shown in fig. 1. By doing this the point where the photoelectric absorption takes place is moved away from the crystal surface and the solid angle

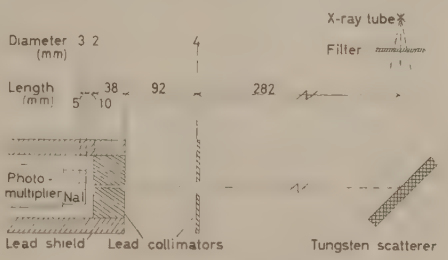

Fig. 1. Experimental arrangement.

in which K X-ray escape is possible is greatly decreased. With a well 3 mm in diameter and 5 mm in depth the calculated ratio between the escape peak and the photopeak is decreased from 30% with no well to 1.2% at an X-ray energy of 33 keV. The corresponding values at 59 keV are 12% and 0.7% respectively.

In order to test the feasibility of this method of decreasing the K X-ray escape fraction of a NaI(Tl) crystal a well having a diameter of 3 mm and a depth of 5 mm was drilled in a Harshaw crystal 37 mm in diameter and 27 mm in length. The drilling was performed with a standard work-shop drilling machine with the crystal protected against the humidity of the air

[1]) T. B. Novey, Phys. Rev. **89** (1953) 672.
[2]) M. J. Sterk and A. H. Wapstra, Physica **19** (1953) 669.
[3]) K. Lidén and N. Starfelt, Arkiv Fysik **7** (1954) 427.
[4]) P. Axel, Rev. Sci. Instr. **25** (1954) 391.
[5]) W. E. Meyerhof and H. I. West, Jr., Rev. Sci. Instr. **25** (1954) 1025.
[6]) N. Starfelt, K. Fysiograf. Sällsk. i Lund Förh. **26** (1956) 5.

by means of silicone oil. After cleaning the crystal surfaces with methylethyl ketone the crystal was placed on a 6292 photomultiplier and covered with an aluminium can. As light reflector magnesium oxide was packed between the cylindric surface of the crystal and the can and a white filter paper was used on the top surface to avoid the risk of getting the well filled with magnesium oxide.

Fig. 2 shows the pulse height distributions obtained when irradiating the crystal with tungsten K X-rays. One run was taken before the well was drilled and the other with the beam entering the crystal through the bottom of the well. The photopeaks are normalized to the same peak counting rate.

The K X-rays were produced by irradiating a piece of tungsten metal with the filtered bremsstrahlung from an X-ray tube. The acceleration potential was 140 kV and the filter consisted of 1.67 mm of Al together with 1.98 mm of Cu[7]). The secondary radiation from the tungsten piece at 90° to the primary beam was used in the experiment.

As can be seen from the fig. 2 the K X-ray escape obtained with the well in the crystal is much smaller than with an ordinary entrance surface. The width of the peak or the resolving power is practically unchanged and so is the background counting rate. It is thus concluded that when studying continuous bremsstrahlung spectra below a few hundred keV it is always worth while to use the method described in this paper. In this way the large amount of numerical work involved in correcting the observed pulse height distributions is avoided.

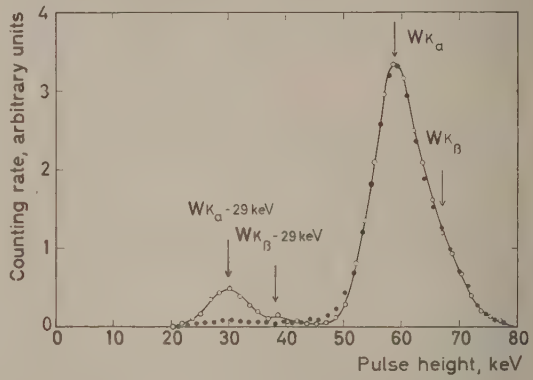

Fig. 2. The pulse height distributions produced in the scintillation spectrometer by tungsten K X-rays. The open circles were obtained before drilling the well and the filled circles with the beam entering the crystal through the bottom of a well 3 mm in diameter and 5 mm deep. The photopeaks are normalized to the same peak counting rate. Below 50 keV the statistical error is smaller than the size of the points.

[7]) G. Hettinger and N. Starfelt, Acta Radiologica (to be published).

NUCLEAR INSTRUMENTS 3 (1958) 27–32; NORTH-HOLLAND PUBLISHING CO. – AMSTERDAM

PHOTOGRAPHIC BENT CRYSTAL GAMMA SPECTROMETER

OLOF BECKMAN

Institute of Physics, Uppsala

Received 20 January 1958

A 1-meter bent crystal gamma-ray spectrometer is described. The gamma lines are registered on Ilford G5 nuclear emulsions. By counting with a microscope the electron tracks forming a line, it is possible to determine gamma intensities. Corrections have to be made for emulsion efficiency, crystal reflectivity and the geometry of the spectrometer. The accuracy of this method is controlled by the measurements of some known lines in Ta^{182}. In addition the energies and intensities of two lines in Sm^{153} are given: 69.66 ± 0.02 keV and 103.18 ± 0.04 keV; intensity ratio 9 to 100.

1. Introduction

Gamma spectroscopy by means of crystal diffraction has been developed to a high precision method for studying nuclear decay schemes by the work of DuMond and collaborators in Pasadena[1]). Notably, however, the high precision that characterizes crystal spectrometers does not seem to have attracted nuclear spectroscopists in general. Apart from several gamma-spectrometers originating from DuMond's laboratory, very few instruments of this kind seem to have been built. So far only a spectrometer designed by Ryde and Andersson[2]) has been reported in literature.

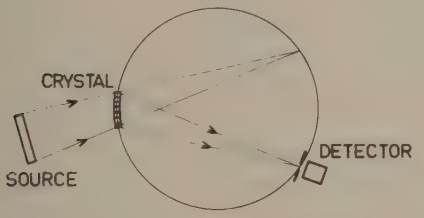

Fig. 1. Curved crystal spectrometer. Arrangement according to Y. Cauchois.

For crystal gamma spectroscopy the transmission bent crystal spectrometer is best suited. In the conventional mounting one uses an extended source, which gives a focussed spectrum along the Rowland circle (fig. 1). It is possible to register the spectrum on a photographic plate or by means of a counter and slit, thus exploring the spectrum point by point.

DuMond's wellknown gamma-spectrometer makes use of an inverted beam direction with the source placed on the Rowland circle and the counter with a collimator on the convex side of the crystal (fig. 2). This type offers several advantages such as high luminosity and the possibility of using very small Bragg angles and thus is applicable to high gamma energies. The ordinary Cauchois spectrometer of fig. 1 gives lower intensity because only the radiation within a very small angle corresponding to the integrated reflection coefficient ($\approx 10^{-4}$ at 100 XU) will be diffracted by the crystal. In the DuMond-type spectrometer the whole aperture of the crystal is used. In the photographic Cauchois spectrometer the problem of shielding the plate from

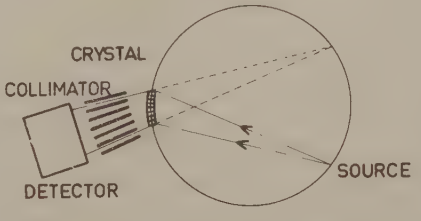

Fig. 2. Curved crystal spectrometer. Arrangement according to J. Dumond.

[1]) J. W. M. DuMond, in K. Siegbahn, Beta- and Gamma-Ray Spectroscopy (Amsterdam, 1955) p. 100.

[2]) N. Ryde, B. Andersson, Proc. Phys. Soc. B 68 (1955) 1117.

direct radiation is great, which restricts the useful region to energies below say 400 keV.

In spite of the disadvantages in luminosity and useful wavelength region the photographic method offers the great advantages of cheap and simple construction and easy handling, however. All lines in the spectrum are exposed simultaneously and corrections for the decay of the source are not necessary.

The DuMond-type spectrometer is well suited for absolute precision measurements (absolute in the sense that only the grating constant of the crystal has to be known) since the Bragg angle itself is determined, which gives the wave-length from the Bragg diffraction law. The angle which hereby has to be accurately known is the angle between the crystal normal and the primary beam direction. The counter only has to receive radiation and its position is not critical to the same extent. From the high precision point of view the source and slit therefore, ought to be fixed and the counter movable. The Bragg angle is then the angle between a fixed bar and the movable crystal normal, which has the advantage of making possible the use of a circular scale for reading the Bragg angle. Thus the accuracy is only to a lesser extent depending on precision screws (viz. in the reading microscopes), and all mechanical link systems are avoided.

The photographic method is restricted to relative measurements, but this is not a serious draw-back, since the wave length region in question is rather rich in known X-ray and gamma-ray lines. The X-ray lines of heavier elements have been measured by Ingelstam[3]) and several gamma lines have been determined by the groups under DuMond and Ryde respectively.

The photographic material used must necessarily have a high sensitivity for short wavelength radiation. Best suited for the actual problem are the Ilford G5 nuclear emulsions, which are available with a thickness of up to 600 μ. Apart from the high absorptivity they offer a great advantage in that it is possible to count the single electron tracks produced by the incoming quanta. From the known composition of the emulsion the absorption coefficient can be calculated, which opens a possibility of determining absolute gamma-ray intensities. The nuclear emulsion is in this respect comparable to an ordinary counter.

2. Experimental

The difficulties of shielding the plate from the direct beam make it necessary to chose a crystal plane with small grating constant in order to get large deflecting angles. Quartz crystals have good elastic properties, which make them very suitable for bent crystal spectrometers. Several quartz planes have good reflecting properties and small grating constants as is seen from table 1.

TABLE 1

Plane	Spacing, d, XU	Structure factor, F
310	1177.63	20.9
223	1012.75	15.6
502	810.00	21.7
550	490.29	14.3

The plane most often used so far is the 310 plane. This plane is, however, inferior to 502 as regards the spacing and comparable as to the luminosity. Since the demands on large Bragg angles is very great in the present spectrometer the plane 502 was chosen.

The crystal holder is of the type described by Brogren[4]), where the crystal is bent between two pairs of steel pins on steel blocks. The crystal radius can be arbitrarily set by proper adjustement of the bending pressure. The free bending will tend to make the crystal saddle-formed, but this will not influence the line width to a greater extent in the actual spectrometer. The measured width of a 67 keV gamma line is about 0.17 XU, which is mainly attributed to the pure diffraction pattern of the crystal. The size of the crystal is 20 × 50 × 1.0 mm and the aperture of the crystal holder 15 × 30 mm.

[3]) E. Ingelstam, Die K-Spektren der Schweren Elemente, Diss. (Uppsala, 1937).

[4]) G. Brogren, Ark. f. Fysik 3 (1951) 515.

Fig. 3 is a schematic drawing of the spectrometer arrangement. The radioactive source S is located at the centre of a heavy lead and iron shield. The source is placed in a lead cube with 20 cm sides. By the use of two identical cubes

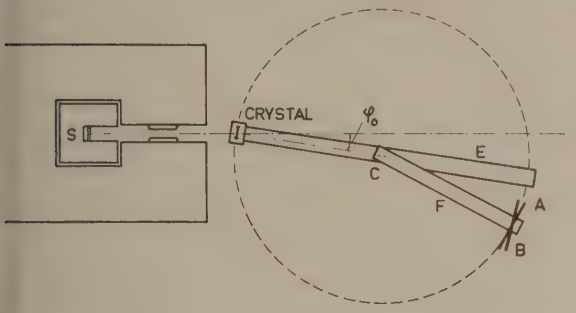

Fig. 3. The experimental arrangement.

the sample is easily replaced by the source used as reference. The exit channel for the radiation is supplied with an aperture, shielding the crystal holder and the walls of the exit hole from direct radiation, that may cause undesired scattering.

Apart from the crystal and plate holders the spectrometer is the same as used by Ingelstam[3]) in his work on the wave-lengths of X-ray K-lines. The beam E (fig. 3) is movable around the crystal axis and represents the crystal normal; the beam F is pivoted at C, the center of the Rowland circle and carries the plate holder. The Bragg angle φ_0 corresponding to gamma lines at the centre of the plate is adjusted by means of simple circular scales. These scales require no precision, since the wave-lengths are determined by the use of known reference lines.

In his thesis, Ingelstam[3]) discusses two positions of plate; pos. A, where the plate is tangential to the Rowland circle and pos. B, where the plate normal is directed towards the crystal axis. For reasons discussed by Ingelstam, pos. B is to be preferred. One of the reasons is that the gamma rays hit the plate under almost normal incidence, which is important in this case, where thick emulsions are used.

A Ta^{182} source from the R 1 reactor of AB Atomenergi, Stockholm, has served as a reference source. The gamma spectrum of Ta^{182} has been measured carefully by DuMond *et al.*[5]). One week's exposure of Ta^{182} produced measurable lines on the plate. With the same spectrometer setting the source under investigation was then exposed. It must be pointed out that the position of the source is not at all critical. The important thing is that the plate and crystal are rigidly connected to each other.

After development the plate is measured in a precicion comparator. The wave-lengths are calculated from a simple interpolation formula. This formula, containing corrections due to the use of a plane plate, that does not follow the Rowland circle, is easily derived from purely geometry conditions. Formulas for pos. A as well as pos. B are given by Ingelstam. The corrections are negligible if the reference lines are close to the unknown lines.

For determinations of the line intensities the electron tracks forming a spectral line are counted in a microscope. The electron tracks produced by gamma quanta result from photoelectric and Compton events and they can be distinguished from fortuitous single grains, contributing to the background. By counting of the electron tracks and discarding single grains it is thus possible to detect fainter lines than by ordinary measurements in a comparator because of the higher signal to noise ratio. Fig. 4 shows the 72 keV line of W^{187}. On the plate, a reproduction of which is seen at the top of fig. 4, the line is barely visible when viewed at a small glancing angle. The photometer curve in the middle of fig. 4 shows nothing, but the line appears at the track-counting, the result of which is seen at the bottom of fig. 4. Of course the counting of tracks is a rather cumbersome method, which presumes a knowledge of approximate position of the lines. However, to a certain extent this is also the case with spectrometers using counting devices. The use of photographic G5 emulsions combines the advantages of the survey character

[5]) J. J. Murray, F. Boehm, P. Marmier, J. W. M. DuMond, Phys. Rev. **97** (1955) 1007.

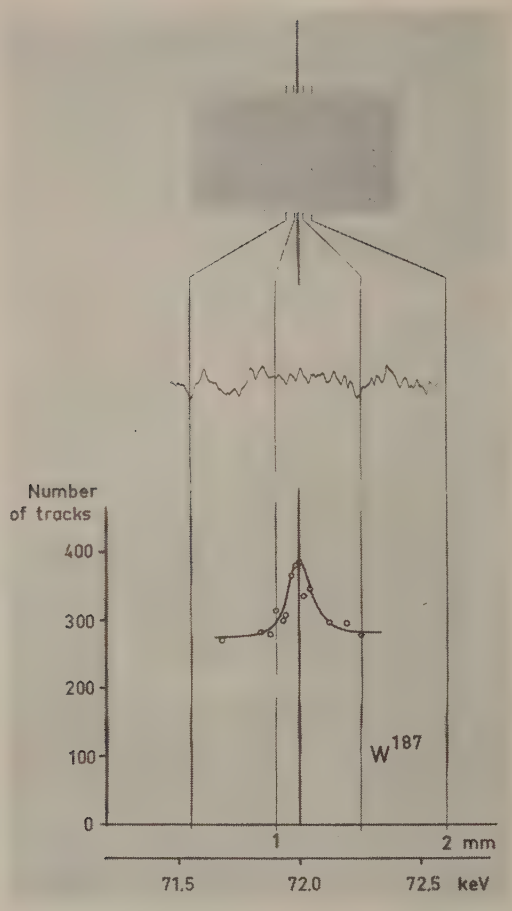

Fig. 4. The 72 keV line of W^{187}. At the top is a reproduction of the photographic plate. The line is barely visible on the original. In the middle a photometric recording and, at the bottom, the result of counting of the electron tracks in a microscope. The track-counting method gives higher signal to noise ratio.

of the photographic method with the intensity measurements of the counter spectrometer method.

3. Results

Ta^{182}

A plate exposed to Ta^{182} shows the gamma lines as well as the K X-ray lines of Ta and W. Two low energy gamma-lines were measured, using the X-ray lines as reference lines in order to check the wave-length values given by DuMond *et al.*[5]). A 100 μ Ilford G5 emulsion was exposed to Ta^{182} for 31 days. By the use of eight X-ray lines (Ta, W; $\alpha_1\alpha_2\beta_1\beta_3$) tabulated by Ingelstam[3]), two low energy gamma lines were determined (table 2). The plate was measured in two different comparators; (1) Precision comparator from Adam Hilger Ltd. London and (2) Projection comparator with a commercial micrometer screw, calibrated by Ingelstam[3]) in his thesis work.

Table 2

Wave-length XU		Energy keV	
Hilger-comp	Proj-comp	Present results	DuMond *et al.*[5])
188.266	188.265	65.72 ± 0.01	65.71 ± 0.01
182.666	182.664	67.73 ± 0.01	67.74 ± 0.01

The agreement with DuMond's values is very good.

An attempt was further made to calculate the line intensities as measured on the plate, starting from the known strength of the radioactive source. During the 31^d exposure of the 0.5 curie Ta source 5×10^{16} disintegrations have occurred. The strong 67.74 keV line has a decay fraction of 0.31 and a total internal conversion of 0.31[5]). After correcting for self-absorption in the source we find that a total number of 2.3×10^{13} quanta has been emitted per unit solid angle towards the crystal.

The reflecting properties of bent quartz crystals have been studied by Lind, West and DuMond[6]). They found that the intergrated reflection coefficient R_θ for an elastically bent quartz crystal varied as if the crystal had an ideal mosaic structure with low primary and secondary extinction. The expression for R_θ is then:

$$R_\theta = \frac{r^2\, d\, K^2\, t}{\cos^2\theta}\left(\frac{|F|}{V}\right)^2 \lambda^2 . \qquad (1)$$

Here r equals e^2/mc^2, d is the lattice constant, t the crystal thickness, F the crystal structure factor and V the volume of the unit cell. Putting

[6]) D. A. Lind, W. J. West, J. W. M. DuMond, Phys. Rev. 77 (1950) 475.

the polarization factor K and cos θ equal to 1, we find approximately for the 502 plane:

$$R_\theta = \frac{1}{E^2} \times 3.6 \times 10^{-2} \qquad (E \text{ in keV}) . \quad (2)$$

The reflection coefficient is thus inversely proportional to the square of the gamma energy. Lind, West and DuMond have justified this for the 310 plane and the present author found the same energy dependence in connection with an investigation on the X-ray intensities of heavier elements[7]). Though this is by no means a rigorous proof for the validity of eq. (2) for the 502 plane, we still use this equation for our intensity calculations.

From eq. (2) and the known geometry of the spectrometer the total amount of 67.74 keV gamma quanta diffracted by the crystal is found to be 1.2×10^5 per mm length of the spectral line at the Rowland circle.

The absorption coefficient of the G5 emulsion is calculated from the known composition[8]) (table 3).

TABLE 3

Composition of G5 emulsion at 58% humidity

Element	g/cm³	Element	g/cm³
Ag	1.817	H	0.0534
Br	1.338	O	0.249
J	0.012	N	0.074
C	0.277	S	0.007

From these figures and the mass absorption coefficients of the elements the percent absorption in 100 and 600 μ G5 emulsions is plotted against gamma energy in fig. 5.

At 67.74 keV 10.6% is absorbed in 100 μ emulsions. If each absorbed quantum produces only one electron track, which is the most probable case, we find that the plate should contain 1.3×10^4 electron tracks per mm length of the spectral line. In order to stop weak stray radiation, a filter of 0.5 mm brass was placed in front of the plate, which diminishes the number to 8.5×10^3 tracks.

[7]) O. Beckman, Ark. f. Fysik 9 (1955) 495.
[8]) A. J. Swinnerton, C. Waller, Priv. comm.

The result obtained by counting the tracks in a microscope was 4.4×10^3 tracks per mm length of spectral line, which considering the great uncertainties in the calculations, is in fairly good agreement with the estimated figure.

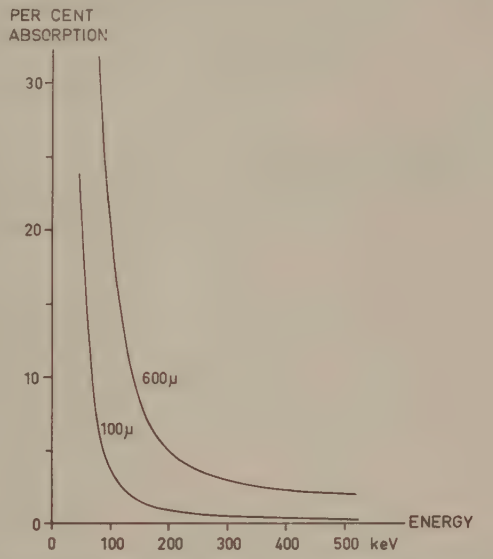

Fig. 5. Per cent absorption of gamma-rays in Ilford G5 nuclear emulsions.

The magnification of the microscope was 950x and all tracks inside a window 10×600 μ were counted. The line profiles obtained are plotted in fig. 6 and the relative intensities of the lines, corrected for source self-absorption, crystal reflectivity and plate efficiency, are quoted in table 4. The agreement with the intensities measured by DuMond *et al.*[5]) may justify the use of the $1/E^2$ dependence of the crystal reflectivity from eq. (2).

TABLE 4

Gamma energy keV	Intensity	
	DuMond *et al.*[5])	Present results†
65.71	7.5	10
67.74	85	85
100,09	40	43

† Normalized to the 67.74 keV line, set equal to 85 by DuMond *et al.*[5]).

Sm^{153}

A sample of Sm^{153} (half-life 47^h) in 0.38 g Sm_2O_3 was obtained from the R 1 reactor of AB Atomenergi, Stockholm, and exposed on a 100 μ G5 plate. Using the 67.74 and 100.09 keV lines of Ta^{182} as reference lines the following energy values were obtained.

The intensity figures are corrected for self-absorption in the source, crystal reflectivity and emulsion efficiency. The intensity of the 69.66 keV is reported by Debey, Mandeville and Rothman[9]) to be 25 and, by Andersson[10]) to be $\approx$ 10, the other line taken as 100.

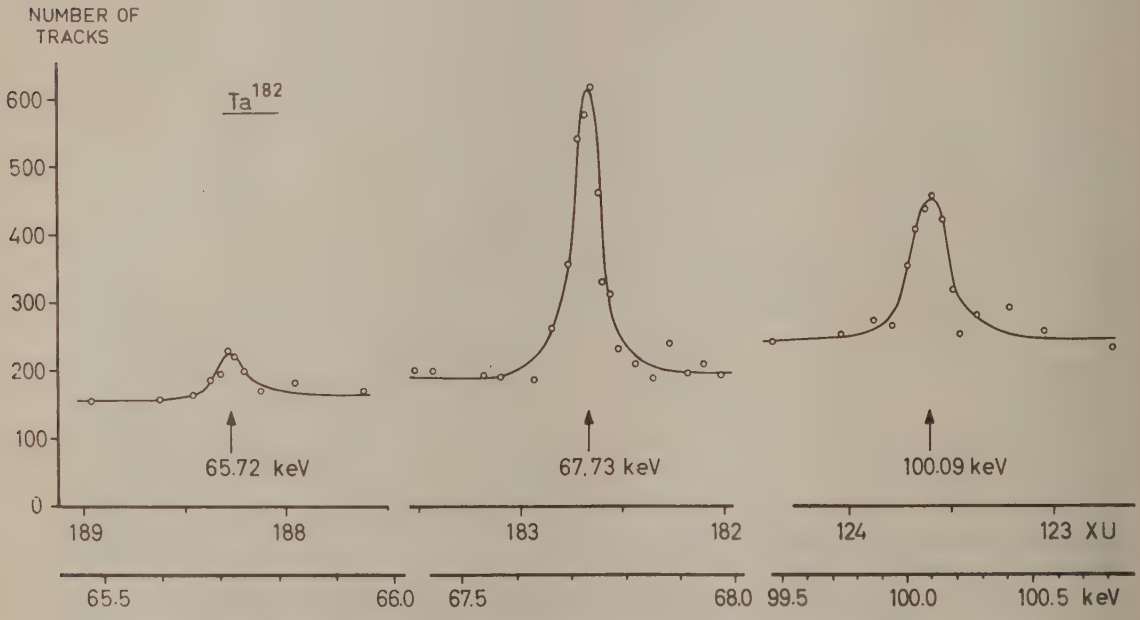

Fig. 6. Three gamma lines from Ta^{182}, registered by counting of the electron tracks in the G5 emulsion.

Table 5

Present values		Andersson[10])
Intensity	Energy keV	Energy keV
9	69.66 $\pm$ 0.02	—
100	103.18 $\pm$ 0.04	103.27 $\pm$ 0.02

The author is greatly indebted to Professor Kai Siegbahn for his continuous interest in this work. Further my thanks are due to the reactor group at R 1, AB Atomenergi, Stockholm, for preparing the strong radioactive sources.

[9]) V. S. Dubey, C. E. Mandeville, M. A. Rothman, Phys. Rev. **103** (1956) 1430.

[10]) B. Andersson, Proc. Phys. Soc. A **69** (1956) 415.

NUCLEAR INSTRUMENTS 3 (1958) 33–42; NORTH-HOLLAND PUBLISHING CO. – AMSTERDAM

ION SOURCE FOR RADIOISOTOPE SEPARATION

J. O. BURGMAN† and G. ANDERSSON††

The Gustaf Werner Institute for Nuclear Chemistry, University of Uppsala

Received 20 January 1958

An ion source of the oscillating electron type with axial magnetic field and end extraction has been constructed for electromagnetic separation of synchrocyclotron-produced radioactive isotopes. A description of the ion source and the results of some systematic investigations of its properties are given.

The performance of the ion source is illustrated by some recent applications to prepare sources for spallation studies and nuclear spectroscopy.

1. Introduction

The electromagnetic isotope separator (mass separator) of the Gustaf Werner Institute for Nuclear Chemistry[1]) is constructed with special regard to the separation of synchrocyclotron-produced radioactive isotopes.

This use in general puts a low upper limit to the available quantities of radioactive material, and great requirements are imposed on the charge economy of the ion source. On the other hand, it is not necessary and not even desirable to reach high ion currents. The total intensity is determined by the amount of stable carrier substance that has to be added for several reasons: to facilitate preceding chemical separations, to make possible mass identification and control of the beam and, most important, to allow the use of a high-efficient plasma ion source. In most cases, an output of a few hundred microamps has proved sufficient.

The rapidity of the separation process is another point of decisive importance when dealing with relatively shortlived nuclides, that means half-lives down to about ten minutes. Vacuum-gating of the charge into the ion source and suitable thermal properties of the discharge chamber and the evaporation furnace must be provided for. Of course the relation between charge quantity, separation time and total ion current has to be considered in planning a separation. It may be worth pointing out that due to the short duration of most runs the power economy of the ion source becomes a minor problem.

The first ion source used with the mass separator had some drawbacks, such as the condensation of evaporated charge material on the oil-cooled electrode leads and chamber walls and the difficulty of controlling the evaporation rate from the internal furnace. A reconstruction aiming at increased efficiency with solid charge material was necessary. The new ion source, as well as the first one, is of the oscillating electron type with an axial magnetic field and ion extraction in the field direction (end extraction)[2]).

Though the reconstruction was initially based on experience gained with the old ion source, it should be remarked that the simultaneously performed investigation of a similar source at Copenhagen[3,4]) influenced the shaping of several details†††.

In this paper a description of the present ion source will be given together with the results of some systematic investigations of its properties, supplementing the more extensive studies

[1]) G. Andersson, Arkiv Fysik **12** (1957) 331.

[2]) A. T. Finkelstein, Rev. Sci. Instr. **11** (1940) 94.

[3]) O. Almén and K. O. Nielsen, Proc. 1955 Harwell Isotope Conf., Ch. 3.

[4]) O. Almén and K. O. Nielsen, Nuclear Instruments **1** (1957) 302.

† Present address: CERN, Geneva, Switzerland.

†† Present address: Nuclear Data Project, National Research Council, Washington 25, D.C., U.S.A.

††† We are indebted to Drs. K. O. Nielsen and O. Almén for frequent communication of results.

carried out by Almén and Nielsen[4]). The performance of the ion source is further demonstrated in a review of recent applications.

To the present work one of the authors (G. A.) has contributed mainly the general layout for the ion source construction.

2. Construction and Operation

The principal features of the ion source are seen in fig. 1. The aim has been to make the discharge chamber closed as far as possible and ($\varnothing = 0.8$ mm) is placed at the inlet end of the discharge chamber. The chamber temperature can be increased by direct heating of the anode, which consists of a helical tungsten wire ($\varnothing =$ 1 mm). Thus charge material is prevented from condensing on the walls.

The discharge chamber is placed inside an oil-cooled magnet coil. The magnetic field strength can be varied from zero up to some hundred oersteds.

Behind the discharge chamber there are two

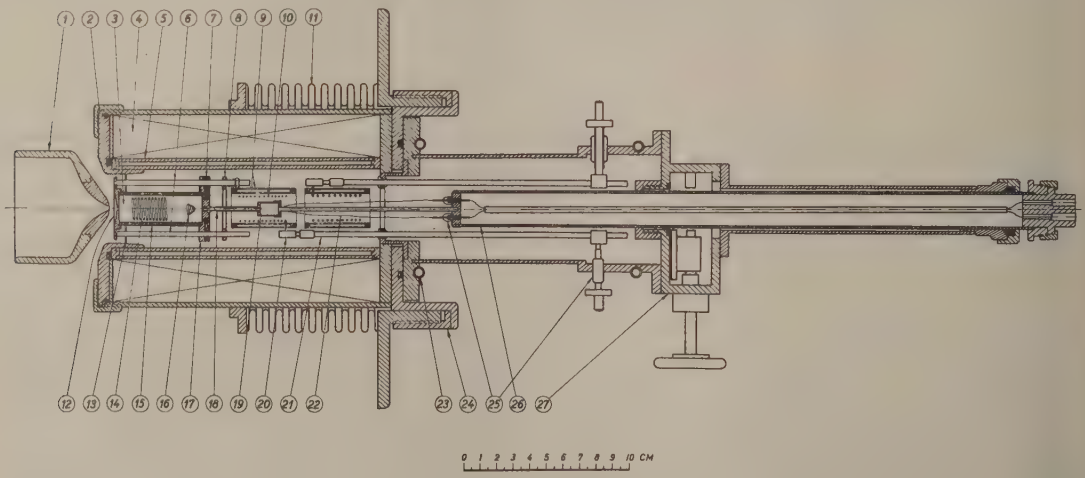

Fig. 1. Axial cross section of the ion source. 1. First electrode of the electrostatic lens system (suction electrode). 2. Iron housing. 3. Discharge chamber. 4. Magnet coil. 5. Cooling mantle. 6. Support rods. 7. Lavite plate. 8. Support ring. 9. Radiation shields for oven. 10. Oven heater. 11. Metal bellows. 12. Outlet plate. 13. Guide ring. 14. Directly heated anode. 15. Lavite cylinder. 16. Filament. 17. Inlet plate. 18. Inlet tube. 19. Container for the charge material. 20. Molybdenum holder. 21. Oven heater lead. 22. Thermocouple leads. 23. Cooling system. 24. Adjuster for axial position. 25. Kovar-glass terminals. 26. Holder for the charge container. 27. Vacuum valve.

keep it at high running temperature by thermal insulation and sufficient heating. It consists of two halfcylinders of lavite, making possible the introduction of cathode and anode connections through the chamber walls, and two end plates (inlet plate and outlet plate) of nickel. Nickel was chosen as a corrosion-resistant material. The discharge chamber is screwed together by two rods of stainless steel and centered relative to the ion source magnet by means of three lugs on a ring of nicrotal (a nickel-chromium alloy) near the outlet plate. The directly heated cathode in the form of a bifilarly wound tungsten wire

furnaces, the nearest one for charge material with low vapour pressure and the other for more volatile substances. The furnace heaters are tungsten spirals ($\varnothing = 1$ mm) each surrounded by two concentric radiation shields of nicrotal. The container for the charge as well as the inlet tube to the discharge chamber are made of stainless steel and can rapidly be gated in through a vacuum valve without breaking the high vacuum. To facilitate the transfer of radioactive samples to the container the material is filled (for instance by direct evaporation) into a small crucible, normally of stainless steel.

The gas pressure is regulated by the furnace temperature and is controlled by a thermocouple and a temperature regulator working on the heater current.

The separation can start as soon as the temperature dependent vapour pressure reaches the threshold value for stable plasma. With plasma ion sources it is necessary to operate at a pressure in the discharge chamber around 10^{-3}–10^{-4} mm Hg (cf. [4]). To obtain this pressure, a certain amount of stable charge material must be present. Alternatively a support gas, for instance argon, can be used in some cases. For this purpose a gas inlet tube of stainless steel is connected to the discharge chamber. The stable isotopes also serve as mass indicators to control the position of the mass-spectrum and the focusing conditions in the collector plane of the separator.

The ion extraction is provided by the first electrode ("suction electrode") of the accelerating system, placed at a distance of 5–6 mm from the outlet. The suction electrode is made of nickel and the diameter of its entrance opening is 3 mm, while the outlet from the ion source has a diameter of 2 mm.

Fig. 2. Front view of the internal parts of the ion source.

A photograph of the discharge chamber and the evaporation furnaces seen from the outlet end of the ion source is shown in fig. 2.

As to power supplies (fig. 3) it should be noted that direct current has been chosen for heating purposes inside the discharge chamber, alternating currents giving rise to plasma oscillations which lead to defocusing. For the same reason the anode voltage and the ion source magnet current are carefully smoothed. Fig. 3 also shows the potential scheme of the electrostatic lens system. In addition two geometrical extraction gap parameters to be discussed in section 3 are indicated.

Typical operating data are:

Accelerating voltage	E_{acc}	= 60 kV
Focusing voltage	E_{foc}	= 47 kV
Suction voltage	E_s	= 5 kV
Anode voltage	E_a	= 100–200 V
Filament heating current	I_f	= 35 A
Anode heating current	I_{ah}	= 20–30 A
Oven heating current	I_{oven}	= 15 A.

3. Performance

As already mentioned, Almén and Nielsen[4]) have systematically studied the characteristics of a magnetic ion source, similar to the present one. In their measurements they used noble gases, in particular argon and krypton, which are known to form atomic ions. In most applications of the mass separator to produce radioactive sources, however, chemical compounds, for instance chlorides, are used as charge material. These compounds have a tendency to form not only atomic ions but also molecular ions. In order to establish the conditions for maximum efficiency of the separation process a systematic investigation of the dependence of the atomic and molecular ion content on some important parameters was performed.

The ion source parameters involved in these measurements are (cf. [4]): the filament heating current I_f, the anode voltage E_a, the ion source magnet current I_m and the pressure p and length l of the discharge chamber. A new parameter of fundamental importance is the

anode heating current I_{ah}. The extraction gap parameters are: the suction voltage E_s, the distance d between the suction electrode and the ion source outlet, the area of the outlet opening

material for the following measurements was thus well founded.

To establish as equal running conditions as possible the furnace temperature was kept

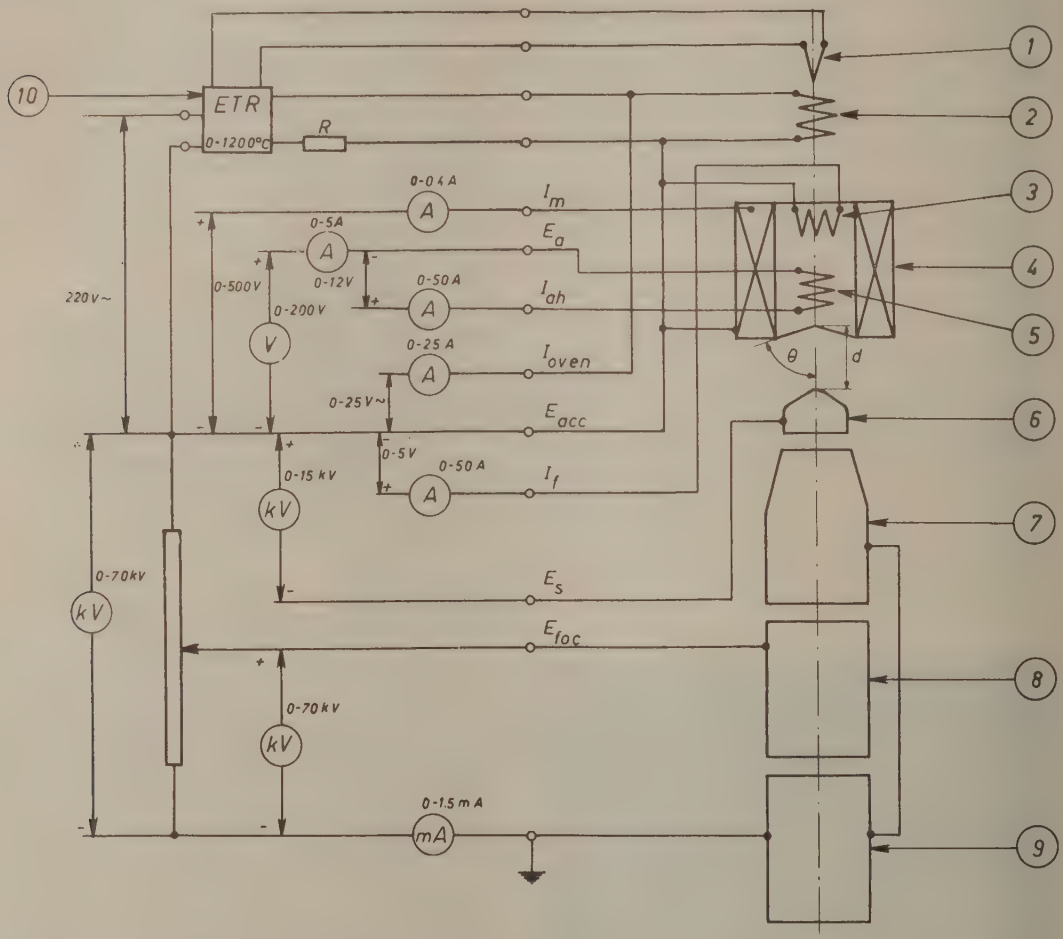

Fig. 3. Power supply and experimental arrangement. 1. Thermocouple. 2. Oven heater. 3. Filament. 4. Magnet coil. 5. Directly heated anode. 6. Suction electrode. 7. First grounded electrode. 8. Focusing electrode. 9. Second grounded electrode. 10. Temperature regulator. d. Distance between the suction electrode and the ion source outlet. θ Outlet angle.

A_o and the outlet angle θ (see fig. 3). In the following measurements d, A_o, θ ($= 80°$) and l ($= 50$ mm) are kept constant.

The application of the mass separator to produce sources for nuclear spectroscopy in the lead region has been the main task during the last year. The choice of stable $PbCl_2$ as charge constant during each series of measurement, keeping the vapour pressure p in the discharge chamber almost constant. The rate of vapour flow to the discharge chamber is proportional to the rate of evaporation and to the surface area of the charge material and thus varies with charge quantity, physical state of the charge

and charge temperature (cf. [5])). As the charge decreases it is necessary to increase the temperature to maintain the same rate of vapour flow. If the amount of substance is too small the rate of flow is not sufficient to maintain stable plasma conditions, that is, p falls below $p_{\min}$, and a phenomenon called hash occurs before the arc goes out. For this reason quite large amounts of charge material were used. The measurements were performed in such a way that the ion current due to stable lead isotopes was collected on a plate of copper situated in the focal plane of the separator. That optimum focusing conditions were fulfilled during the investigation was controlled by observing the mass spectrum on a fluorescent screen.

Optimum focusing, that is maximum resolution of the mass spectrum, can be obtained in two different ways. In the first way, most frequently used, the filament heating current is changed without changing the anode voltage setting. Due to the negative current-voltage characteristics of the arc, however, the instrument reading E_a of the anode voltage drops with increasing filament current. In the second way the anode voltage is changed together with the filament current to maintain a constant instrument reading of E_a. It is evident that different results will be obtained in the two cases as the ionization cross section σ_1 for electrons varies with electron energy.

Two different types of measurement were performed:

(a) Measurements of the ion beam current I_1^m at maximum resolution as a function of the suction voltage E_s.

(b) Measurements of the ion beam current I_1^m at maximum resolution as a function of the ion source magnet current, that is the magnetic field strength in the discharge region.

The measurements were carried out in the following way: First the atomic ion current of the Pb^+ mass spectrum was measured. Then the accelerating voltage was slightly decreased in order to measure the molecular ion current from the $(PbCl)^+$ mass spectrum, keeping the ion source parameters constant. In the same manner also the $(PbCl_2)^+$ ion current was measured but as it contributed with less than one per cent to the total lead ion current it could be neglected.

3.1. I_1^m AS A FUNCTION OF THE SUCTION VOLTAGE E_s

The space charge limited current I_1 of ions of mass M is expected to vary with the suction voltage E_s according to the Langmuir formula[6])

$$I_1 = \text{const.} \frac{A_0 \times E_s^k}{d^2 \times M^{1/2}}$$

The theoretical value of the exponential coefficient k is 3/2. In a work with a plasma ion source, however, O. Reifenschweiler[7]) obtained an E^2 law for the dependence of ion current on extraction voltage. Almén and Nielsen[4]) on the other hand, concluded that $k = 3/2$ was in accord with their measurements.

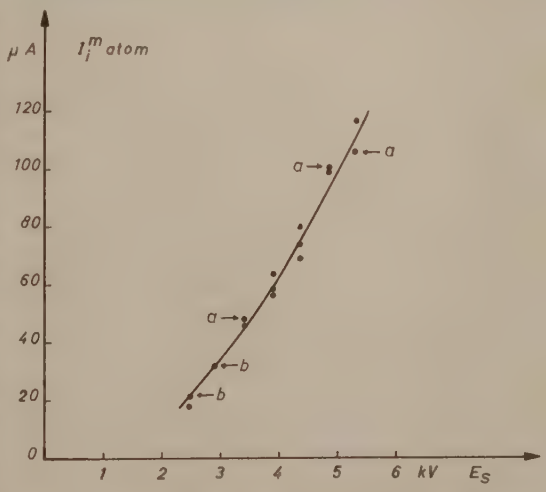

Fig. 4. The atomic ion current as a function of the suction voltage. Anode voltage decreases with increasing filament current. $91V < E_a < 140V$ $31.7A < I_f < 34.0A$.
a = double point, b = triple point.

The present measurements seemed to indicate roughly an E^2 dependence when only the atomic ion current was measured (fig. 4). Different

[5]) K. O. Nielsen, Nuclear Instruments **1** (1957) 289.
[6]) I. Langmuir and K. T. Compton, Revs. Mod. Phys. **3** (1931) 191.
[7]) O. Reifenschweiler, Ann. Physik **14** (1954) 3.

series of measurements, however, gave different k values. These discrepancies made it necessary to measure both the atomic and the molecular ion currents of the lead isotopes.

It was observed that the content of atomic and molecular ions was strongly dependent on the filament heating current and the discharge chamber temperature as well as the arc voltage drop. This explains the different values obtained in different series of measurement.

The renewed measurements with $(PbCl)^+$ included in I_1 gave a mean value for the exponent $k = 1.8$ which is still different from the Langmuir law (fig. 5). A closer examination of Almén's and Nielsen's experimental values shows, however, that also in their measurements the 3/2-power law is not quite satisfied. The exponent is found to be around $k = 1.6$–1.8. Considering the difficulties inherent in measurements of this type and particularly the fact that only a fraction of the total ion current is measured, no far-reaching conclusions as to the

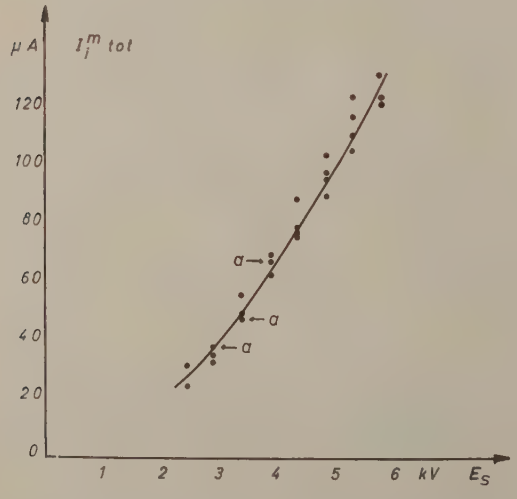

Fig. 5. The total ion current as a function of the suction voltage. Anode voltage decreases with increasing filament current. $147V < E_a < 170V$ $31.4A < I_f < 34.1A$.
a = double point.

validity of the Langmuir formula can be drawn. The tendency of $k > 3/2$ for the useful ion currents, however, emphasizes the importance of a high electrostatic field strength for the extraction of the beam.

The measurements show further that the

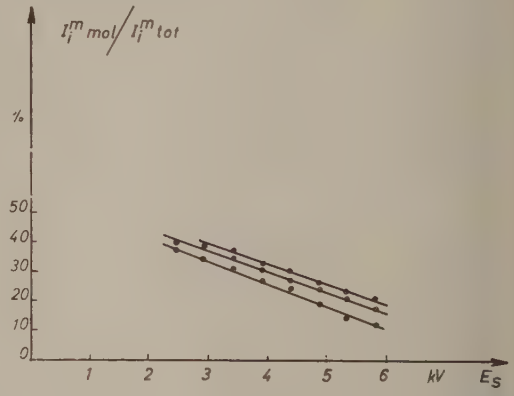

Fig. 6. The molecular ion current percentage of the total ion current as a function of the suction voltage. Anode voltage decreases with increasing filament current.
$147V < E_a < 170V$ $31.4A < I_f < 34.1A$.

molecular ion percentage of the total ion current decreases linearly with increasing E_s (fig. 6). As increasing E_s demands increasing filament current for sharp focusing, the conclusion can be drawn that the increase of the current density in the discharge decreases the molecular ion current. As dissociation is proportional to the discharge current density[8]), the atomic ion current increases with increasing heating power.

3.2. I_1^m AS A FUNCTION OF THE ION SOURCE MAGNETIC FIELD AT CONSTANT SUCTION VOLTAGE $E_s = 5$ kV

The ion currents I_1^m of the atomic and molecular ions were measured for gradually decreased magnet current values.

The experimental curves show a linear dependence of the ion current on the magnet current (figs. 7 and 8). The atomic ion current decreases with decreasing magnetic field strength, whereas the molecular ion current increases with decreasing field strength. The total ion current, the sum of atomic and molecular ion current, remains almost constant or shows only

[8]) J. Flinta, AB. Atomenergi, Stockholm, private communication.

a slight decrease with decreasing field strength. At small values of the magnet current good focusing can no longer be obtained and finally the arc extinguishes.

It is interesting to note (fig. 9) that the molecular ion percentage decreases linearly with increasing magnet current. Systematic investigations show further that the molecular ion content decreases with increasing discharge chamber temperature. It was shown that the molecular ion current at maximal magnet current falls from 25% at no anode heating current to 5% at an anode heating current of 30 A.

That the efficiency of the separation process is much greater in the latter case is clear as only the atomic ion beams are collected in the actual applications.

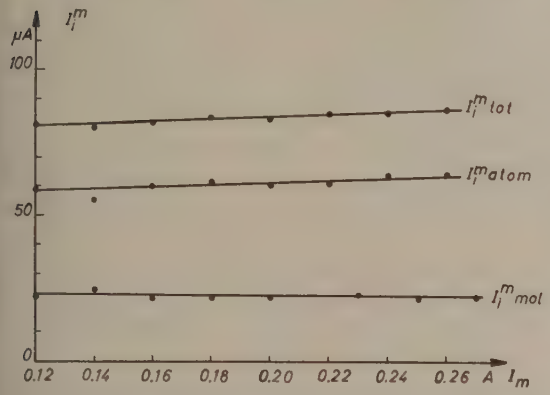

Fig. 7. Ion currents as functions of the ion source magnet current. Anode voltage decreases with increasing filament current. No anode heating current.
$149\text{V} < E_a < 153\text{V}$ $34.3\text{A} < I_f < 35.2\text{A}$.

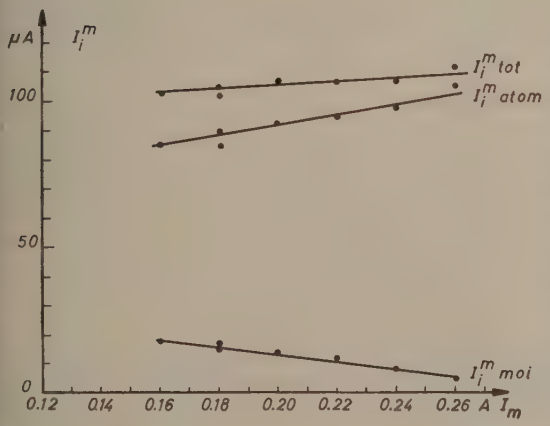

Fig. 8. Ion currents as functions of the ion source magnet current. Anode voltage decreases with increasing filament current. Anode heating current, $I_{ah} = 30\text{A}$.
$120\text{V} < E_a < 135\text{V}$ $34.0\text{A} < I_f < 35.8\text{A}$.

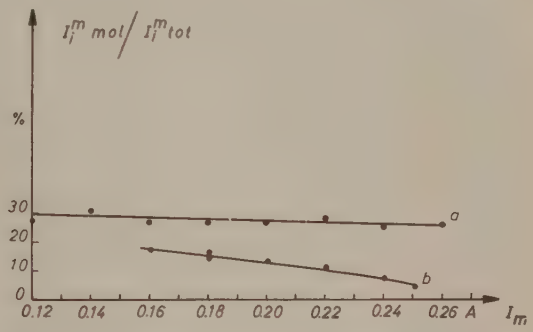

Fig. 9. The molecular ion current percentage of the total ion current as a function of the ion source magnet current. a) No anode heating current; b) Anode heating current, $I_{ah} = 30\text{A}$.

From the experimental results the conclusion can be drawn that the dissociation is more complete at higher discharge chamber temperature. It seems plausible to assume that the recombination of atoms to molecules at the chamber walls is restrained by the higher temperature.

The conditions for highest efficiency of this ion source are fulfilled at high discharge current density, high discharge chamber temperature and maximal magnetic field strength in the discharge region. To obtain maximum efficiency it is further necessary to work at the lowest pressure that is consistent with stable arc conditions and optimum ion current output. With increasing pressure the loss of neutral atoms or molecules through the outlet increases.

3.3. THE MECHANISM OF ION PRODUCTION AND BEAM FORMATION

For the understanding of the behaviour of a plasma ion source a short description of the fundamental processes for ion production and beam formation will be given although more

complete treatments have been published by various authors[4,9-12]).

The ionization is produced by medium fast primary electrons (about 100 eV energy) obtained by a low-tension arc discharge between the cathode and anode. The electrons leaving the cathode are accelerated by the electrical field in the plasma boundary sheath adjacent to the filament. The ionization efficiency of the primary electrons is increased because the magnetic field in the discharge region causes the electrons to move in helical paths, oscillating back and forth between the cathode and anti-cathode (outlet plate). The electrons thus form a column of high ion density, a plasma. The plasma is characterized as the state of an ionized gas where the concentration of positive and negative charges is almost equal. The maximal potential drop that can be sustained in a plasma is about half the electron temperature. Greater drops would cause space charge to redistribute itself until it is neutralized. The plasma is separated from the chamber walls and filament by a positive ion sheath.

At optimal focusing conditions for the external beam, the electrostatic field maintained by the suction electrode (fig. 3) pushes the plasma inward forming a concave interface, the meniscus, between sheath and plasma at the outlet opening. The curvature of this boundary sheath determines to a great extent the degree of focusing of the ion beam. The position and curvature of the meniscus is determined by the rate of ion diffusion from the plasma and the field intensity at the outlet, so that an equilibrium between the ion current density at the plasma boundary sheath and the space-charge current density of the extraction gap is maintained. The total ion beam current is further determined by the area of the meniscus. If the filament current is increased the ion current density is increased and the ion supply to the meniscus becomes greater. This causes the meniscus to move forward, reducing the curvature, which results in a defocusing of the ion beam, if the suction voltage is left unchanged. To restore optimum focusing conditions the suction voltage must be increased.

At optimum focusing conditions, a beam cross-over, that is a minimum beam cross section, exists between the outlet and the first accelerating electrode.

To prohibit beam-broadening because of space-charge repulsion of the ions in the extraction gap the potential field between the ion source and the first electrode must be fitted to the space charge determined potential along the boundary surface of the beam by choice of a suitable geometrical shape of the outlet plate and first electrode[10,13]). The ion beam must not touch the first electrode in order to prevent electrical breakdowns between ion source and electrode.

4. Applications

A brief review of some investigations in which the mass separator has been used after the reconstruction of the ion source will be given in this concluding chapter.

Gallium isotopes from the spallation of arsenic were separated in order to determine relative formation cross sections of 9.6 h ^{66}Ga, 79 h ^{67}Ga, 68 min ^{68}Ga, 22 min ^{70}Ga, 14 h ^{72}Ga, and 4.8 h ^{73}Ga[14]). GaF_3 was chosen as the charge material and about 10% overall efficiency of the separation process was estimated at a stable ^{69}Ga ion current of more than 100 μA.

Similar figures of charge economy and focused ion currents have been obtained with Br in an investigation of the yield ratio 4.5 h ^{80}Br/18 min ^{80}Br from various high energy reactions[15]).

As indicated earlier, much interest has been

[9]) P. C. Thonemann, Progr. Nucl. Phys. 3 (1953) 219.

[10]) M. von Ardenne, Tabellen der Electronenphysik, Ionenphysik und Übermikroskopie, Bd I und II (VEB Deutscher Verlag der Wissenschaften, Berlin, 1956).

[11]) D. Bohm, The Characteristics of Electrical Discharges in Magnetic Fields, Ed. A. Cuthrie and R. K. Wakerling, (McGraw-Hill Book Company, New York 1949) Chs. 2, 3, 4, 9.

[12]) A. H. Barnes, S. M. MacNeille and C. Starr, Problems of Physics in the Ion Source, TID-5219 (United States Atomic Energy Commission, 1951).

[13]) J. R. Pierce, J. Appl. Phys. 11 (1940) 548.

[14]) G. Rudstam, Thesis (Univ. of Uppsala, 1957).

[15]) I. B. Svensson and G. Andersson, work in progress.

concentrated on the preparation of sources for nuclear spectroscopy in the lead region. $PbCl_2$ and TlCl proved to be suitable charge materials, allowing satisfactorily strong samples of various nuclei in the mass range 195–199 to be prepared for measurements of internal conversion lines in the double focusing beta spectrometer of the institute[16]) (see fig. 10).

Mass separated sources are often desirable in coincidence arrangements, even when one or two electron channels are involved. As beta spectrometers of the lens type are normally used and thus circular samples are wanted, the mass separator is not altogether ideal in this application because its "lines" are mainly extended in one direction (1–2 mm by 20 mm). That is, only part of the activity can be used and intensity difficulties are to be expected. A combination of a lens spectrometer and a 100 channel γ-ray spectrometer at the Physics Department of this University, however, has been run with some success on samples of 17 min

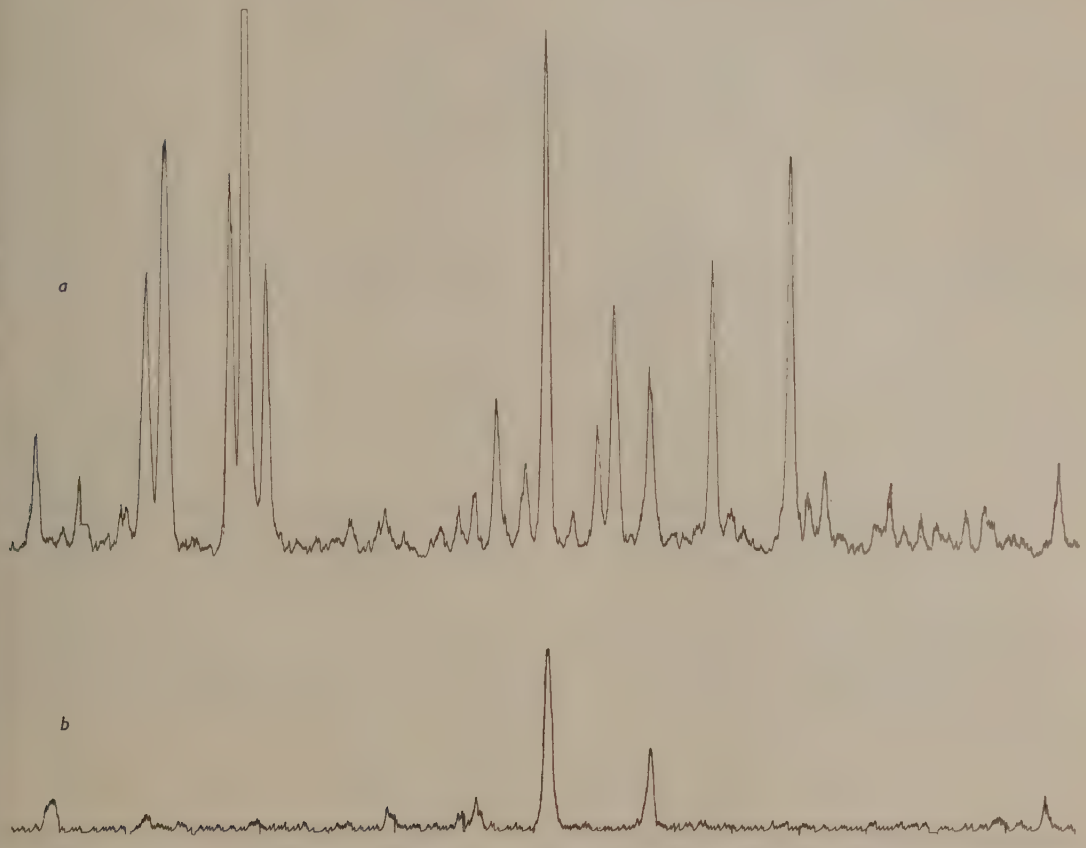

Fig. 10. Automatically recorded conversion electron spectra in the energy region 100–250 keV of lead samples from the irradiation of natural thallium with 105 MeV protons. a) Sample by chemical separation and vacuum evaporation. b) Mass separated $A = 196$ sample. Spectrometer resolution about 0.3%. The same intensity scale in both cases.

In the decay of 2.4 h ^{198}Pb, to give one actual example, the conversion lines of 15 γ-transitions have so far been measured at about 0.3% resolution[17]).

[16]) E. Arbman and N. Svartholm, Arkiv Fysik 10 (1956) 1.
[17]) B. Jung, work in progress.

^{195m}Pb and 42 min ^{197m}Pb[18]). In this case the strips were cut into pieces which were pasted together to a more suitable geometric shape.

More decent requirements on sample strength are characteristic of lifetime measurements in the μs-ms region by means of electronic time analysis[19]). On the other hand a good isotopic purity is highly demanded. Using mass separated 3.6 h ^{202m}Pb, Tove succeeded in determining the half-life of a level in ^{202}Tl as 475 μs[20]). Similar measurements on a 1.8 h ^{198m}Tl sample placed upper and lower half-life-limits (100 μs–50 mμs) to a 48 keV E2 transition in ^{198}Hg[21]).

There have been comparatively small intensity problems also in preparing samples for a multi-channel goniometer set up at the Institute of Physics, Uppsala[22]). Gerholm *et al.*[23]) have studied angular correlation of γ-rays in a series of odd mass thallium isotopes, using sources of 17 min ^{195m}Pb, 42 min ^{197m}Pb, 1.5 h ^{199}Pb, and 9.4 h ^{201}Pb. The results, which are still preliminary, seem to give interesting contributions to the systematics of *l*-forbidden M1 transitions.

From the examples quoted above it is seen that the present efficiency of the ion source, which in the Pb and Tl separations has varied between approximately 1% and 10%, makes possible quite an extensive use of the mass separator in nuclear spectroscopy. However, an increase of the charge economy even with as little as a factor 2 would mean a significant improvement in many cases, for instance in the study of positron spectra of the above-mentioned Pb and Tl isotopes. It is our opinion that the efficiency limit of the present type of ion source has not yet been reached and that the development work must be continued. This, however, should not exclude the search for essentially new ideas concerning ion source construction.

5. Acknowledgements

To the head of the Institute, Professor The Svedberg, we wish to express our sincere gratitude for the various facilities he has put at our disposal. Thanks are further due to Mr. B. Jung for interesting discussions on ion source problems and to Mr. R. Ringh for qualified technical assistance. Among the skilled mechanics whose contributions made the ion source constructions possible we would like to mention in particular Mr. O. Peterson and Mr. R. Östlund.

[18]) B. Jung and I. Marklund, unpublished work.

[19]) P. A. Tove, Nuclear Instruments 1 (1957) 95.

[20]) P. A. Tove, to be published.

[21]) G. Andersson, E. Arbman, J. O. Burgman and P. A. Tove, unpublished work.

[22]) T. R. Gerholm, T. Lindqvist and H. de Waard, Nuclear Instruments 1 (1957) 107.

[23]) T. R. Gerholm, E. Karlsson, J. Lindskog and J. O. Burgman, work in progress.

NUCLEAR INSTRUMENTS 3 (1958) 43–44; NORTH-HOLLAND PUBLISHING CO. – AMSTERDAM

NATURAL MODULATION OF HIGH FREQUENCY ION SOURCE BEAMS

G. C. PHILLIPS†, E. B. PAUL, A. T. G. FERGUSON and A. B. WHITEHEAD

Atomic Energy Research Establishment, Harwell, Berks.

and

T. GRJEBINE, R. MOREAU and B. OLKOWSKY

Centre d'Etudes Nucléaires de Saclay, Gif sur Yvette (S. et O.)

Received 7 January 1958

In the course of developing techniques to allow time-of-flight measurements using the Harwell 5 MeV Van de Graaff accelerator, it was discovered that the beam is naturally strongly modulated in time with the frequency of the R.F. ion source. Similar experiments on the two Van de Graaff accelerators at Saclay have indicated that they are modulated in the same way. At Harwell, the beam from the accelerator, after 90° magnetic deflection, was allowed to strike a fine lead glass fibre whose scintillations were observed with a photomultiplier and fast oscilloscope. A saw-tooth wave, with each alternate peak more intense, was observed; the two principal frequencies in these pulses were about 15 and 30 Mc/sec. By interposing parallel plates excited by a radio frequency oscillator between the magnetic analyser and the glass fibre (a device designed to pulse the beam) it was possible to allow only short bursts of the natural beam to strike the glass fibre. The variation of signal with deflector oscillator frequency demonstrated that the natural modulation was near 100% and that the beam naturally consists of short pulses of a repetition period of 33 msec. The oscillator driving the ion source discharge has two strong frequencies present: 15 and 30 Mc/sec. The construction of the discharge vessel is conventional[1]).

It also proved to be quite easy to detect the beam modulation with an ordinary communications radio receiver by placing a short antennae near the brass vacuum tube transmitting the proton beam. At Harwell this effect appears as strong signals at 15 and 30 Mc/sec. At Saclay, where the 2 and 5 MeV Van de Graaff's have ion source oscillator frequencies of 52 and 10 Mc/sec respectively, strong signals at those frequencies were observed. In addition, at Saclay, similar observations have been made on the Cockcroft-Walton machine.

While the radio signals are detectable for beams inside brass vacuum tubes the signals are much enhanced if the beam is allowed to strike metal near the antennae, but the effect is diminished if the beam is stopped in a quartz plate. It has been demonstrated at Saclay that the signals are more intense if the vacuum tube is of glass.

For the 5 MeV Van de Graaff at Saclay, whose beam is modulated at 10 Mc/sec, the percentage modulation has been estimated by direct observations of the radio frequency voltage imposed by the beam on a low capacitance target arrangement: the capacitance to ground, the average beam current, and the radio frequency voltage wave measured. These measurements indicated that the beam was as much as 70% modulated.

Thus there appears to be a high percentage modulation of the beams from these three Van de Graaff accelerators and in each case the

† John Simon Guggenheim Memorial Foundation Fellow, 1957, on leave from the Rice Institute, Houston, Texas.

[1]) P. C. Thonemann, D. Roaf, J. Moffatt and J. H. Sanders, Proc. Phys. Soc. (London) **61** (1948) 483.

modulation has the principal frequencies of its ion source oscillator. All three ion sources have the oscillator tank coil wound about the discharge tube of the ion source. Within the available range of variation of ion source parameters the character of the modulation does not qualitatively change.

Since this beam modulation is quite probably a general characteristic of such high frequency sources there seem to be several practical experimental consequences worth pointing out. 1) It should be possible to increase the intensity of pulsed beams produced by radio frequency deflection (such as the Harwell device mentioned above) by imposing suitable frequency and phase relationships between the ion source oscillator and the deflector oscillator. 2) It may be possible to produce very intense beams, consisting of very short pulses of current at any desired repetition rate, from conventional ion source tubes by replacing the conventional oscillator with a pulse oscillator. 3) The ease of detection of the radio-frequency signals of the naturally modulated proton beam while in flight suggests various interesting ways of measuring Van de Graaff beam current intensities without stopping the beam; such a technique might be useful, for example, for current measurements of low energy beams used with gas targets. 4) The natural beam modulation necessitates special care in using such beams for fast coincidence measurements when the resolving time of the coincidence circuits and the period of the beam modulation are comparable. Since, for example, fortuitious two-fold coincidences are proportional to the product of the two individual counting rates, the chance rates will be largely proportional to the square of the beam modulation. This effect, for example, makes questionable the accuracy of all past measurements of chance rates of radiations produced by high frequency ion source beams, where the counting rare *versus* delay curve has not extended over at least one beam modulation cycle.

NUCLEAR INSTRUMENTS 3 (1958) 45–48; NORTH-HOLLAND PUBLISHING CO. – AMSTERDAM

RESPONSE CURVES OF ALKALI HALIDE SCINTILLATORS WITH SPECIAL REFERENCE TO THE $Li^6(n,\alpha)$ REACTION IN LITHIUM IODIDE

T. R. OPHEL

Research School of Physical Sciences, Australian National University, Canberra

Received 1 March 1958

Proton and gamma-ray responses of the alkali halide scintillators, NaI, KI, CsI, LiI and Li^6I have been obtained and the response of a 5-MeV proton was found to be approximately equivalent to the response of a 7-MeV electron for all five scintillators.

Special emphasis was given to the responses of LiI and Li^6I in an attempt to clarify various anomalies which have arisen in the course of neutron energy measurements with LiI by means of the $Li^6(n,\alpha)$ reaction. From an estimate of the triton response of LiI and Li^6I, which was derived from the proton and gamma-ray data in conjunction with the alpha-particle response and measurements of the pulse height of the $Li^6(n,\alpha)$ group, it has been shown that energy calibration of the $Li^6(n,\alpha)$ group with gamma rays is unsatisfactory.

1. Introduction

Scintillation detection of neutrons with lithium iodide by means of the $Li^6(n,t)He^4$ reaction has been reported by several workers [1–5]). The cross-section of the reaction is large (≈ 930 barns) at thermal energies and monoenergetic group which is due to the energy loss of the triton plus alpha particle ($Q = 4.785$ MeV) within the crystal, allows discrimination in the presence of a γ-ray background.

The energy of the $(t + \alpha)$ group produced by thermal neutrons has been given as 4.0 (Nicholson and Snelling), 4.1 (Hofstadter *et al.*), 4.5 (Schenk and Heath), and to within 6% of 4.8 MeV (Bernstein and Shardt). Each energy measurement was made by comparing the pulse heights of the $(t + \alpha)$ group and the 661 keV γ-ray line of Cs^{137} or, in the case of Hofstadter *et al.*, the 1.17 and 1.33 MeV γ-rays of Co^{60}. Schenk and Neiler extended the measurements to higher neutron energies and found that the energy of the group was not a linear function of $(E_n + Q)$ in the energy region $E_n = 0 - 16$ MeV; the neutron points lay below the γ-ray response for values of $(E_n + Q)$ less than 8 MeV and above for values of $(E_n + Q)$ in excess of 8 MeV.

There is no a priori reason to suppose that the properties of LiI will differ greatly from those of NaI, but in relation to the known relative responses of the latter phosphor, the above data are difficult to explain. Taylor *et al.*[6]) showed that, for NaI, the proton and deuteron response curves were linear and almost coincident, while the α response was non-linear and, at any given energy, considerably less than the proton response. It has been commonly supposed that both the electron (γ-ray) and triton responses would be linear and identical, or very nearly so, to the proton curve. No measurements to confirm the latter assumption have been reported in the literature.

Assuming similar responses for LiI, two inconsistencies in the data become apparent. Firstly, it is surprising that the energy release of the $(t + \alpha)$ within the crystal is as large as 4 — 4.8 MeV. The same particles would give rise to a group at approximately 3.5 MeV in NaI, the

[1]) R. Hofstadter, J. A. McIntyre, H. Roderick and H. I. West, Phys. Rev. **82** (1951) 749.

[2]) J. Schenk and R. L. Heath, Phys. Rev. **85** (1952) 923.

[3]) W. Bernstein and A. W. Shardt, Phys. Rev. **85** (1952) 919.

[4]) J. Schenk and J. H. Neiler, Nucleonics **12** (1954).

[5]) K. P. Nicholson and G. F. Snelling, Brit. J. App. Phys. **6** (1955) 104.

[6]) C. J. Taylor, W. K. Jentschke, M. E. Remley, F. S. Eby and P. G. Kruger, Phys. Rev. **84** (1951) 1034.

exact energy being determined by the activator concentration[7]). Secondly, the release of energy exceeding $(E_n + Q)$ for some values of E_n is inadmissible. In an attempt to clarify this anomaly, Schenk and Neiler investigated the effect of europium concentration on the energy of the $(t + \alpha)$ group produced by thermal neutrons. The energy of the group increased with the amount of activation until a concentration was attained for which the group energy exceeded the anticipated maximum of 4.8 MeV. The energy release of a $(t + \alpha)$ (total energy 4.8 MeV) in NaI would behave in much the same way as the activator concentration is increased since the p–α ratio (for any given energy) decreases with increasing activation[7]). However, the data for NaI indicate that the maximum energy would not exceed 4.8 MeV.

Both difficulties are removed if the assumption is made that the triton and γ-ray responses do not coincide. Measurements of the proton, γ-ray and α responses of natural LiI and Li^6I (96% Li^6) (obtained from the Harshaw Chemical Company, Cleveland, Ohio, U.S.A.) in conjunction with the $Li^6(n,t)$ group, were made to test the validity of this assumption. The proton and γ-ray responses of NaI, KI and CsI were also determined.

2. Experimental Procedure

The counter assembly employed was essentially similar to that described by Ophel and Wright[8]) for the calibration of photoproton spectra produced within scintillating materials. Protons from the $B^{10}(d,p)$ reaction at a deuteron bombarding energy of 300 keV were used to determine the proton response curve and aluminium absorbers of various thicknesses were interposed between the detecting crystal and the boron target to increase the number of proton points. The protons were observed at 90^0 rather than at 0^0 as was previously the case. The 8.78 and 6.1 MeV α groups from a (ThC + ThC′) source and γ-rays from Cs^{137} and Na^{22} were employed to establish the α and γ-ray responses. Crystal mounting and protection were as before. The $Li^6(n,t)$ group was obtained with an uncollimated Ra–Be source. A paraffin block, placed between the source and the detector, moderated the neutrons.

3. Results

Two sets of measurements were recorded with natural LiI using different crystals and foil thicknesses, and were in excellent agreement. The crystal dimensions were $\frac{1}{2}'' \times 1'' \times 0.15''$ and $\frac{1}{4}'' \times \frac{1}{4}'' \times 0.050''$. The larger crystal resolved the highest energy γ-ray used, viz. 1.28 MeV line of Na^{22}, with resolution better than 12% and the $Li^6(n,t)$ group with 7% resolution. The Na^{22} and $Li^6(n,t)$ spectra for this crystal are given in fig. 1. The smaller crystal, though of inferior resolution, was sufficiently large to obtain the γ-ray response up to 1.28 MeV.

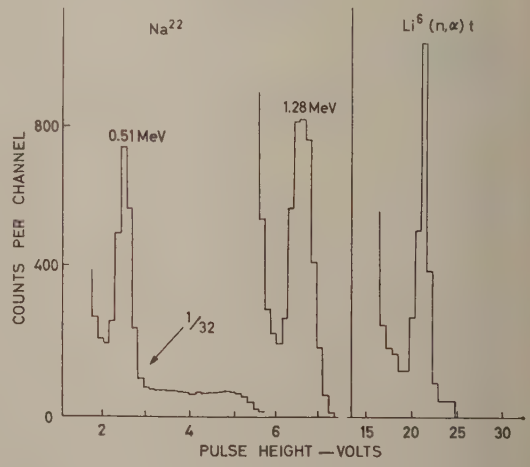

Fig. 1. Gamma-ray spectrum and $Li^6(n,\alpha)t$ group obtained with natural LiI crystal of dimensions $1'' \times \frac{1}{2}'' \times 0.15''$.

One measurement was made with a Li^6I crystal of dimensions $\frac{1}{2}'' \times \frac{1}{2}'' \times 0.15''$.

Figs. 2 and 3 show the proton, γ-ray and α responses which were obtained for each of the crystals along with the position of the $Li^6(n,t)$ group. It will be seen that there is a difference between the γ-ray and proton responses, and a linearity check of the electronics (fig. 4) ruled

[7]) F. S. Eby and W. K. Jentschke, Phys. Rev. **96** (1954) 911.

[8]) T. R. Ophel and I. F. Wright, to be published in Proc. Phys. Soc. (1958).

out the possibility that the proton and γ-ray points might be fitted to a common line of non-zero intercept.

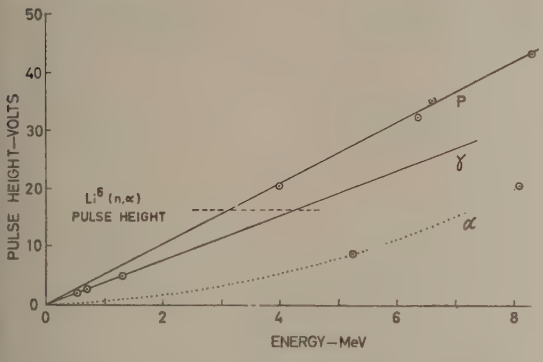

Fig. 2. Proton, gamma-ray and alpha-particle responses of natural LiI.

The energy of the α-particle produced in the $Li^6(n,t)$ reaction is 2.16 MeV, and the pulse

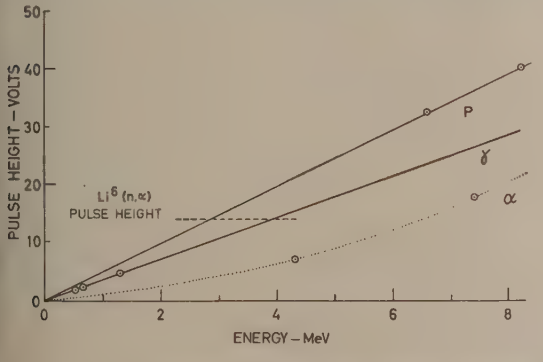

Fig. 3. Proton, gamma-ray and alpha-particle responses of Li^6I.

height of an α-particle of this energy in natural LiI (fig. 2) is approximately equivalent to that of a 0.5 MeV proton. The (t + α) group corresponds to 3.25 MeV proton energy so that the residual energy of the group, viz. 2.75 MeV, corresponds to the triton contribution. The triton energy is 2.6 MeV; thus the proton and

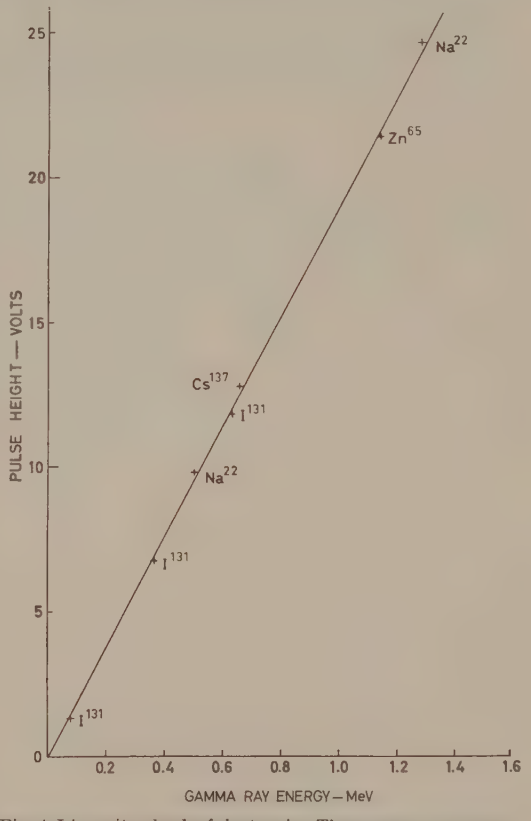

Fig. 4. Linearity check of electronics. The gamma-ray sources used to obtain the points are indicated on the diagram.

triton response curves are identical within the accuracy of the present measurement, which is

TABLE 1

Summary of LiI and Li^6I data

	Dimensions of Crystal	Energy of $Li^6(n,t)$ Group		Contribution of 2.6 MeV triton
		†(1)	†(2)	
Natural lithium iodide	$1'' \times \frac{1}{2}'' \times 0.15''$	3.2 MeV	4.1 MeV	2.8 MeV
Natural lithium iodide	$\frac{1}{4}'' \times \frac{1}{4}'' \times 0.040''$	3.3 MeV	4.2 MeV	2.7 MeV
Separated Li^6I	$\frac{1}{2}'' \times \frac{1}{2}'' \times 0.15''$	2.9 MeV	3.8 MeV	2.4 MeV

† (1) Energy relative to proton calibration. † (2) Energy relative to γ-ray calibration.

limited by the α response curve because only two points were used to determine this.

A similar result follows for Li^6I. A summary of the results for both scintillators is given in table 1. Differences between the γ-ray and proton responses were also obtained for NaI, KI and CsI and the electron energies equivalent to a 5 MeV proton for each scintillator are tabulated in table 2.

TABLE 2

Phosphor	Electron energy equivalent to a 5 MeV proton
NaI	7.2 MeV
NaI	$\approx$ 7.5 MeV
CsI	7.3 MeV
Natural LiI	6.7 MeV
Li^6I	6.95 MeV

4. Discussion

Having established that the triton and γ-ray responses of LiI are considerably different, the apparent anemalies discussed in the introduction are easily resolved. Clearly, neutron energy measurements are only possible if protons are used for calibrations of the crystal (unless the relative proton (triton)-γ-ray responses are known) or the actual neutron response determined.

No explanation is offered for the proton-gamma ray response difference, but it is to be noted that a similar effect has been reported for anthracene[6]). For a given rate of energy loss in anthracene, the fluorescence efficiency is greater for protons than electrons.

This work was done as part of a programme of nuclear photodisintegration studies carried out under Professor E. W. Titterton.

NUCLEAR INSTRUMENTS 3 (1958) 49–51; NORTH-HOLLAND PUBLISHING CO. – AMSTERDAM

PROPOSITION FOR A NEW METHOD FOR MEASURING SHORT HALF-LIVES

B. JOHANSSON and T. ALVÄGER

Nobel Institute of Physics, Stockholm 50

Received 16 January 1958

In the usual method of measuring short half-lives, employing fast scintillators and photo-multipliers, the measurements are limited by the decay time of the scintillation flash and more seriously by the time-spread in the photo-multipliers. These complications seems to make it impossible to measure half-lives shorter than about 5×10^{-11} s. In other indirect ways, as e.g. in resonant scattering, it is possible to estimate half-lives which are at least a factor of 10 faster, but this is limited to some very special cases. With the method proposed here, which in a direct way determines the half-lives, it is hoped that isomeric states decaying slower than 10^{-14} s could be reached.

The principle is as follows. Suppose that an element emits two K-conversion electrons in cascade. The time between these two events can then be determined in the following way. The start time of the first electron is determined by its phase-position in a high-frequency voltage supplied between two condenser-plates. The second electron emitted in coincidence with the first one obtains a deflection which is a function of the phase difference with respect to the first one. The principle is indicated in the fig. 1, which shows a block-diagram of the test-arrangement. (The magnetic focusing is necessary in practice, but not in principle.) For simplicity the source, S, is assumed to emit two electrons of the same energy in coincidence with each other. The plane parallel condensors C_1 and C_2 are connected to a high-frequency AC source. If the electron, e_1, reaches C_1 at time t_1, indicated in the sine-curve, it will undergo zero deflection. (This will be the most sensitive point and will be used in practice.) If e_2 is an electron in prompt coincidence with e_1 it will also obtain zero deflection, but if it had been emitted a short time later (e'_2), then it would have obtained a deflection proportional to the shaded area, A_2, indicated in the sine-curve. Thus, if the coincidence counting-rate versus the position of the aperture, a_2, along the line L is measured, a coincidence resolution curve will be obtained.

A test arrangement with two sector-magnets before the deflecting plates is in the process of being constructed at the Nobel Institute.

The condensers C_1 and C_2, indicated in the figure, are connected to the same high-frequency source. The phase-difference between the voltage on the two condensors will be made variable in order to obtain an artificial delay. The angle, θ, is chosen to be 90° in order that the electrons will pass through as little material as possible. A frequency of 144 Mc/s of the HF-source will be employed with an estimated voltage of 10 kV. With a distance of 60 cm between the condenser and the detector the resolving-time τ of the arrangement for 1 MeV electrons can be estimated to be 0.1 mμs. The figure is calculated from the following expression:

$$\tau = \frac{\Delta b}{\delta} + \Delta t$$

where Δb = the width of the spectrometer-line at half maximum.
δ = deflection sensitivity at the detector in mm/mμs (at $t = t_1$).
Δt = the difference in the transit time of the electrons through the magnet.

In the actual case: $\Delta b = 1$ mm corresponding to a transmission of about 0.2%, $\delta = 20$ and $\Delta t = 0.05$ mμs. The H.F.-deflection is carried

out after the magnetic deflection because this will give the highest deflection sensitivity or time-dispersion and because an energy discrimination before the H.F.-deflection will be obtained. The differences in length of the electron paths in the magnet are with good approximation (α is small) equal to

$$\alpha[R(1 - \cos\beta) + l_1 \sin\beta], \text{ where}$$

R = radius of curvature of the electron paths,
α = angle between the electron paths (at S),
β = angle of sector magnet,
l_1 = source to magnet distance.

Because these differences are linear functions of α they can be corrected for by using a small angle magnet with reversed field-direction in front of the spectrometer. By properly chosen parameters, this will not cause a serious decrease of the dispersion. However, a better method is to use two magnets with the same field-direction before the deflection plates, arranged in such a way that a first focus is obtained in between them. An aperture in the first focus will allow electrons with one energy only (within the energy resolution) to pass on to the second

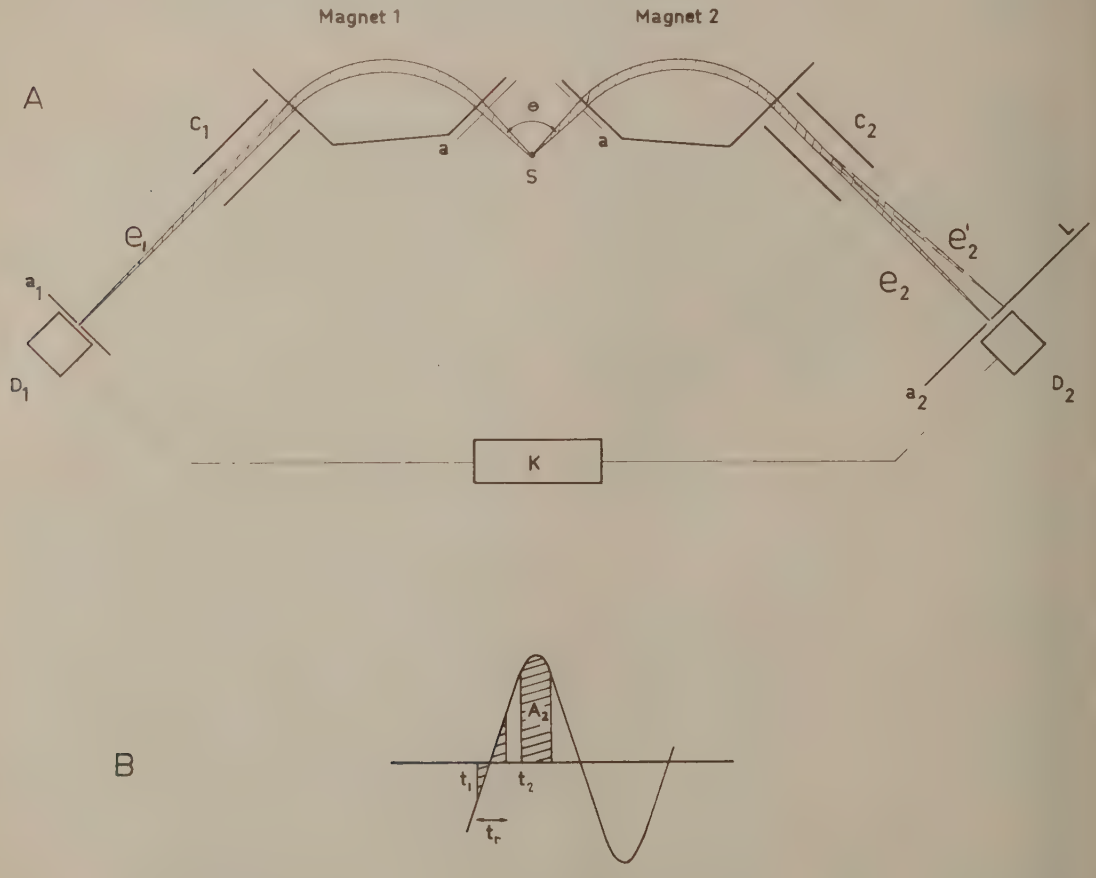

Fig. 1. A. Block-diagram of the test arrangement. S = sample; $C_{1,2}$ = deflection condensors; $D_{1,2}$ = detectors; a, $a_{1,2}$ = apertures; $e_{1,2}$ = electron paths; K = coincidence unit. (The resolving time is equal to one half-period of the H.F.-voltage. Thus, $\tau_{chance} = \tau$.) B. The high frequency voltage which is supplied to the condenser plates C_1 and C_2. t_r is the transit time of the electron through the condensors.

magnet. The differences in the length of the electron path will then be corrected for by the second magnet and moreover the final line-shape will be improved, which is important for the time-determination. However, the resolving time is of less importance in the time-measurement provided that the deflection is small within the condenser-plates and that the resolution curve is sharp.

Another method to obtain a displacement of the focus is to modulate the energy of the electrons†. This will, however, give rise to mixing of electrons with different energies so that the time-dispersion is limited. In the deflection-method this mixing can be held within the energy-resolution of the spectrometer and furthermore, the time-dispersion for the deflection-method is much larger for the same modulation conditions.

In further development of the method, double-focusing magnets will be employed, and by increasing the frequency and the voltage it seems to be possible to decrease the resolving time to about 10^{-12} sec and the shortest measurable half-life to about 10^{-14} sec for 1 MeV electrons and may be still less for lower energies.

The sector-magnets will give low transmission and thus low coincidence counting rate, but fortunately the arrangement described above is very convenient to supply with a multi-channel (or multi-detector) system. Then it should be possible to obtain all points of the coincidence resolution-curve at the same time.

† Energy modulation in order to determine short half-lives has been proposed by Gerholm and Tove, to be used in connection with lens spectrometers (Ark. f. Fysik **11** (1956) nr. 2, p. 75). A possible resolving time of $\tau = 0.3$ mμs was estimated for an electron-energy at 100 keV. The frequency required is 500 Mc/s.

NUCLEAR INSTRUMENTS 3 (1958) 52–56; NORTH-HOLLAND PUBLISHING CO. – AMSTERDAM

GENERAL FORMULAS FOR GAP-EXCITED LINEAR DUCTS

J. VAN BLADEL

Midwestern Universities Research Association† and Department of Electrical Engineering, University of Wisconsin

Received 6 February 1958

Equations allowing determination of the electric and magnetic fields at each point within a gap-excited metallic duct are derived. With the application to accelerators in mind, formulas are established for the energy and lateral momentum kicks to which a particle is subjected upon crossing the gap region. The configuration where the gap is in a plane perpendicular to the duct's axis is given some special attention.

1. Introduction

The purpose of the present investigation is to derive, in fairly general terms, formulas for the electromagnetic field in a metallic cylinder of arbitrary cross-section, cut in two by a gap of equally arbitrary contour (see fig. 1). The field is

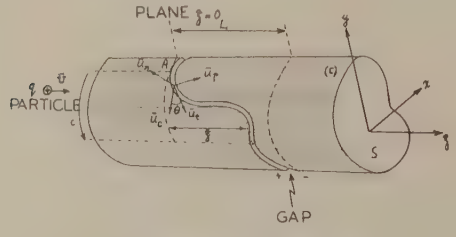

Fig. 1. Gap-excited linear duct.

excited by a voltage impressed across the lips of the gap, a voltage which varies continuously in phase and amplitude all along the gap contour. This variation, which depends on the external sources of excitation (cavities, two-wire lines, etc.), is assumed to be given, and is the starting point of the present analysis. The problem is tackled with one well-defined application in mind: gap-excited accelerators, either linear, or so slightly curved that they can be considered as linear in the region surrounding the gap. In accordance with that point of view, the following restrictions to the generality of the approach will be made:

(1) The operating frequency is less than the general cut-off frequency of the duct. As a result, fields are confined to the vicinity of the gap, and are not propagated, The tube will

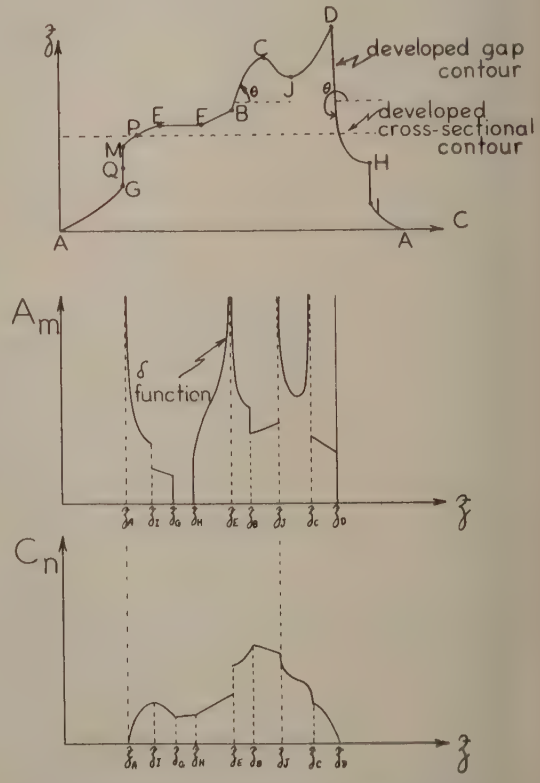

Fig. 2. Developed gap-contour, and general behaviour of the A_m and C_n integrals which appear in the calculation of the fields.

† Supported by Contract AEC No. AT (11-1)-384.

therefore be treated as an infinitely long wave-guide below cut-off.

(2) The cross-section of the duct is simply-connected, and the walls are perfectly conducting.

(3) The gap can be considered as infinitely narrow, its width being negligible with respect to wavelength and cross-sectional dimensions.

(4) The gap contour, when developed, takes the aspect depicted in fig. 2, where c denotes a coordinate measured along the perimeter of the cross-section (see fig. 1). It is seen that the gap is allowed to run parallel to the guide axis for a certain distance, but that no two of its points are otherwise permitted to lie on a parallel to that axis. In other words, the situation where the gap would "wind back" on itself is specifically excluded. Except for the segments parallel to the axis, therefore, z is a single-valued function of c.

2. Field Calculations

The fields within the duct are excited by the tangential component of the electric field in the gap. When the gap is very narrow, excitation takes place through the component of the field perpendicular to the gap[1]). If v and φ are respectively the magnitude and phase of the gap voltage, this component can be represented in δ function form by

$$\mathbf{e}_{tang}(c,t) = \delta(p)\, v(c) \cos\left[\omega t + \varphi(c)\right] \mathbf{u}_p \qquad (1)$$

where $\mathbf{u}_p$ is the unit vector lying in the tangent plane, and perpendicular to the profile of the gap. It will be convenient to work with complex vectors, and to represent the tangential field in phasor form by

$$\mathbf{E}_{tang}(c) = \delta(p)\, V(c)\, \mathbf{u}_p \qquad (2)$$

with

$$V(c) = v(c)\, e^{\,j\,\varphi\,(c)} .$$

The fields inside the wave-guide can be calculated by normal mode methods[2]). Adapted to the present situation, these consist of expanding $\mathbf{E}$ and $\mathbf{H}$ as †

$$\begin{aligned}
\mathbf{E}\,(x,y,z) &= \sum_m a_m(z)\, \boldsymbol{\mathscr{E}}_{tm}(x,y) + \sum_n b_n(z)\, \boldsymbol{\mathscr{E}}_{tn}(x,y) \\
&\quad + \sum_m c_m(z)\, \boldsymbol{\mathscr{E}}_{zm}(x,y) \\
\mathbf{H}\,(x,y,z) &= \sum_m \alpha_m(z) \boldsymbol{\mathscr{H}}_{tm}(x,y) + \sum_n \beta_n(z) \boldsymbol{\mathscr{H}}_{tn}(x,y) \\
&\quad + \sum_n \gamma_n(z) \boldsymbol{\mathscr{H}}_{zn}(x,y) \ .
\end{aligned} \qquad (3)$$

The unknowns are the complex expansion coefficients a_m, b_n etc.; these satisfy the set of equations:

$$\begin{cases}
\dfrac{da_m}{dz} + j\omega\mu\alpha_m - c_m = -\dfrac{1}{N_m{}^2}\displaystyle\int_c (\mathbf{u}_n \times \mathbf{E}_t)\cdot\boldsymbol{\mathscr{H}}_{tm}\,dc = A_m(z) \\
\dfrac{d\alpha_m}{dz} + j\omega\varepsilon a_m = 0 \\
\alpha_m + \dfrac{j\omega\varepsilon}{k_m{}^2}\, c_m = 0
\end{cases} \qquad (4)$$

$$\begin{cases}
\dfrac{d\beta_n}{dz} - j\omega\varepsilon b_n - \gamma_n = 0 \\
\dfrac{db_n}{dz} - j\omega\mu\beta_n = \dfrac{1}{N_n{}^2}\displaystyle\int_c (\mathbf{u}_n \times \mathbf{E}_t)\cdot\boldsymbol{\mathscr{H}}_{tn}\,dc = B_n(z) \\
b_n - \dfrac{j\omega\mu}{k_n{}^2}\,\gamma_n = \dfrac{1}{N_n{}^2}\displaystyle\int_c (\mathbf{u}_n \times \mathbf{E}_t)\cdot\boldsymbol{\mathscr{H}}_{zn}\,dc = C_n(z) \ .
\end{cases}$$

The integrals appearing in the right-hand members of the equations are known functions of z. Their actual value, which depends on the gap contour, gap voltage, etc., will ultimately determine the six unknown functions. The following general statements can be made about the behavior of A_m, B_n and C_n. Let the developed curve consist of k arcs along which z varies monotonically with c (fig. 2). Then each integral consists of the sum of k contributions, one for each intersection of the gap with the cross-sectional contour.

(a) If this intersection is an ordinary point such as P, the contribution takes the following form:

[1]) A. F. Stevenson, Journal of Applied Physics, 19 (1948) 24.

[2]) J. van Bladel, Paper accepted for publication in the Zeitschrift für Angewandte Mathematik und Physik.

† Let $\mathscr{E}_{zm}(x,y)$ and $\mathscr{H}_{zn}(x,y)$ be the eigenfunctions of the following two-dimensional problems:

$$\nabla_{xy}{}^2\,\mathscr{E}_{zm} + k_m{}^2\,\mathscr{E}_{zm} = 0$$

with $\mathscr{E}_{zm} = 0$ on the cross-section contour

$$\nabla_{xy}{}^2\,\mathscr{H}_{zn} + k_n{}^2\,\mathscr{H}_{zn} = 0$$

with $\partial\mathscr{H}_{zn}/\partial n = 0$ on the cross-section contour

where a subscript such as m stands for a pair of indices. One defines: $\boldsymbol{\mathscr{E}}_{zm} = \mathscr{E}_{zm}\,\mathbf{u}_z$; $\boldsymbol{\mathscr{H}}_{zn} = \mathscr{H}_{zn}\,\mathbf{u}_z$; $\boldsymbol{\mathscr{E}}_{tm} = \operatorname{grad}\mathscr{E}_{zm}$; $\boldsymbol{\mathscr{E}}_{tn} = \mathbf{u}_z \times \operatorname{grad}\mathscr{H}_{zn}$; $\boldsymbol{\mathscr{H}}_{tm} = \mathbf{u}_z \times \operatorname{grad}\mathscr{E}_{zm}$; $\boldsymbol{\mathscr{H}}_{tn} = \operatorname{grad}\mathscr{H}_{zn}$ with the norms: $N_m{}^2 = \iint_s |\,\boldsymbol{\mathscr{E}}_{tm}|^2\,dS$ and $N_n{}^2 = \iint_s |\,\boldsymbol{\mathscr{E}}_{tn}\,|^2\,dS$.

$$A_m = \frac{1}{N_m^2}\left[V\cdot\frac{\partial \mathscr{E}_{zm}}{\partial n}\cdot\frac{1}{|\operatorname{tg}\theta|}\right]_{\text{at P}}$$
$$= \frac{1}{N_m^2}\left[V\cdot\frac{\partial \mathscr{E}_{zm}}{\partial n}\cdot\left|\frac{dc}{dz}\right|\right]_{\text{at P}}$$
$$B_n = -\frac{1}{N_n^2}\left[V\cdot\frac{\partial \mathscr{H}_{zn}}{\partial c}\cdot\frac{1}{|\operatorname{tg}\theta|}\right]_{\text{at P}}$$
$$= -\frac{1}{N_n^2}\left[V\cdot\frac{\partial \mathscr{H}_{zn}}{\partial c}\cdot\left|\frac{\partial c}{\partial z}\right|\right]_{\text{at P}} \qquad (5)$$
$$C_n = -\frac{1}{N_n^2}\left[V\mathscr{H}_{zn}\right]_{\text{at P}}$$

when θ is between 0 and $\pi/2$

$$C_n = +\frac{1}{N_n^2}\left[V\mathscr{H}_{zn}\right]_{\text{at P}}$$

when θ is between 0 and $-\pi/2$.

These formulas can also be applied for a point such as Q, where the gap runs parallel to the z axis, provided a value of $\pi/2$ (or $-\pi/2$) is substituted for θ.

(b) At point B, where a change of slope from $\operatorname{tg}\theta^-$ to $\operatorname{tg}\theta^+$ is experienced, A_m and B_n are subjected to a jump in value equal to, respectively,

$$\frac{1}{N_m^2}\left[V\frac{\partial \mathscr{E}_{zm}}{\partial n}\right]_{\text{at B}}\cdot\left[\left|\frac{1}{\operatorname{tg}\theta^+}\right| - \left|\frac{1}{\operatorname{tg}\theta^-}\right|\right]$$

and

$$-\frac{1}{N_n^2}\left[V\frac{\partial \mathscr{H}_{zn}}{\partial c}\right]_{\text{at B}}\cdot\left[\left|\frac{1}{\operatorname{tg}\theta^+}\right| - \left|\frac{1}{\operatorname{tg}\theta^-}\right|\right].$$

C_n is continuous, but with a jump in its derivative (easily calculated from (5)).

(c) At an axial distance z where the gap runs perpendicular to the axis for a while, such as between points E and F, the various integrals become:

$$A_m = \frac{1}{N_m^2}\,\delta(z - z_E)\int_E^F V(c)\,\frac{\partial \mathscr{E}_{zm}}{\partial n}\,dc$$
$$B_n = -\frac{1}{N_n^2}\,\delta(z - z_E)\int_E^F V(c)\,\frac{\partial \mathscr{H}_{zn}}{\partial c}\,dc \qquad (6)$$
$$C_n = 0\ .$$

(d) At point C, where the developed curve has a horizontal tangent, and a radius of curvature R, A_m and B_n become infinite as

$$A_m = \frac{\sqrt{2R}}{N_m^2}\cdot\left[V\frac{\partial \mathscr{E}_{zm}}{\partial n}\right]_{\text{at C}}\cdot\frac{1}{\sqrt{|z - z_c|}} \qquad z < z_c$$
$$B_n = -\frac{\sqrt{2R}}{N_n^2}\left[V\frac{\partial \mathscr{H}_{zn}}{\partial c}\right]_{\text{at C}}\cdot\frac{1}{\sqrt{|z - z_c|}} \qquad (7)$$

formulas which can be derived from (5) by substituting $[2\,|z - z_c|/R]^{1/2}$ for $\operatorname{tg}\theta$. The infinity of A_m and B_n is weaker than a δ function discontinuity in that the "area under the curve" around C, i.e.,

$$\lim_{\varepsilon\to 0}\int_{z_c-\varepsilon}^{z_c} A_m(z)\,dz\ ,$$

is equal to zero. Function C_n goes to zero at C, with a vertical tangent, and has the form

$$C_n = \frac{2\sqrt{R}}{N_n^2}\left[\frac{\partial}{\partial c}(\mathscr{H}V_{zn})\right]_{\text{at C}}\sqrt{|z - z_c|} \qquad z < z_c\ .$$

The behaviour of A_m, B_n and C_n at point D, where the developed curve has an angular peak, can be deduced from the behaviour at C by letting the radius of curvature R approach zero.

To summarize the preceding considerations in a graphical way, typical curves for A_m and C_n are shown in fig. 2. A curve for B_n would have the same general aspect as its A_m counterpart. At the discountinuity points, the unknown functions, a_m, b_n, etc., behave in a manner which can easily be deduced from a consideration of eq. (4). For example:

a_m, b_n, γ_n suffer a discontinuity in slope at B and D, a jump in value and slope at EF, and possess a vertical tangent at $z = z_c$.

α_m, β_n, c_m are smoother; they are subjected to a jump in slope at EF, but are continuous, with continuous first derivative, at all other singular points. Finally, complete determination of the six unknown functions requires taking into account that they vanish at infinity (i.e., for $z = \pm\infty$), the guide being operated below cut-off.

3. Energy and Momentum Kicks

Calculation of a_m, b_n, etc., along the lines sketched in the preceding paragraph, allows determination of the electric and magnetic fields at each point of the vacuum chamber of the accelerator. In many situations, however, one is not so much interested in a detailed knowledge of these fields as in their integrated effect on a particle which flies through the gap region. Of particular physical significance, for instance, are the energy and lateral momentum

kicks impressed on a particle which was originally travelling parallel to the accelerator axis. Remarkably simple formulas can be found for these kicks if one assumes that the gap voltage is not of such magnitude as to materially alter the particle's linear motion during the crossing of the gap region. Derivation of these formulas proceeds as follows:

3.1. ENERGY KICK $\Delta\mathscr{E}$

Let v and q be the velocity and charge of the particle, φ_0 the phase of the voltage at A (see fig. 1) at the moment the particle crosses the $z = 0$ plane. The longitudinal energy kick is equal to

$$\Delta\varepsilon(x,y) = q\int_{-\infty}^{\infty} e_z(x,y,z,t)\mathrm{d}z = q \times \text{real part of}$$

$$\int_{-\infty}^{\infty}\sum_m \mathscr{E}_{zm}(x,y)\, c_m(z)\quad \mathrm{e}^{j\left(\varphi_0+\frac{2\pi}{\beta}\frac{z}{\lambda}\right)}\mathrm{d}z\ .$$

There, as usual, β is equal to v/c, and λ is the free-space wavelength of the applied voltage. To evaluate an integral such as

$$\int_{-\infty}^{+\infty} c_m(z)\ \mathrm{e}^{j\left(\varphi_0+\frac{2\pi}{\beta}\frac{z}{\lambda}\right)}\mathrm{d}z\ ,$$

one first establishes a relation satisfied by c_m alone. This can be obtained from (4) as:

$$\frac{\mathrm{d}^2 c_m}{\mathrm{d}z^2} - (k_m{}^2 - k^2)\, c_m = k_m{}^2\, A_m(z)$$

$$(\text{with } k = \omega/c = 2\pi/\lambda)\ .$$

The integral involving c_m is then obtained by multiplication of both members by

$$\mathrm{e}^{j\left(\varphi_0+\frac{2\pi}{\beta}\frac{z}{\lambda}\right)},$$

and integration between $z = -\infty$ and $z = +\infty$. The integral involving $A_m(z)$ can be computed by applying the results derived in the preceding section. Detailed calculations will not be given here: they are fairly straightforward. The expression one ends up with is

$$\Delta\mathscr{E}(x,y) = -q\sum_m \frac{\mathscr{E}_{zm}(x,y)}{N_m{}^2}\,\frac{k_m{}^2}{k_m{}^2 + k^2\left(\frac{1}{\beta^2}-1\right)}$$

$$\int_c v(c)\,\frac{\partial\mathscr{E}_{zm}}{\partial n}\cos\left[\varphi_0 + \Delta\varphi + \frac{kz}{\beta}\right]\mathrm{d}c\ . \qquad (8)$$

There, $\Delta\varphi$ is the phase difference between the voltage at a gap point c and the voltage at A. Expressed as a formula: $\Delta\varphi = \varphi(c) - \varphi(0)$. The angle appearing after the cosine has an interesting physical significance: it is the phase of the voltage in c, at the very moment the particle shoots through the cross-sectional plane to which c belongs.

3.2. LATERAL MOMENTUM KICK $\Delta\mathbf{p}$

The lateral momentum kick due to the electric fields is

$$\Delta\mathbf{p}_E = q\int_{-\infty}^{+\infty}\mathbf{e}_{\text{transverse}}(x,y,z,t)\,\mathrm{d}t$$

which, upon substitution of the expansion for the electric fields, yields:

$$\Delta\mathbf{p}_E = \frac{q}{v} \times \text{real part of}\left[\sum_m \boldsymbol{\mathscr{E}}_{tm}(x,y)\right.$$

$$\int_{-\infty}^{+\infty} a_m(z)\cdot \mathrm{e}^{j\left(\varphi_0+\frac{2\pi}{\beta}\frac{z}{\lambda}\right)}\mathrm{d}z + \sum_n \boldsymbol{\mathscr{E}}_{tn}(x,y)$$

$$\left.\int_{-\infty}^{+\infty} b_n(z)\ \mathrm{e}^{j\left(\varphi_0+\frac{2\pi}{\beta}\frac{z}{\lambda}\right)}\mathrm{d}z\right]\ .$$

The lateral momentum kick due to the magnetic field is

$$\Delta\mathbf{p}_H = q\mu_0\int_{-\infty}^{+\infty} v[\mathbf{u}_z \times \mathbf{h}(x,y,z,t)]\,\mathrm{d}t = q\mu_0\int_{-\infty}^{+\infty}(\mathbf{u}_z \times \mathbf{h})\,\mathrm{d}z$$

an expression which can similarly be rewritten, by insertion of the expansion for the magnetic field, as:

$$\Delta\mathbf{p}_H = q\mu_0 \times \text{real part of}\left[-\sum_m \boldsymbol{\mathscr{E}}_{tm}(x,y)\right.$$

$$\int_{-\infty}^{+\infty}\alpha_m(z)\cdot \mathrm{e}^{j\left(\varphi_0+\frac{2\pi}{\beta}\frac{z}{\lambda}\right)}\mathrm{d}z + \sum_n \boldsymbol{\mathscr{E}}_{tn}(x,y)$$

$$\left.\int_{-\infty}^{+\infty}\beta_n(z)\ \mathrm{e}^{j\left(\varphi_0+\frac{2\pi}{\beta}\frac{z}{\lambda}\right)}\mathrm{d}z\right]\ .$$

Upon computation of the integrals, the electric and magnetic kicks, consolidated in one expression, yield the fairly simple formula:

$$\Delta\mathbf{p}(x,y) = \frac{qk}{c}\left(1-\frac{1}{\beta^2}\right)\sum_m \frac{\boldsymbol{\mathscr{E}}_{tm}(x,y)}{N_m{}^2}\cdot\frac{1}{k_m{}^2 + k^2\left(\frac{1}{\beta^2}-1\right)}$$

$$\int_c v(c)\cdot\frac{\partial\mathscr{E}_{zm}}{\partial n}\cdot\sin\left(\varphi_0 + \Delta\varphi + \frac{kz}{\beta}\right)\mathrm{d}c + \frac{q}{kc}\sum_n \frac{\boldsymbol{\mathscr{E}}_{tn}(x,y)}{N_n{}^2}$$

$$\int_c v(c)\cdot\frac{\partial\mathscr{H}_{zn}}{\partial c}\sin\left(\varphi_0 + \Delta\varphi + \frac{kz}{\beta}\right)\mathrm{d}c\ . \qquad (9)$$

The value of the lateral momentum kick can now be obtained by merely substituting actual magnitude and phase of the applied voltage in the indicated integrals, and performing the required summations†. The shape of the gap's profile enters the formula through the term $(k/\beta)\, z\,(c)$, the shape of the cross-section through the transverse vectors $\boldsymbol{\mathscr{E}}_{tm}$ and $\boldsymbol{\mathscr{E}}_{tn}$ and the eigenvalues $k_m{}^2$.

4. Gap Perpendicular to the Tube's Axis

A gap situated in a plane perpendicular to the z axis is often used in practical applications. The formulas relative to this important configuration are obtained by merely setting $z = 0$ in the expressions derived in the preceding paragraphs. Two particular situations deserve some special attention.

4.1. THE PARTICLE TRAVELLING AT THE VELOCITY OF LIGHT

The relevant expressions for voltage and momentum kick show that, if magnitude and phase of the applied voltage are maintained constant as frequency varies:

The voltage kick is frequency independent at each point of the cross-section.

The lateral momentum kick has a direction independent of frequency, and a magnitude inversely proportional to the latter††.

† The application of the formulas to a duct with rectangular cross-section, excited by a constant voltage (in magnitude and phase) all along the gap contour, will appear in a forthcoming issue of "Nuclear Instruments".

†† As the frequency approaches zero, any phase difference along the gap will be reflected in a rapid increase in the wall currents and the magnetic fields associated with the latter. This, in turn, increases the lateral magnetic kick.

4.2. THE GAP VOLTAGE CONSTANT IN PHASE AND AMPLITUDE ALL ALONG THE CONTOUR

Important simplifications in the formulas are associated with this voltage distribution, which is often desired in those applications where constant voltage throughout the cross-section is hoped for:

$$\Delta\mathscr{E} = qV\cos\varphi_0 \sum_m \mathscr{E}_{zm}(x,y)\,\frac{k_m{}^2}{k_m{}^2 + k^2\left(\dfrac{1}{\beta^2} - 1\right)}\cdot\frac{\iint \mathscr{E}_{zm}\,\mathrm{d}S}{\iint \mathscr{E}^2{}_{zm}\,\mathrm{d}S}$$

$$\Delta\mathbf{p} = \frac{qV\sin\varphi_0}{c}\,k\left(\frac{1}{\beta^2} - 1\right)$$

$$\left[\sum_m \frac{\boldsymbol{\mathscr{E}}_{tm}(x,y)}{k_m{}^2 + k^2\left(\dfrac{1}{\beta^2} - 1\right)}\cdot\frac{\iint \mathscr{E}_{zm}\,\mathrm{d}S}{\iint \mathscr{E}^2{}_{zm}\mathrm{d}S}\right]$$

It turns out that $\Delta\mathbf{p}$ is also equal to $-\,(\mathrm{tg}\,\varphi_0/kc)\,\mathrm{grad}_{xy}\,(\Delta\mathscr{E})$. In consequense, an accurate plot of the energy kick $\Delta\mathscr{E}$ throughout the cross-section allows one the dispence with the lengthy calculations associated with the lateral momentum kick. The latter is, for instance, perpendicular to the constant energy curves. *In particular, a particle travelling at the velocity of light experiences a constant voltage throughout the cross-section, and is not subjected to any net lateral momentum kick:* magnetic and electric kicks balance each other.

The results obtained for a gap perpendicular to the z axis can be extrapolated to a gap of negligible longitudinal extent L (see fig. 1). Such an extrapolation is valid as long as the term kz/β remains sufficiently small, i.e., as long as the particle flies through the gap region in a time negligible with respect to a quarter of a period.